



**Univeristà degli Studi di Firenze**  
**LENS - European Laboratory for Nonlinear Spectroscopy**

---

Phd degree in Atomic and Molecular Spectroscopy  
XXVI Cycle - FIS/03

PHD THESIS

**One-dimensional disordered bosons  
from weak to strong interactions:  
the Bose glass**

Candidate:  
**Luca Tanzi**

Supervisor:  
**Prof. Giovanni Modugno**

Coordinator:  
**Prof. Francesco Pavone**



# Contents

<b>Introduction</b>	<b>1</b>
<b>1 Interacting bosons in disorder</b>	<b>5</b>
1.1 The weakly-interacting Bose glass . . . . .	5
1.2 Disordered phases at strong interactions . . . . .	8
1.3 Bosons in a disordered lattice . . . . .	10
1.4 Experimental observation of the Bose glass . . . . .	12
<b>2 Experimental procedures</b>	<b>17</b>
2.1 Experimental realization of the $^{39}\text{K}$ BEC . . . . .	17
2.2 Tuning the interactions in dilute Bose gases . . . . .	19
2.3 Optical dipole potentials . . . . .	20
2.4 Low-dimensional systems . . . . .	21
2.5 Disordered optical potential . . . . .	24
<b>3 Theoretical framework</b>	<b>27</b>
3.1 The Bose-Hubbard Hamiltonian . . . . .	27
3.2 The Aubry-André model . . . . .	30
3.3 Disorder and interactions in 1D . . . . .	32
3.3.1 The Tomonaga-Luttinger liquid . . . . .	32
3.3.2 Perturbation on 1D superfluids . . . . .	33
3.4 Open questions . . . . .	35
<b>4 Coherence</b>	<b>37</b>
4.1 Momentum distribution and correlation function . . . . .	38
4.2 Experimental procedure . . . . .	39
4.3 Experimental $U$ - $\Delta$ diagram . . . . .	41
4.4 Comparison with theory . . . . .	43
4.4.1 Zero- $T$ phase diagram in inhomogeneous systems . . . . .	45
4.4.2 Finite-temperature: a phenomenological approach . . . . .	46
4.5 Finite temperature effects . . . . .	48
4.5.1 Weakly-interacting side: an experimental thermometer . . . . .	48
4.5.2 Strongly-correlated phases . . . . .	50
4.5.3 Thermal effects in the $U$ - $\Delta$ plane . . . . .	50

<b>5</b>	<b>Transport</b>	<b>53</b>
5.1	Experimental procedure . . . . .	54
5.2	Dynamics in a clean lattice . . . . .	55
5.2.1	Physical picture and theoretical expectations . . . . .	55
5.2.2	Experimental observation . . . . .	57
5.3	Dynamics in a disordered lattice . . . . .	60
5.3.1	Transport diagram . . . . .	62
5.4	Mobility from weak to strong interactions . . . . .	65
<b>6</b>	<b>Excitation spectrum</b>	<b>69</b>
6.1	Inelastic scattering and Bragg spectroscopy . . . . .	69
6.2	Experimental procedure . . . . .	71
6.3	Excitations in the strongly-correlated regime . . . . .	72
6.4	Excitations from weak to strong interactions . . . . .	76
	<b>Conclusions</b>	<b>79</b>
	<b>Bibliography</b>	<b>89</b>

# Introduction

The interplay between disorder and interactions lies at the heart of many physical phenomena and its study has recently aroused more and more interest. In fact, disorder is ubiquitous in nature, since any physical structure is disordered if observed on small enough length scales (e.g., impurities in crystals, fractals surfaces, etc), and it strongly affects the transport properties of a system. Non-interacting particles can be localized by disorder; the celebrated phenomenon of Anderson localization<sup>6</sup> has been observed in the last fifty years in many physical systems. On the other hand, interactions play a fundamental role in the physics of condensed matter, altering the effects of disorder; for instance, the large electron-electron and electron-phonon interactions prevent a direct observation of the Anderson transition for electrons in a crystal. Despite its relevance, the fate of the localized phase in the presence of nonlinearities is still debated, and new unconventional behaviors are expected to appear.

The case of bosons is a paradigm of disorder-related phenomena. Here, interactions alone lead to superfluidity, a peculiar conducting state of matter, normally resistant to disorder. The combined effects of disorder and interactions strongly affect superfluidity, leading to a new localized quantum phase, the so-called *Bose glass*. This particular glassy phase was initially predicted in 1988 by Giamarchi and Schulz<sup>42</sup>, treating the disorder as a small perturbation to the strongly-correlated 1D bosonic system. In this context, a large repulsion between bosons plays the role of the Pauli exclusion principle in a fermionic system, cooperating with disorder in destroying superfluidity. As a consequence, the Bose glass phase can be described as an Anderson localized Fermi gas in a weak disordered potential<sup>37</sup>, and is expected<sup>42,37</sup> to behave as a *compressible* insulator, thus characterized by the absence of a finite energy gap in the excitations spectrum.

While large interactions cooperate with disorder in localizing bosons, weak interactions tend to establish coherence between the single-particle (Anderson) localized states, thus competing with disorder and possibly leading to a delocalizing transition from an insulator to a superfluid. In this regime, the resulting Bose glass phase is well described by several coherent puddles weakly coupled through the disorder potential. Despite a flurry of theoretical studies during the last 25 years, how exactly this glassy phase develops and connects to the strongly-interacting regime is still highly debated.

Also on the experimental side, a characterization of the Bose glass from weak to strong interactions is still missing. Recently, doped quantum magnets immersed in a magnetic field<sup>93</sup> provided the evidence of a gapless strongly-correlated Bose glass but, lacking the ability to simultaneously control disorder and interactions,

they did not probe this glassy phase in the whole phase diagram. This control is instead possible in ultracold atomic systems. In these systems, a laser light can create optical potentials for the atoms, enabling to engineer controllable and tunable disordered potentials. Pioneering experiments<sup>32,68,39</sup> studied the disordered phases of a  $^{87}\text{Rb}$  BEC by measuring its spectral response and its transport properties at strong interactions, distinguishing between insulating and superfluid regimes. However, they could not discriminate the Bose glass from a more conventional gapped insulator (a disordered Mott insulator), because of the impossibility to easily control the atom-atom interaction and the inhomogeneity due to the confining potentials. Other atomic species, such as  $^{39}\text{K}$ , do provide the possibility to easily tune the inter-particle interaction by means of Feshbach resonances. Exploiting this feature, some works<sup>79,26</sup> explored the coherence properties of a  $^{39}\text{K}$  BEC in a disordered lattice, providing the experimental diagram in the disorder-interaction plane, but only at weak interactions.

In this thesis we describe an extensive experimental investigation of the disordered bosons problem. We employ a degenerate Bose gas of  $^{39}\text{K}$  atoms with tunable interactions in a quasiperiodic lattice, and, for the first time, we explore the whole disorder-interaction plane at low temperature, exploiting our ability to control both the energy scales. We realize the one-dimensional system, the most studied in theory. We study both the equilibrium and the transport properties of the system, by combining various experimental techniques. In particular, we study three experimental observables: the system coherence, the mobility and the excitation spectrum. Cold atoms experiments do not allow to measure phase transitions, due to the unavoidable inhomogeneity and the finite temperature of the samples, but allow to distinguish the different phases. Combining coherence and transport measurements we give evidence of an insulating regime with a peculiar reentrant behavior from weak to strong interactions, surrounding a conducting one. At strong interactions, we use an excitation technique to spectrally resolve a gapless insulator well described by the Bose glass theory at low-temperature, and a disordered Mott insulator. We test the spectral response of the insulating regimes in the whole interaction range and we find a contrasting behavior at weak and at strong interactions, confirming a different interplay of interaction and disorder in the two regimes. We compare our finite- $T$  observations to the established  $T=0$  theory, finding good agreement. The theoretical studies are performed in cooperation with Guillaume Roux and Thierry Giamarchi, using a combination of density-matrix renormalization group (DMRG), exact diagonalization and fermionization approaches, adapted to the inhomogeneous experimental system.

The thesis is organized as follows. In Chapter 1 we give the intuitive physical picture of the phases predicted for interacting disordered bosons (the so-called *dirty bosons*). We briefly discuss their experimental realization with quantum magnets and with ultracold atoms. In Chapter 2 we illustrate the experimental apparatus, describing how the physical properties of the system can be tuned and controlled, especially the interaction energy and the disorder strength. In Chapter 3 we introduce few theoretical models which describe the experimental system.

The last three chapters report the experimental observation of the dirty-bosons regimes. In Chapter 4 we explore the coherence properties of the system, by measuring the atomic momentum distribution in a wide range of disorder and interaction. We

provide the first full experimental disorder-interaction diagram showing a broad crossover between coherent and incoherent regimes. We probe the different phases, by comparing the experimental diagram with numerical studies which account the system inhomogeneity, and with finite temperature simulations.

In Chapter 5 we measure the mobility and the momentum-dependent transport of the system, in the single lattice and in the disordered potential. We observe a crossover from a weakly dissipative regime at small momenta to a strongly unstable one at a disorder-dependent critical momentum. We compare the experimental results with theory suggesting a contribution of quantum phase slips to the dissipation. The combination of these measurements with the coherence diagram give the evidence of a reentrant insulating (incoherent) regime surrounding the superfluid phase in the disorder-interaction diagram.

Finally, in Chapter 6 we test the excitation spectrum of the insulating regions. In the strongly-correlated limit this measure allows to differentiate two insulating regimes: the Bose glass and the disordered Mott insulator. We compare the experimental response with the low- $T$  theory for the Bose glass, finding good agreement, consistent with a gapless insulator. At weak interactions the disordered phase response is quite different suggesting the presence of a distinct glassy phase.



# Chapter 1

## Interacting bosons in disorder

Disorder may have very strong effects on quantum fluids. The problem of the metal-insulator transition in interacting Bose systems is not easily addressable neither in theory nor in experiments. At the end of the eighties some theoretical studies tackled the problem using similar techniques to those employed in localized fermionic systems. Subsequently, many theoretical approaches have been developed, predicting the onset of a new insulating phase, the Bose glass, but the actual shape of the full phase-diagram is still debated. In this chapter we give the intuitive physical picture of the phases expected to appear in an interacting Bose gas in disorder. Few theoretical models will be discussed more in detail in Chapter 3.

### 1.1 The weakly-interacting Bose glass

Actually, the problem of interacting disordered bosons is very general, concerning a variety of real physical systems, such as superfluid Helium in porous media<sup>21,22</sup>, Cooper pairs in disordered superconductors<sup>82</sup>, and cold atoms in random optical potentials<sup>32,68,39</sup>. Basically, it consists in addressing the quantum phases induced by disorder in fundamental states of matter, such as superfluidity or superconductivity. In fact, at zero temperature the de Broglie wavelength associated to the bosonic particles is larger than the inter-particles separation. The bosons behave as coherent waves and they all occupy the same quantum state, giving rise to a Bose Einstein condensate (BEC). In the presence of interactions this macroscopic phenomenon imply superfluidity, a peculiar fluid state characterized by the complete absence of viscosity. If the condensed particles are Cooper pairs, the resulting gas is instead a superconductor. At small velocity no excitations can be created in the superfluid flow. Indeed, a nonzero critical velocity ( $v_c > 0$ ) for the creation of excitations was predicted by Landau, corresponding to a linear spectrum in the superfluid dispersion relation.

In the absence of interactions, the bosonic system is not superfluid ( $v_c = 0$ ), since its dispersion is that of free particles,  $E = p^2/2m$ , with  $m$  the atomic mass and  $p$  the momentum. The system is in fact less resistant to excitations. Nevertheless it is still a BEC, thus delocalized and describable as a coherent quantum state. The presence of disorder strongly influences the transport properties of the system, causing its localization. This phenomenon was formerly predicted by Anderson<sup>6</sup>

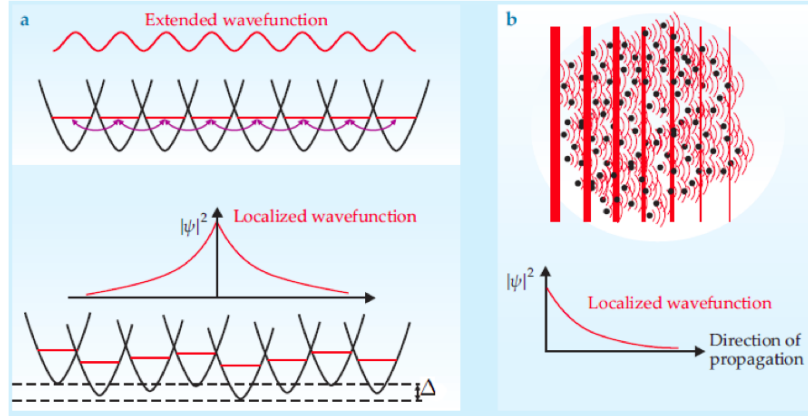


**Figure 1.1:** Schematic of the Anderson localization<sup>7</sup>. (a) Anderson localization can be thought in terms of particles tunneling. In an ordered lattice particles can tunnel between neighboring sites, freely propagating across the lattice. If the regularity of the lattice is broken by randomly changing the depth of the potential at each lattice site, the tunneling is suppressed and particles localize with an exponentially decaying wave-function. (b) From another point of view, Anderson localization can be understood in terms of destructive interference of waves propagating in a medium with large concentration of randomly distributed scatterers.

in 1958; Anderson studied the transport of generic ‘entities’, originally electrons, in a crystal by using a single particle tight-binding model with random on-site energies, finding localized eigenstates. The onset of localization can be understood by considering the quantum-wave nature of particles. In this wave picture, the Anderson localization relies on the destructive interference of several multiple scattering paths, which prevents any diffusion, exponentially localizing in space the wave-functions, see Fig. 1.1. In fact the Anderson localization is a very general phenomenon and has been observed in many different physical systems, such as disordered metals and superconductors<sup>55,82</sup>, light in random media<sup>92,89,83</sup>, sound waves<sup>48</sup>, ultracold atoms<sup>10,79</sup>. While in 1D any finite disorder provides localization, in 2D and 3D systems a metal-insulator transition occurs, and there exist mobility edges for the particle energy above which the disordered system is delocalized.

In this context the presence of a weak repulsive inter-particles interaction can weaken the Anderson localization, restoring phase coherence between localized states. As sketched in Fig. 1.2, the presence of interactions breaks the orthogonality of localized states; the energies of different states can become degenerate due to the interaction energy and their shape might change, giving rise to the formation of locally coherent fragments and allowing the transfer of population between neighboring states. Generally, if the interaction energy is smaller than the disorder strength (i.e. the standard deviation of the energies in the disordered potential), phase coherence cannot be restored in the whole system. In this case a new insulating phase, composed of many local superfluid puddles, arises from the competition between disorder and interactions, i.e. the *weakly-interacting Bose glass* (or sometimes also called fragmented BEC). This glassy phase is characterized by a large correlation length, i.e. is coherent on large length scales. Indeed, the main mechanism restoring coherence in the localized system is the resonant coupling due to the interaction energy,

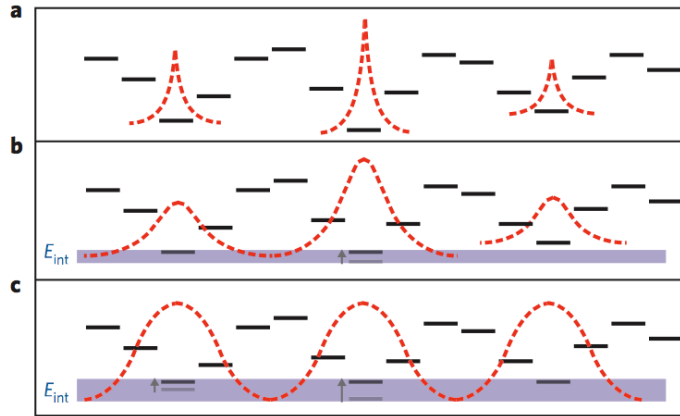


**Figure 1.2:** Schematic of the interaction-induced delocalization<sup>26</sup>. (a) In a very weakly interacting system with sufficiently large disorder, the eigenstates are exponentially localized, populating the lowest-energy states. (b) When the energies of different states becomes degenerate due to repulsive interactions, their shape modifies, giving rise to the formation of locally coherent fragments (weakly-interacting Bose glass). (c) The global phase coherence is restored only at large interaction strengths, where the entire system forms a coherent, extended state (BEC)

which preferentially couples states near in energy, and in space. As a consequence, every coherent puddle composing the Bose glass may extend over several unit length  $\ell$ , with  $\ell$  the mean inter-particle distance. For large enough interactions (naively, larger than the disorder strength) all the single-particle states are coupled, thus restoring superfluidity.

Many theoretical works tried to locate this metal-insulator transition from a superfluid to a weakly-interacting Bose glass in the disorder-interaction plane. Different approaches have been used. In 1D a Josephson array model considering the Josephson coupling between coherent puddles, can be used to map the system and gives a correction to the mean-field approach. In particular in Sec. 5.3.1 we will briefly describe these two methods for the one-dimensional case, in comparison with experimental data.

The weakly-interacting Bose glass phase can be found in any dimensionality, in the presence or in the absence of a lattice, since analogous arguments apply in one, two or three dimensions. It is a very general phenomenon occurring in disordered bosonic samples, which has been studied in different physical systems. For example, the delocalizing effects of a weak interaction was experimentally observed with light waves in nonlinear media<sup>83,56</sup>. These experiments investigate the evolution of linear and nonlinear waves in disordered waveguide lattices. The Anderson transition results as a transition from ballistic transport to diffusion and eventually exponential localization for the propagating light-wave, for increasing disorder. Generally, the presence of a weak positive nonlinearity corresponds to an attractive interaction, thus it tends to further localize the localized modes; anyway, it was shown<sup>56</sup> that nonlinear perturbations enhance delocalization in the higher-band localized modes, where, due to the inverted effective mass, they result in a weak repulsion.

In the last years we performed similar experiments, not reported in this thesis, with ultracold atoms in optical lattices, investigating both the dynamical regime and the

equilibrium properties of 3D condensates in the weakly-interacting regime<sup>26,27,59,60</sup>. In Lucioni et al.<sup>59</sup> we addressed the out-of-equilibrium dynamics of a 3D interacting BEC in a disordered lattice, showing that the Anderson-localized non-interacting state slowly expands when a controlled repulsive interaction is added. This expansion has a peculiar subdiffusive behavior, completely different from the ballistic one expected for a delocalized Bloch wave, which is induced by the interaction-assisted hopping between localized states. The ground-state properties of the system can be also studied. In Deissler et al.<sup>26</sup> we measured the metal-insulator crossover for 3D weakly-interacting bosons in a quasiperiodic lattice, studying the average local shape of the wave-function, its spatial correlations and its phase coherence. In this system a (weak) repulsive interaction energy screens the disorder restoring coherence in the wave-functions and inducing a Bose glass insulating phase. The boundary of this regime are experimentally mapped in the disorder-interaction plane, and found in good agreement with a mean-field theory.

## 1.2 Disordered phases at strong interactions

Up to now, we focused on the physical properties of weakly-interacting bosons in disorder. However, the Bose glass phase was initially found in the strongly-correlated regime. While a weak interaction competes with disorder and restores the coherence between localized states, at strong interactions the physical picture changes.

Let us consider the case of  $N$  bosons in the continuum confined in a  $d$ -dimensional box with volume  $L^d$ . Then  $\ell = L/\sqrt[d]{N}$  is the mean separation between the particles. Two energy scales determine the system properties: the average kinetic energy  $E_k \propto \hbar^2/m\ell^2$  and the interaction energy between particles, which in general scales as  $E_{\text{int}} \propto gn$ , where the mean-density  $n$  is dimension-dependent ( $n=N/L^d$ ). Here  $g$  describes the coupling between the particles and depends on their scattering properties, i.e. is proportional to the  $d$ -dimensional scattering length  $a_d$ . In 3D  $n = N/L^3$ ; as a consequence  $E_{\text{int}} \propto g/\ell^3$ . Therefore the ratio between the interaction and the kinetic energy scales as  $E_{\text{int}}/E_k = a_{3D}/\ell$ , i.e. the strongly correlated regime can be achieved only if the three-body scattering length  $a_{3D}$  is comparable the inter-particles separation  $\ell$ , at large interactions and large density. In our experimental dilute system, the mean separation is about 500 nm. To enter in the strongly correlated limit we would need a scattering length of the order of 10.000  $a_0$ , with  $a_0 \sim 0,05$  nm the Bohr radius. This is the so-called unitary regime; in this regime the two-body description of the collisions fails, and one deals with a many-body system. Due to the large three-body (and more) recombinations, this regime is very difficult to realize experimentally. Usually a 3D system is always weakly-interacting.

On the other hand, in 1D the interaction energy scales as  $E_{\text{int}} \propto g_{1D}/\ell$ , where  $g_{1D}$  is the one-dimensional coupling constant. The 1D system can be thought as a 3D system with two directions strongly confined by some external potential. As a consequence the atoms are forced to stay in the ground-state of the two confined directions, while they can propagate in the other one. In cold atoms experiments the external confinement is usually a harmonic trap, and the typical dimension of the confined directions is  $a_{\perp} \sim 50$  nm, much larger than  $a_{3D} \sim 100a_0 \sim 5$  nm. To a first approximation the collisional properties of the 1D system are three-dimensional and  $g_{1D} \propto a_{3D}/a_{\perp}^2$  (see Sec. 2.4). Therefore  $E_{\text{int}}/E_k = a_{3D}\ell/a_{\perp}^2$ , i.e. the interactions

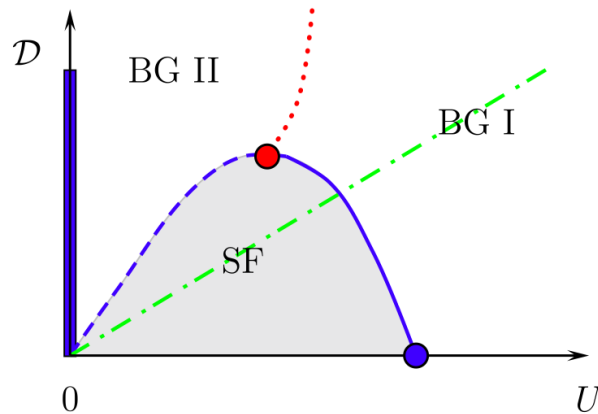


**Figure 1.3:** Phase diagram for a disordered one-dimensional Bose gas.  $U$  is the interaction energy,  $\mathcal{D}$  is the disorder strength. In the presence of disorder at strong enough interactions the ‘fermionized’ Bose gas Anderson-localizes. The green dash-dotted line schematically indicates the boundary below which an analytical approach can be used to treat the one-dimensional problem. The blue continuous line represents the strongly-correlated metal-insulator transition, the blue dashed line argues the weakly-interacting transition. How the two insulating phases connects is still an open problem. One possibility is that they are two distinct BG phases, separated by the red dotted line. The picture is taken from Ristivojevic et al.<sup>76</sup>.

dominate at low densities. In 1D the strongly-correlated regime is easily accessible, since  $a_{\perp}$  can be very small; indeed one needs scattering lengths even 10 times smaller than the inter-particles separation to reach  $E_{\text{int}} \sim E_k$ .

In general, in 1D one has two regimes: at weak interactions and high density  $E_{\text{int}} < E_k$ , i.e. the system prefers to lose its energy in interactions rather than into kinetic energy, in order to minimize the total energy. In general, the kinetic energy depends on the curvature of the wave-function,  $E_k = \hbar^2 \nabla^2 / 2m$ , i.e. it strongly increases if the wave-function is corrugated. Therefore at weak interactions the wave-function is smooth, though allowing the interaction between several atoms. On the other hand at strong interactions and low density,  $E_k < E_{\text{int}}$ ; then the total energy is minimized by avoiding interactions between the atoms. The resulting wave-function is corrugated; bosons minimize their interaction energy by avoiding spatial overlap and acquire fermionic properties<sup>43,67,53</sup>. In the absence of any perturbation, the system is a strongly correlated superfluid (the so-called Tonks-Girardeau gas). This mechanism is known as ‘fermionization’.

In the presence of disorder the one-dimensional strongly correlated superfluid undergoes a new phase transition. Indeed, the fermionized Tonks wave-functions Anderson localize in the disordered potential. The resulting insulating phase is a compressible Bose glass. Anyway, it is not yet clear whether the nature of this glassy phase is analogous to the weakly-interacting one. Of course, the correlation length characterizing its coherence properties is short, of the order of the mean particles separation  $\ell$ , contrary to the weakly-interacting case. This phase transition was initially predicted in 1988 by Giamarchi and Schulz<sup>42</sup>, treating the disorder as a small perturbation onto the one-dimensional bosonic problem. Using a renormalization-group approach the boundary of the transition was quantitatively established. In

Sec. 3.3 we will briefly discuss more in detail the phase transition, in the context of the Luttinger liquid theory. A sketch of the phases of the 1D disordered bosons is plotted in Fig. 1.3. Here  $U$  is the interaction energy energy per particle, while  $\mathcal{D}$  is the disorder strength. The theoretical diagram shows the typical reentrant shape of the Bose glass phase for increasing interactions. The continuous line represents the strongly-correlated metal-insulator transition, described by universal exponents, while the dashed line argues the weakly-interacting transition; how the two glassy phases connects is an open problem.

### 1.3 Bosons in a disordered lattice

As shown in Fig. 1.4a, the presence of a lattice introduces a new length and energy scale, i.e. the lattice periodicity  $\ell_0$  and the tunneling energy between neighboring sites  $J$ , which depends on the lattice depth  $s$ . In general  $s$  expresses the lattice depth in units of recoil energy  $E_r = \pi^2 \hbar^2 / 2m\ell_0^2$  (see Sec. 2.3). In the periodic potential the single-particle dispersion relation shows a band structure. For a vanishing lattice depth, the dispersion equals the free particle energy-momentum parabola; as already said, in a box the energy is  $1/L^2 < E_k < 1/\ell^2$ , with  $1/L^2 \rightarrow 0$  since  $L \gg \ell$ . When the lattice depth is increased, some gaps open and widen in the energy dispersion, and the width of the energy bands becomes exponentially smaller, see Fig. 1.4b. The total energy of the system is minimized if the wave-function is an extended (Bloch) state. In the tight binding limit ( $s > 5$ ), the single-particle energy dispersion in the first band reads:  $E(q) = E_0 - 2dJ \cos(q\ell_0)$ , where  $E_0 = \hbar\omega_{\text{lat}}/2 \propto \hbar^2 \sqrt{s}/m\ell_0^2$  is the ground-state energy in the single site,  $q$  is the quasi momentum of particles and  $d$  the lattice dimensionality.  $E_0$  depends on the lattice periodicity  $\ell_0$  (about 500 nm in our experimental setup) and on the lattice depth  $s$  (about 8 in our typical experiment), thus increases for increasing  $s$ . The kinetic energy of a Bloch wave is thus larger than the typical kinetic energy for particles in the continuum ( $\hbar^2/2m\ell^2$ ), since the wave function readapts to follow the lattice periodicity. On the other hand, in a lattice the energy is bounded and particles can not have kinetic energy larger than  $E_0 + 2dJ$  or smaller than  $E_0 - 2dJ$ . The width of the first band is  $4J$  and depends only on the tunneling energy which decreases for increasing  $s$ . Therefore, the interaction energy required to enter the strongly correlated regime is a function of  $J$ , which defines the bandwidth (i.e. the separation between the minimum and the maximum of energy). Roughly speaking, for interactions larger than the bandwidth the system is strongly correlated, i.e.  $E_{\text{int}} > E_k$ . The interaction energy in the single lattice site is still proportional to the density. It can be written as  $E_{\text{int}} \propto U(n-1)$ , where  $U$  is proportional to  $g$  and quantifies the energy-cost to put two atoms in the same lattice site, while  $n$  is the average atom number per site.

At weak interactions  $U < J$ , a delocalized wave-function minimizes the dominant kinetic energy, therefore minimizing the total energy of the many-body system. In the presence of disorder the physical picture is as described before: a finite disorder induces Anderson localization in the single particle problem but can be screened by a weak interaction, restoring coherence between particles. Two competing terms, the interaction energy  $E_{\text{int}}$  and the disorder strength, determine the phases of the system in any dimensionality.

In the opposite limit, when the repulsive atom-atom interactions are large com-

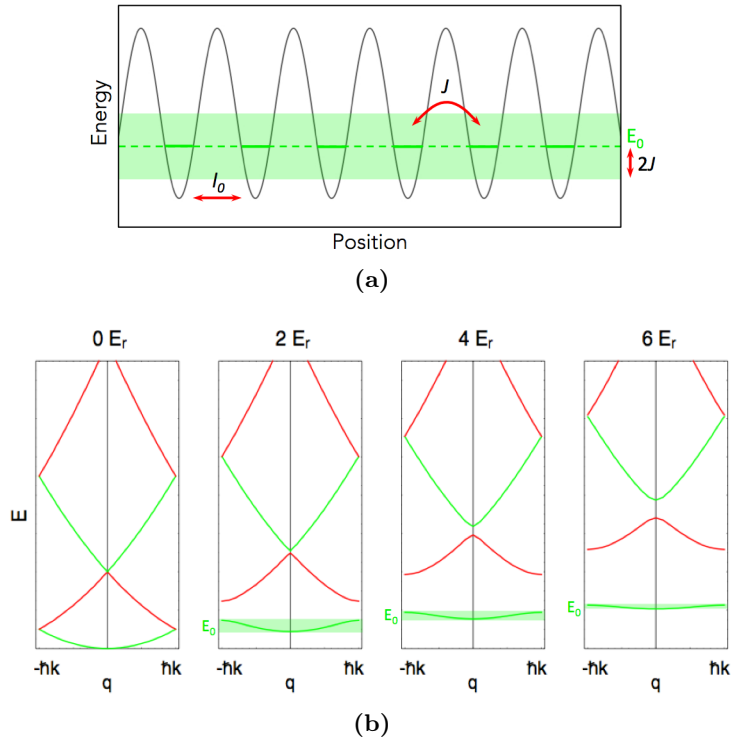


**Figure 1.4:** (a) In a regular lattice with periodicity  $\ell_0$  and tunnel coupling between neighboring sites  $J$ , the single-particle dispersion has a band structure (green region). The eigenfunctions are delocalized. The minimum kinetic energy is  $E_k \approx E_0 - 2J$ , with  $E_0$  the ground-state energy in the single hole (green line). (b) Band structure in a lattice. Energy of the Bloch state versus quasi momentum  $q$  in the first Brillouin zone, plotted for different lattice depths between 0 and  $6 E_r$ . For deep lattices the lowest band flattens and the width of the first band gap corresponds to the level spacing  $\hbar\omega_{\text{lat}}$  on each lattice site.

pared to the tunneling ( $U \gg J$ ), the system enters the strongly correlated regime and ‘fermionizes’. The interactions are larger than the bounded kinetic energy. Therefore the system prefers to localize increasing the (small) kinetic cost, in order to avoid (large) interactions between particles. The resulting ground-state is no longer a Bloch wave. A new metal-insulator transition arises already in the absence of disorder and the total energy is minimized when each lattice site is filled with the same number of atoms. This interaction-induced insulating state, known as Mott insulator (MI), occurs in any dimensionality as a consequence of the presence of the lattice. As the fermionic Mott insulator found in solid state systems because of the electron-electron interaction, it is characterized by the opening of an energy gap in the excitation spectrum, due to the competition between the interaction energy  $U$  and the tunnel coupling  $J$ . Indeed, a finite energy is required to create a particle-hole excitation. In Sec. 3.1 we will discuss this phase transition in the context of the Bose-Hubbard model, and its experimental realizations in the context of cold atoms.

The presence of disorder has a dual effect on the strongly interacting ( $U \gg J$ ) lattice system<sup>37</sup>. On the one hand, it induces a disordered Mott insulator in regions with commensurate  $n$  particles per site. On the other hand, in regions where the site occupation is not commensurate, i.e. each site contains  $n$  or  $n+1$  bosons which can hop to neighboring sites for non-zero tunneling  $J$ , perturbative arguments similar to those used for the strongly correlated 1D system in the continuum can be applied to the lattice system. Once again, the repulsive interactions dominate the kinetic energy and play a role analogous to the Pauli exclusion between fermions<sup>37</sup>; the ‘fermionized’ system localizes in the disorder, causing a Bose glass phase. In a lattice, where the kinetic energy is bounded, the Bose glass phase arises in any dimensionality. This phase is expected to be in intermediate between the gapped Mott phase and the superfluid phase<sup>37</sup>, even though the topic is highly debated. Once again the correlation length of this new insulating phase will be quite short, of the order of the lattice spacing  $\ell_0$ , contrary to what happens at weak interactions.

In this context, one can discuss the effects of a finite temperature onto these zero-temperature phases<sup>71,72,51</sup>. Generally, in one-dimension the presence of a finite temperature transforms the phase transition into crossover. This topic is not easily addressable either with analytical arguments or numerical simulations. Anyway a simple picture might be the following. While at strong interactions a finite  $T$  introduces a new energy scale ( $E_{th} \approx k_B T$ ) which breaks the zero- $T$  insulating phases (the MI and the BG), restoring (normal) conductivity, at weak interactions the temperature may have an opposite effect. In fact in this regime the thermal energy may compete with the interaction energy, since, at not too high  $T$ , the increase of the temperature causes the decrease of the mean density. Therefore the temperature effect would be to reduce the interactions, helping the localization of the system. This phenomenon, much debated in theory<sup>2</sup>, is known as *many-body localization*, and could be observed in weakly-interacting disordered systems.

## 1.4 Experimental observation of the Bose glass

The experimental observation of the Bose glass phase is a very difficult task. As already mentioned, bosons with disorder can be realized in a number of different ways, including Cooper pairs in thin superconducting films, Josephson junction arrays

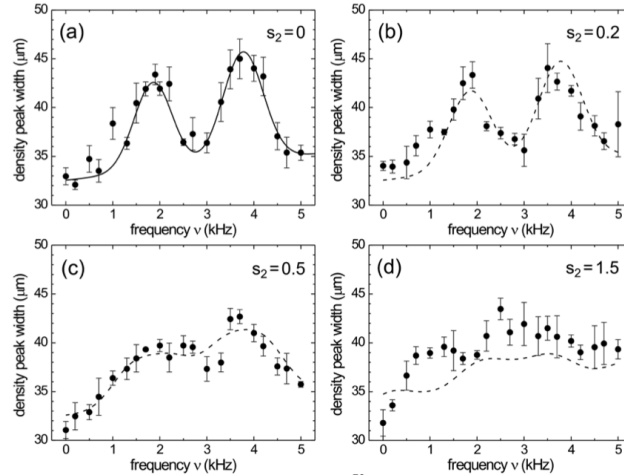


**Figure 1.5:** Excitation spectra in a disordered lattice at fixed tunneling  $J$  and increasing disorder.  $s_2$  is proportional to the disorder strength<sup>32</sup>. The progressive vanishing of the Mott insulator excitation peaks is clearly visible.

and  $^4\text{He}$  in porous media and on substrates, but none of these methods provided the unambiguous detection of this glassy phase, rather suggested indications of its presence.

**Cold atoms.** Cold atoms experiments are good candidates to study disorder-related phenomena. No phase transitions can be observed with cold atoms systems, since they are always confined in harmonic potentials causing inhomogeneous samples and their temperature is not zero. Anyway, they give access to several experimental observables, which can be used to distinguish the different phases. Furthermore, they allow to engineer controllable disordered potentials using laser light (laser speckles or bichromatic potentials has been successfully used), and to tune the interaction energy with Feshbach resonances, thus giving access to all the regions in the disorder-interaction plane.

Up to now, only few regions in the disorder-interaction diagram were studied. Using time-of-flight interference images and transport measurements, few experiments<sup>68,39</sup> explored the strongly-interacting region, distinguishing between insulating and superfluid phases. An important experimental observation towards the Bose glass was performed in Florence in 2007 by Fallani et al.<sup>32</sup>. Here the authors used a spectroscopic technique to study the energy excitation spectrum of disordered bosons at strong interactions. Furthermore, they characterized the system phase-coherence with a time-of-flight technique, detecting a strongly interacting insulator. An example of the system response to the excitation is shown in Fig. 1.5. For increasing disorder the gapped Mott-insulator resonances clearly broaden, giving the evidence of a disordered insulating phase, the first prerequisite for the formation of a Bose glass. However this spectral response does not allow to distinguish this phase from a disordered Mott insulator.

In Pasienski et al.<sup>68</sup> the authors studied the effect of disorder on the transport properties of  $^{87}\text{Rb}$  gas in a speckle potential superimposed on a clean lattice. Fig 1.6 shows the centre-of-mass velocity of the gas along the transverse ( $v_T$ ) and

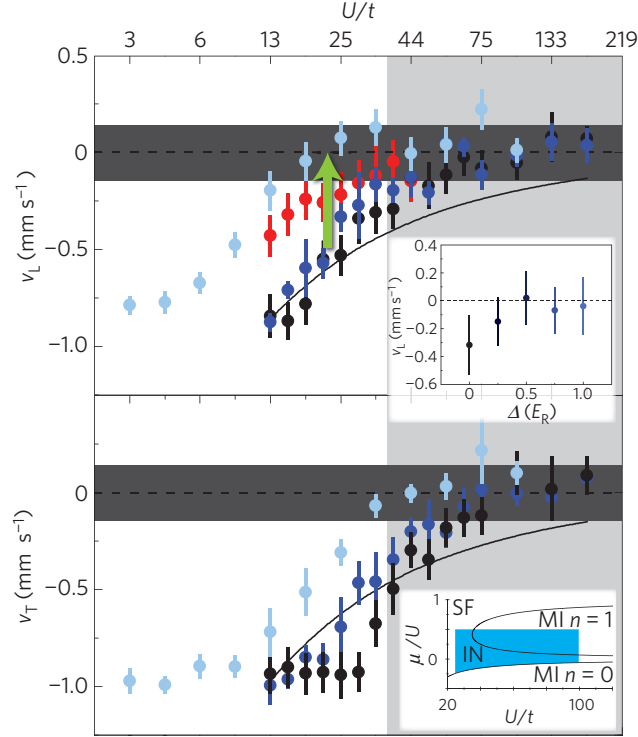


**Figure 1.6:** Effect of disorder on the transport of interacting bosons<sup>68</sup>. Dependence of the center of mass velocity on the interaction energy for increasing disorder strengths (black, dark blue, light blue) along the transverse ( $v_T$ ) and longitudinal ( $v_L$ ) speckle directions. The conductor-insulator transition is shifted towards smaller value of  $U/J$  as the disorder increases. Red points refer to high temperature transport in a clean (without disorder) lattice. The top inset shows how disorder affects  $v_L$  for  $s=14$

longitudinal ( $v_L$ ) speckle directions immediately after an applied impulse for three disorder strength,  $\Delta=0, 0.75$  and  $3 E_R$  (black, dark blue and light blue points respectively) and for a range of interactions  $U/J$  spanning the superfluid and Mott insulator regimes in a clean lattice. Here the disorder transforms the clean superfluid phase to an insulator, as indicated by the vertical green arrow. The impact of finite temperature is assessed by measuring the transport properties in the clean lattice at higher temperature (red points); the gas is not insulating, indicating that the observed metal-insulator transition is not exclusively caused by heating introduced by the speckle field. In fact, the disorder-induced insulating phase found at strong interactions is compatible with a Bose glass. However, the gapless nature of this insulating phase was not successfully addressed. Disentangling the strongly-correlated Bose glass from the Mott insulator with cold atoms experiments was so far not possible, in particular because of the inhomogeneity due to the confining potentials.

As already mentioned, Deissler et al.<sup>26</sup> exploited the possibility to tune the interactions in a  $^{39}\text{K}$  BEC with a Feshbach resonance, and experimentally probed the coherence properties of disordered bosons at weak interactions, by detecting their momentum distribution. However, this experiment was performed with an essentially 3D system which did not allow to explore the strongly-correlated regime.

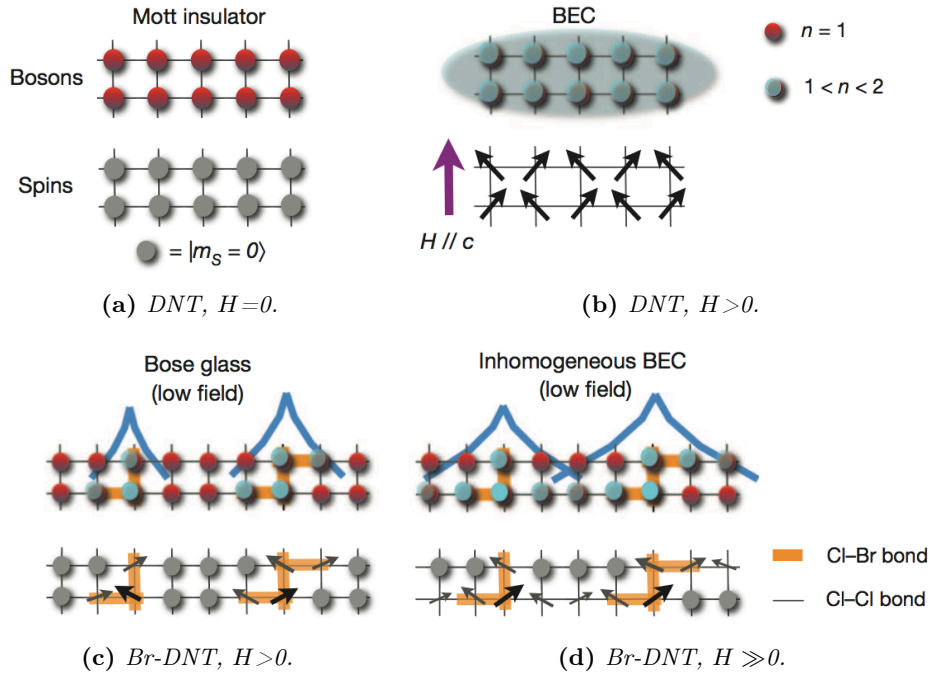


**Figure 1.7:** Sketch of the bosonic phases<sup>93</sup> of DTN and Br-doped DTN. In the undoped case, an increasing magnetic field (purple arrow) drives the system from a Mott insulator (a) to a BEC phase (b) by injecting delocalized excess bosons (indicated in cyan). (c) In the doped case, an arbitrarily weak magnetic field can inject extra bosons in the rare Br-rich regions (the orange bonds) which are localized and incoherent in the (low-field) Bose glass phase. The corresponding local orientations of the spins are sketched by the arrows (the darker the arrow, the larger the fluctuating transverse moment induced by the field). (d) Further increasing the magnetic field leads to the percolation of phase coherence via coherent tunneling of the excess bosons between the localized regions, giving rise to an inhomogeneous BEC.

**Quantum magnets.** The first experimental observation of a strongly-correlated Bose glass phase was achieved only in 2012 by Yu et al.<sup>93</sup>, with a completely different system. The authors observed a Bose glass of quasiparticles in a doped quantum magnet (bromine-doped dichloro-tetrakis-thiourea-nickel, DTN). The physics of pure DNT in a magnetic field  $H$  is equivalent to that of a lattice gas of bosons in the grand canonical ensemble (see Yu et al.<sup>93</sup> and references therein). The ground-state of such a system without disorder and in zero field, is a  $S=1$  quantum paramagnet in the  $|m_S = 0\rangle$  state (with  $m_S$  the  $S$  eigenvalue), corresponding to a gapped Mott insulator of bosons with  $n=1$  particles per site, see Fig 1.7a. By applying a critical magnetic field which overcomes the MI gap one can inject extra bosons into the system, driving a transition to a superfluid state (a magnetic BEC), see Fig. 1.7b. The pure DNT temperature-magnetic field phase diagram is plotted in Fig. 1.8a, showing the MI-SF-MI (with  $n=2$  particles per site) transition at zero temperature for increasing fields.

In this system disorder is introduced by substituting Cl with Br atoms. Bromine doping produces disorder into the hopping and interaction strength of the bosons,

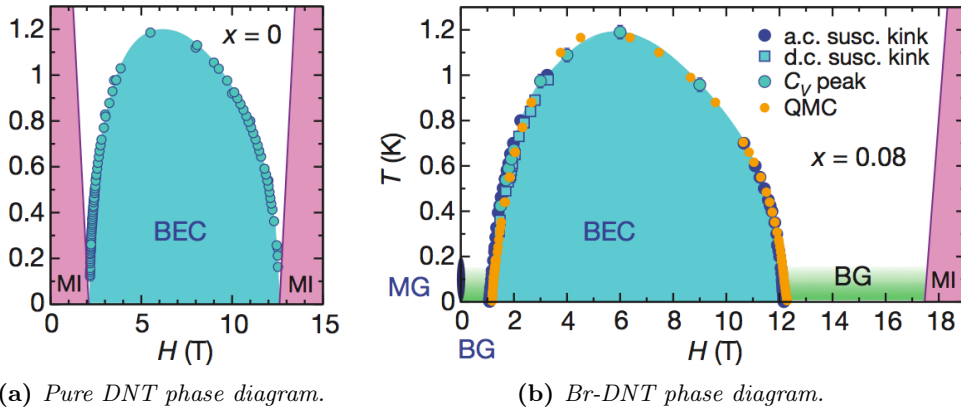


**Figure 1.8:** Phase diagrams in the field-temperature plane<sup>93</sup>. (a) Experimental phase diagram of pure DTN, based on specific heat and the magnetocaloric effect. (b) Experimental phase diagram of Br-doped DTN from specific heat and susceptometry, compared to QMC data.

due to the larger atomic radius of Br respect to Cl. At nonzero magnetic field a Bose glass phase occurs as shown in Fig. 1.7c: when the magnetic field is applied, excess of bosons are injected, and Anderson localize around the rare Br-rich regions. In the spin language, spins in the Br-rich regions acquire a finite magnetization, and their transverse components correlate antiferromagnetically over a finite range, but the local phase of the antiferromagnetic order is different from region to region so that the system remains globally paramagnetic. As shown in Fig. 1.7d the further increase of the magnetic field leads to coherent tunneling of bosons between neighboring localized states, resulting in a highly inhomogeneous BEC.

The  $\mu$ - $T$  phase diagram of Br-DNT is shown in Fig. 1.8b. The gapless nature of the Bose glass is probed by measuring the magnetic susceptibility (corresponding to the compressibility of quasiparticles), and the low temperatures specific heat, which in the MI regime are expected to vanish exponentially for  $T \rightarrow 0$ , due to the presence of the finite energy gap. As shown in Fig. 1.8a-1.8b, Br doping deeply affects the pure DNT phase diagram: both the lower and the upper critical fields for the onset of the magnetic BEC at  $T \rightarrow 0$  are shifted. Most importantly, the magnetic behavior of Br-DNT outside the BEC region is completely different from that of the pure system, showing a finite uniform magnetic susceptibility and a non-exponential decay of the specific heat at low temperatures. This corresponds to a gapless bosonic insulator, i.e. the Bose glass. The experimental results are confirmed by quantum Monte Carlo simulations, which allow to trace boundaries for the different phases.

Quantum magnetic systems allows to investigate the Bose glass properties in the  $\mu$ - $T$  plane at fixed disorder and interaction, addressing the dirty-bosons problem from a point of view orthogonal and complementary to that carried out with ultracold atoms experiments. They can study the properties of the homogeneous system at zero temperature, observing quantum phase transitions. On the other hand these systems do not have the possibility to tune the disorder and the interaction strength exploring the whole disorder-interaction diagram from weak to strong interactions.

## Chapter 2

# Experimental procedures

The main tool we use to investigate the physics of interacting particles in disordered media is a Bose-Einstein condensate (BEC) of  $^{39}\text{K}$  confined in optical potentials. In this chapter we briefly present the experimental techniques to produce the  $^{39}\text{K}$  BEC, and to create and control the one-dimensional disordered systems. The chapter is organized as follows: first of all, we summarize the experimental methods we used to produce the  $^{39}\text{K}$  condensate, the starting point of all the experiments performed in this thesis. In Sec. 2.2 we present a model treating the two-body interaction in a dilute cold gas; then, we introduce the Feshbach resonance phenomenon, as the method used to tune the atom-atom interaction. In Sec. 2.3 we review few basic concepts concerning the dipole interaction between atoms and the electromagnetic field, giving rise to the possibility to trap atoms into optical potentials. Exploiting optical lattices, we can experimentally tune the system dimensionality, as described Sec. 2.4, in particular we focus on the realization of the one-dimensional setup. The experimental realization of a disordered potential is discussed in Sec. 2.5; especially, we concentrate on the particular features of the quasiperiodic lattice, the kind of disorder we employ in the experiment.

### 2.1 Experimental realization of the $^{39}\text{K}$ BEC

The particular level structure of  $^{39}\text{K}$  and its collisional properties at zero magnetic field do not favor direct evaporative cooling; we therefore employ  $^{87}\text{Rb}$  to sympathetically cool  $^{39}\text{K}$  atoms. In spite of the small heteronuclear scattering length for Rb-K collisions, the sympathetic cooling has been proven to work efficiently<sup>78</sup>. Recently, a new experiment in Florence<sup>57</sup> however showed how it is possible to condense  $^{39}\text{K}$  without employing other atomic species, by performing an efficient sub-doppler cooling and using deep optical dipole traps.

The apparatus and experimental procedure used to produce the  $^{39}\text{K}$  condensate is accurately described in previous thesis<sup>77,34,28,94</sup> of our group. In the following I will shortly list the main steps required.

- $^{87}\text{Rb}$  and  $^{39}\text{K}$  atoms are laser cooled in two magneto-optical traps, producing samples at temperatures  $T \approx 100 \mu\text{K}$  and densities of about  $10^{10}$  atoms/cm<sup>3</sup>.
- The two species are prepared in their low-field seeking state  $|F = 2, m_F = 2\rangle$ ,

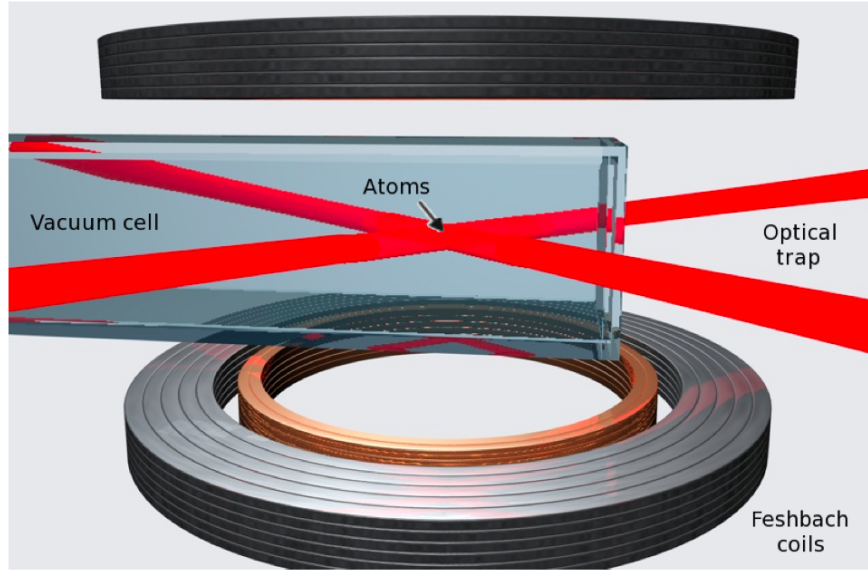


**Figure 2.1:** Schematic representation of the experimental setup. The  $^{39}\text{K}$  Bose-Einstein condensate is achieved in a crossed optical dipole trap obtained with two perpendicular focused laser beams. The laser wavelength,  $\lambda=1064\text{nm}$ , is red-detuned with respect to the atomic transition. A couple of coils in Helmholtz configuration provide a homogeneous magnetic field (Feshbach field) used to tune the inter-particle scattering length. Another couple of coils creates a magnetic field gradient used to compensate gravity.

and trapped in a QUIC magnetic trap. A forced, selective microwave evaporation of Rb atoms to the  $|F = 1, m_F = 1\rangle$  state cools the both samples to  $T \approx 1.5 \mu\text{K}$ .

- To further cool and finally condense the sample, it is required to tune the atomic scattering length. This can be done using a magnetic Feshbach resonance (see Sec. 2.2). The mixture is thus loaded into an optical dipole trap (see Sec. 2.3) and both the species are transferred in their absolute ground state  $|F = 1, m_F = 1\rangle$ , which presents a broad Feshbach resonance around 400 G. The optical trap is produced with two focused laser beams at wavelength  $\lambda = 1064 \text{ nm}$ .
- An homogeneous magnetic field is applied in order to tune inter- and intra-species interactions. The atoms are further cooled by reducing the intensity of the optical trap. The evaporation in the optical trap is performed in two steps. During the first step the magnetic field is set to about 316 G, where a heteronuclear Feshbach resonance exists<sup>78</sup>, thus enhancing collisions between Rb and K atoms. The evaporation is performed such that the atoms are lost in the vertical direction, in order to evaporate mainly the heavier Rb atoms, and sympathetically cool K atoms. When K is close to quantum degeneracy, the magnetic field is tuned to the homonuclear Feshbach resonance around 400 G, in order to set a positive value for the K-K scattering length. In this second step, K is cooled only through intra-species collisions. The final vertical depth of the trap does not compensate gravity for Rb atoms, which are lost. We thus

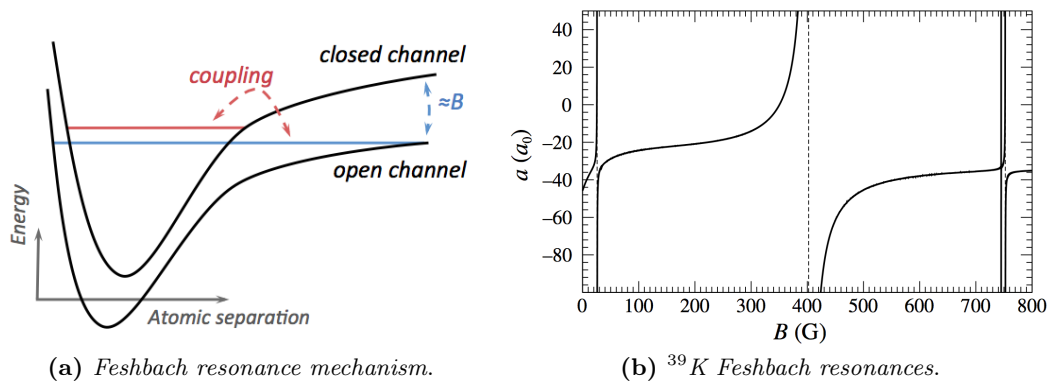


**Figure 2.2:** (a) Basic two-channel model for a Feshbach resonance. The phenomenon occurs when the scattering collision energy (blue line) is resonantly coupled with a molecular bound state (red line) by the application of an homogeneous magnetic field  $B$ . (b) Magnetic field dependence of the scattering length  $a$  for  $|1, 1\rangle + |1, 1\rangle$   $^{39}\text{K}$  collisions. Dashed lines indicate the resonance positions. A broad Feshbach resonance is centered at  $B_0=400$  G;  $a$  vanishes at the zero-crossing magnetic field  $B_{zc}\approx 350$  G. The picture is taken from D’Errico et al.<sup>30</sup>.

achieve a pure  $^{39}\text{K}$  condensate. The final trap average frequency is around 50 Hz. The typical number of atoms in the condensate is around  $3\times 10^4$  at a temperature of few tens of nK.

## 2.2 Tuning the interactions in dilute Bose gases

An important tool available in cold atoms experiments is the possibility to easily tune the interactions between atoms. Here we briefly discuss the method used to tune the atom-atom interaction in  $^{39}\text{K}$  condensates.

In a bosonic gas at low temperature and in a dilute regime, only binary collisions are relevant; consequently, the two-body interaction potential can be written in terms of a contact pseudo-potential:

$$v(r - r') = g\delta(r - r') \quad \text{with} \quad g = \frac{4\pi\hbar^2}{m}a. \quad (2.1)$$

The contact interaction between atoms is thus described by a single parameter, the s-wave scattering length  $a$ , which depends on the details of the interatomic potential. The sign of  $a$  determines the type of interaction: positive values of the scattering length correspond to repulsive interaction between atoms, negative values to attractive ones. The possibility to tune the interaction in these systems, or rather to tune the value of  $a$ , is offered by the presence of magnetic Feshbach resonances.

The Feshbach resonances phenomenon has been initially studied in nuclear physics<sup>36,33</sup> and has become successively important in atom physics<sup>49</sup>, since it offers the great opportunity to control the interatomic interaction in a resonant way. A Feshbach resonance occurs in the process of scattering between two atoms when the collision energy is tuned to resonance with a molecular bound state by the application of an homogeneous magnetic field (Fig. 2.2a). In this case the possibility to have a

transition of the atoms pair to the molecular state produces an enhancement of the collisional cross section. Near a Feshbach resonance, in fact, the scattering length varies dispersively as a function of the magnetic field  $B$ :

$$a(B) = a_{bg} \left( 1 - \frac{W}{B - B_0} \right), \quad (2.2)$$

where  $B_0$  is the resonance center,  $W$  is the resonance width and  $a_{bg}$  is the background scattering length. Applying an homogeneous magnetic field, it is then possible to control the interatomic interaction from strongly attractive to strongly repulsive, passing from zero.

$^{39}\text{K}$  is characterized by several magnetic Feshbach resonances<sup>30</sup>. Its natural scattering length is negative,  $a_{bg} \approx -29$  G, corresponding to an attractive interaction, which would induce the BEC to collapse. Feshbach resonances allow not only to achieve and stabilize the BEC, but also to tune the interactions between the condensed atoms at will. In particular, we use the broad Feshbach resonance that  $^{39}\text{K}$  shows in its absolute ground state  $|F = 1, m_F = 1\rangle$ , centered at  $B_0 \approx 402$  G, with width  $W \approx 52$  G, as shown in Fig. 2.2b.

### 2.3 Optical dipole potentials

A second powerful tool is given by the possibility to address cold atoms with optical potentials. Laser light can be exploited to trap neutral atoms in attractive or repulsive conservative potentials, whose shape and depth can be easily engineered and dynamically controlled. The mechanism underlying this property is the *dipole force*, i.e. the conservative force arising from the dispersive interaction between the intensity gradient of a light field  $\mathbf{E}$  and the induced atomic dipole moment  $\mathbf{d}$ . It can be shown from a semiclassical approach<sup>46</sup>, that if the laser beam is far-off resonance, i.e. the detuning  $\Delta = \omega - \omega_0$  between the field frequency  $\omega$  and the atomic resonance frequency  $\omega_0$  is much larger than the atomic radiative line-width  $\Gamma$ , the dipolar potential generated by the beam can be expressed as,

$$V_{dip}(\mathbf{r}) = \frac{3\pi c^2}{2\omega_0^2} \frac{\Gamma}{\Delta} I(\mathbf{r}), \quad (2.3)$$

where  $c$  is the speed of light in vacuum and  $I(\mathbf{r}) = 2\epsilon_0 c |E(\mathbf{r})|^2$  is the light intensity. On the other hand, the *scattering rate* due to the far-detuned photon absorbed and subsequently spontaneously remitted by the atoms, is

$$\Gamma_{sc}(\mathbf{r}) = \frac{3\pi c^2}{2\omega_0^2} \left( \frac{\Gamma}{\Delta} \right)^2 I(\mathbf{r}). \quad (2.4)$$

If, as it happens in the experimental situation,  $\Delta$  is much larger than the line-width  $\Gamma$ ,  $\Gamma_{sc}$  can be neglected and the optical potential is conservative.

Optical traps are commonly realized in cold atoms experiments by focusing a gaussian laser beam on the atomic cloud. In particular, in our experiment we use a solid state Nd:YAG laser pumped by a diode laser, with wavelength  $\lambda=1064$  nm and spectral linewidth  $\Delta\nu \leq 1$  kHz. The typical trap depth is in the millikelvin range, orders of magnitude smaller than the thermal energy of atoms at room temperature. Anyway, Bose-Einstein condensates can be easily trapped in these weak potentials.

**Optical lattices.** The dipole potential can be used to create periodic potentials for the atoms, for example generating a standing wave as the interference of two counter-propagating beams. This configuration is called *optical lattice*. The optical potential felt by the atoms can be derived considering two sinusoidal counter-propagating fields  $\mathbf{E}_1$  and  $\mathbf{E}_2$  with the same wave number  $k$ , amplitude  $E_0$  and polarization. The time-averaged interference pattern is given by  $I(x) \propto |\mathbf{E}_1 + \mathbf{E}_2|^2 = I_0 \cos^2(kx)$ , with  $I_0 = 2\epsilon_0 c E_0^2$ . Replacing this expression in (2.3) we obtain the potential exerted by the standing wave on the atoms,

$$V_l(x) = \frac{3\pi c^2}{2\omega_0^2} \frac{\Gamma}{\Delta} I_0 \cos^2(kx) = V_0 \cos^2(kx). \quad (2.5)$$

This corresponds to a perfect sinusoid whose spatial periodicity  $\pi/k = \lambda/2$  depends on the wavelength of the laser light  $\lambda$ . Commonly the lattice depth is expressed in terms of energy recoil  $E_r = \hbar^2 k^2 / 2m$ :

$$s = V_0 / E_r. \quad (2.6)$$

In deep lattices, it is possible to approximate the potential well of each lattice site with a harmonic well,  $V_{lat}(x) = V_0 \cos^2(kx) \simeq s E_r k^2 x^2$ . The oscillation frequency  $\omega_{lat}$  of the lattice site can be obtained solving the equation,  $s E_r k^2 x^2 = m \omega_{lat}^2 x^2 / 2$ , resulting

$$\omega_{lat} = \frac{2E_r}{\hbar} \sqrt{s}. \quad (2.7)$$

Various techniques<sup>62</sup> allow to directly calibrate the lattice depth  $s$  in cold atoms experiments, measuring the magnitude of a well-understood effect of the optical standing wave on the atoms. In particular, we exploit two methods based on the Raman-Nath diffraction and the Bragg oscillations of atoms in the lattice, respectively.

## 2.4 Low-dimensional systems

For a system in thermal equilibrium, the condition for the motion in a particular direction to be frozen out is that the energy difference between the ground state and the lowest excited state for the motion must be much greater than the thermal energy  $k_B T$ . In harmonic traps, this energy difference in the  $i$ -th direction is  $\hbar \omega_i$ ; the condition for motion to be frozen out is thus  $\hbar \omega_i \gg k_B T$ . Optical lattices can be used to freeze out the motion in one or two directions, tuning the dimensionality of the system. This occurs when the tunneling from site to site is small enough to prevent hopping from one site to the others on the experimental time scales. At strong lattice depths, the trapping frequency in the single site is large enough to confine the system into the ground-state, see Fig. 2.3. When a three-dimensional BEC is loaded into a strong one-dimensional optical lattice, an array of two-dimensional systems is created. In the experiments described in this thesis, we realize a matrix of one-dimensional (1D) systems (tubes), loading the three-dimensional condensate into a pair of orthogonal optical lattices aligned along horizontal directions, as shown in Fig. 2.4.

At typical lattice depths of 30 recoil energies, the radial trapping frequency of each tube  $\omega_{\perp}$  can be estimated using Eq. 2.9 and is of the order of  $2\pi \times 50$  kHz.

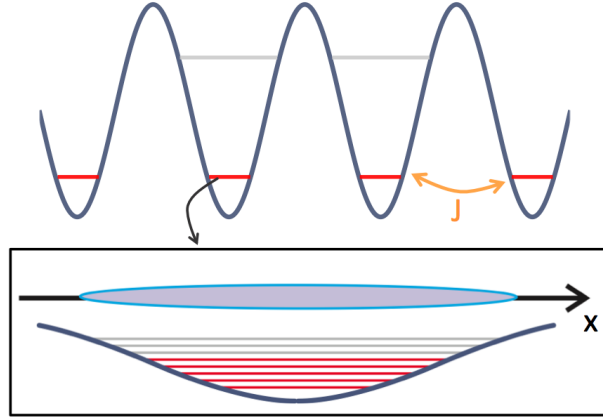


**Figure 2.3:** Schematics of a system confined to one dimension. An optical lattice can be used to freeze some directions: if the coupling  $J$  is small enough every 1D system is independent from the others. Due to the strong confinement, the transverse degrees of freedom are frozen and only transverse ground-state level is occupied, in contrast to what happens in the axial direction. Occupied levels are represented in red; empty levels in gray.

The radial energy is larger than any other energy scale, including the axial trapping frequency (typically  $\omega_x \approx 2\pi \times 150$  Hz) always present in cold atoms experiments,  $\hbar\omega_\perp \gg E_{int}, k_B T \geq \hbar\omega_x$ ; therefore atoms occupy only the radial ground-state. The transverse direction is thus frozen out, and the system is effectively one-dimensional. Moreover, the tunneling rate from tube to tube is about 2 Hz, negligible on the experimental timescale (few-hundred milliseconds). As a consequence, each tube can be considered as an independent system.

The atom number per tube can be determined by integrating the Thomas-Fermi profile of the interacting sample along the tubes. In the tube  $(i, j)$  the number of atoms is

$$N_{i,j} = N_{0,0} \left[ 1 - \frac{2\pi N_{0,0}}{5N_{tot}} (i^2 + j^2) \right]^{3/2} \quad (2.8)$$

where  $N_{tot}$  is the total atom number,  $N_{0,0} = 5N_{tot}d^2/2\pi R_z R_y$  is the atom number in the central tube,  $R_{z,y}$  are the Thomas-Fermi radii in the horizontal directions, which depend on the atomic scattering length  $a$  set by the Feshbach field, and  $d = \lambda/2$  is the spacing of the tubes. For typical  $N_{tot} = 3 \times 10^4$  and  $a = 210a_0$ , we estimate an upper limit of  $N_{0,0} = 96$ , and an average  $N_{i,j} \approx 60$ .

**One-dimensional bosons.** When a strong transverse confinement is applied to an ultracold bosonic sample, the interaction potential between the atoms is modified, as pointed out by Olshanii<sup>65</sup>. Anyway, in cold atoms experiments the typical dimension of the confined directions  $a_\perp = \sqrt{\hbar/m\omega_\perp} \approx 70$  nm (for  $\omega_\perp = 2\pi \times 50$  kHz) is much larger than the three-dimensional scattering length  $a = 100a_0 \approx 5$  nm. Here  $a_\perp$  is the harmonic oscillator length in the transverse direction. To a first approximation the collisional properties of the 1D system are therefore three-dimensional. The asymptotic scattering states have the form  $\psi_0(y, z) \exp(\pm ikx)$ , where  $\psi_0(y, z)$  is the Gaussian ground-state wave-function for the transverse motion and  $k$  is the wave-vector for the motion along the axial direction<sup>11</sup>. In this weak-confinement

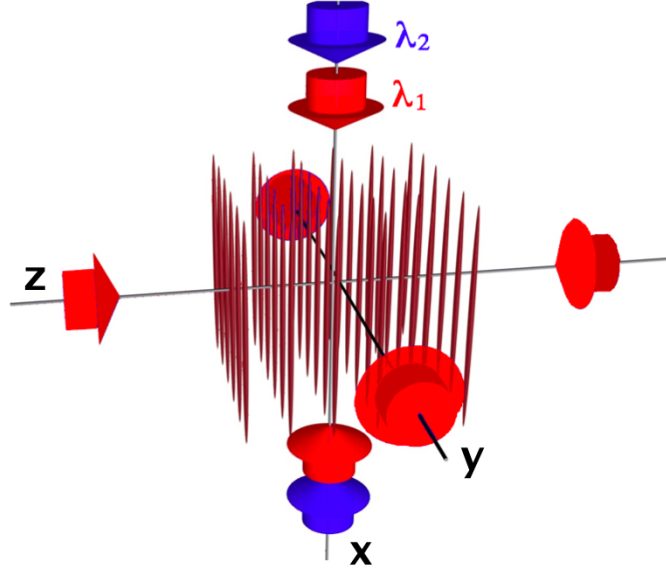


**Figure 2.4:** Schematic representation of the experimental configuration. Two tight lattices, aligned along  $\hat{z}$  and  $\hat{y}$ , form a two dimensional array of one dimensional tubes. The quasiperiodic lattice propagates along  $\hat{x}$ , the axial direction of the tubes.

limit,  $|a| \ll a_{\perp}$ , the effective 1D interaction is obtained by integrating the 3D pseudo-potential (2.1),  $g \int d^3x |\psi_0(y, z)|^2 \delta(x-x')$ , over the ground-state density of the transverse motion. The resulting effective 1D interaction is then  $v(x-x') = \tilde{g} \delta(x-x')$ , with  $\tilde{g} = 2\hbar^2 a / m a_{\perp}^2$ . Near a Feshbach resonance the weak-confinement assumption breaks down; in this case the presence of confinement-induced bound states modifies the expression of  $\tilde{g}$  in:

$$\tilde{g} = \hbar^2 / m a_{1D} \quad \text{with} \quad a_{1D} = \frac{a_{\perp}^2}{2a} \left( 1 - C \frac{a}{a_{\perp}} \right), \quad (2.9)$$

where  $C=1.0326$  and  $a_{1D}$  is the effective 1D scattering length. This formula is valid at any value of  $a/a_{\perp}$ .

An important parameter describing 1D bosons in the continuum<sup>58</sup>, is the ratio between the mean-field interaction energy ( $E_{int} \approx \tilde{g} n_{1D}$ , with  $n_{1D}$  the 1D mean density) and the kinetic energy required to bring particles at distance  $n_{1D}^{-1}$  ( $E_k \approx \hbar^2 n_{1D}^2 / m$ ),

$$\gamma = \frac{m \tilde{g}}{\hbar^2 n_{1D}}. \quad (2.10)$$

$\gamma$  scales inversely with  $n_{1D}$ , leading to the peculiarity that in one-dimensional systems the interactions grow with respect to the kinetic energy as the density decreases, in direct contrast to the three-dimensional situation. As introduced in Sec. 1.2, the parameter  $\gamma$  characterizes the peculiar regimes of degeneracy in the trapped 1D bosonic gas at low temperature ( $T < T_d$ , with  $T_d \approx N \hbar \omega_x$  the 1D degeneracy temperature), see Petrov et al.<sup>71</sup> and Petrov et al.<sup>72</sup>. When  $\gamma \rightarrow \infty$  the sample behaves as a gas of hard-core bosons (Tonks-Girardeau gas<sup>43</sup>); in this limit the 1D boson problem can be mapped onto a system of non-interacting fermions. The infinitely strong contact repulsion between atoms imposes the constraint that the

many-body wave-function must vanish each time two particles meet at the same point. In general, for  $\gamma \gg 1$ , i.e. for sufficiently large inter-particle interactions or for small enough mean density, a trapped Tonks gas occurs, with a typical Fermi-gas density profile. On the other hand,  $\gamma = 0$  corresponds to the free bosons limit. In general, for  $\gamma \ll 1$  the gas is weakly interacting. At relatively high temperature (still below  $T_d$ ), the system is a quasicondensate, i.e. a Bose-condensed state where density fluctuations are suppressed but the phase still fluctuates. At very low temperature, also the long-wave fluctuations of the phase are suppressed due to a finite size of the system, and there exist a true condensate.

Exploiting the ability to widely tune the three-dimensional scattering length with a Feshbach resonance in  $^{39}\text{K}$  atoms, in the experiment we can reach high values of  $\gamma$ , up to 5. Indeed, we can tune both the scattering length  $a$ , therefore the coupling  $\tilde{g}$  (2.9), and the number of particle per unit length  $n_{1D}$ , since the Thomas-Fermi radius change with the interaction. As a consequence, we can explore several regimes of degeneracy.

## 2.5 Disordered optical potential

The optical dipole force can be used to engineer also disordered potentials for the atoms. In natural systems, disorder is intrinsically present and cannot be removed or controlled; ultracold atoms setups give the remarkable possibility to artificially add a controllable disorder to ‘clean’ systems. Many techniques have been exploited to create disordered potentials; a standard way is to employ the speckle pattern<sup>44</sup> produced by a laser beam shined onto a rough surface. The typical length-scale  $\ell$  of the speckle grains strongly depends on the numerical aperture (NA) of the optical system,  $\ell \simeq \lambda/\text{NA}$ , with  $\lambda$  the laser wavelength (1064 nm, in our case). In our setup this limits the minimum speckle size achievable to about 10  $\mu\text{m}$ , reducing the disorder efficacy. Another possibility is to use a quasiperiodic lattice, which introduces an energy disorder on each minimum of a main lattice; in this case the typical size of the disorder is given by the periodicity of the main lattice. This is the kind of disorder we use in the experiments described in this thesis.

A quasiperiodic potential is realized by a *bichromatic lattice*, i.e. by two overlapping lattices with incommensurate wavelength, as shown in Fig. 2.5. It is obtained by superposing to the primary optical lattice a weaker secondary one with incommensurate wavelength  $\lambda_1/\lambda_2 \in \mathbb{R}/\mathbb{Q}$

$$V_b(x) = s_1 E_{r_1} \sin^2(k_1 x) + s_2 E_{r_2} \sin^2(k_2 x), \quad (2.11)$$

with  $k_i = 2\pi/\lambda_i$  the lattice wavenumber and  $s_i$  the lattice heights in unit of recoil energy  $E_{r_i}$ . Generally, if the depth of the two lattices is comparable, the perturbation induced by the secondary lattice on the primary one results in a non-periodic modulation of the potential energy minima, and in an inhomogeneous shift on its minima positions. When instead, the secondary lattice is a small perturbation to the first one, i.e.  $V_2 \ll V_1$ , the lattice spacing of the bichromatic potential is to good approximation given by that of the primary lattice,  $d = \lambda_1/2$ . The essential features of such a potential are visible in Fig. 2.5. The potential energy minima of the primary lattice are modulated by the second one, giving rise to characteristic

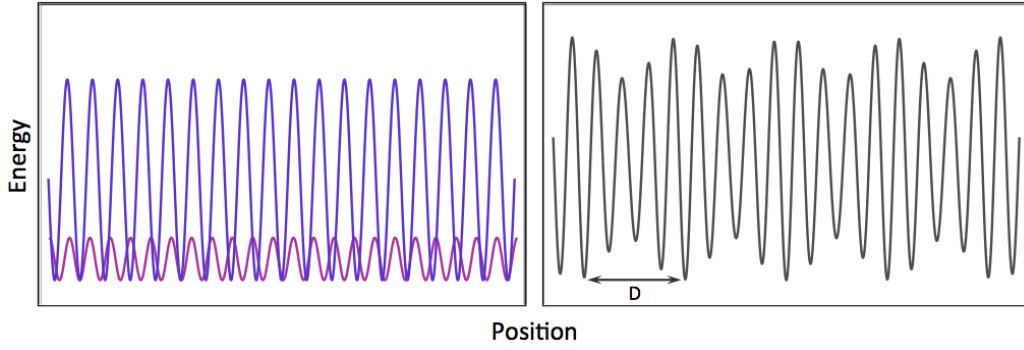


**Figure 2.5:** Quasiperiodic potential. The quasiperiodic potential is experimentally realized for lattice incommensurability  $\beta=1.238\dots$  by superimposing two lattices with wavelengths  $\lambda_1=1064$  nm and  $\lambda_2=859$  nm, respectively. The quasiperiodic lattice is characterized by potential wells approximately every  $D=d/(\beta-1)=4.2$  lattice sites, which arise from the beating of the two lattices.

wells separated on average by the quasi-period  $D = d/(\beta - 1)$ , where  $\beta = k_1/k_2$  measures the incommensurability.

In the experiment a Nd:YAG laser with wavelength  $\lambda_1=1064$  nm creates the main lattice and a Ti:Sapphire laser with wavelength  $\lambda_2=859$  nm generates the secondary one. The quasi-period is thus approximately  $D=4.2$  lattice sites. We note that the disorder introduced by the bichromatic lattice is not a random disorder because of its quasiperiodic structure. In fact, the correlation function of the bichromatic potential shows a well defined sinusoidal shape, resulting in a deterministic and spatially correlated distribution of the energy across the lattice sites. Anyway, the translational symmetry of a perfect lattice is broken in a non-trivial way and it is thus suitable for the study of disorder physics.

The single particle properties of the bichromatic potential (2.11) have been discussed in literature<sup>61</sup> and can be obtained by diagonalizing the Hamiltonian  $H = -(\hbar\nabla_x)^2/2m + V_b(x)$ . In the tight-binding limit, the system can be mapped onto the Aubry-André model, which predicts an Anderson-like transition from extended to localized state for a finite value of the secondary lattice  $s_2$ . The details of this model will be discussed in Sec. 3.2, in the framework of the Bose-Hubbard model.



# Chapter 3

## Theoretical framework

In this chapter we introduce few analytical methods which describe disordered interacting bosons, providing the theoretical framework for the experiments performed in this thesis. In Sec. 3.1, we introduce a microscopic approach for bosons in a lattice, resulting in the Bose-Hubbard Hamiltonian, which relates the system local properties to the experimental parameters. The two limiting cases of interacting bosons in a periodic lattice and non-interacting particles in a disordered (quasiperiodic) potential (Sec. 3.2) are discussed within this Bose-Hubbard framework, showing the well known metal-insulator transitions driven respectively by interactions (Mott transition) and disorder (Anderson and Aubry-André transition). The competition between disorder and interactions is instead taken into account in Sec. 3.3, within a specific model, the Haldane's harmonic fluid approach. This peculiar description, well describing 1D systems, allows to re-express the Hamiltonian in a simple quadratic form, providing a convenient starting point to study the effects of various external potentials, such as disorder.

### 3.1 The Bose-Hubbard Hamiltonian

When a Bose-Einstein condensate is loaded into an optical lattice its local properties can be microscopically traced out, and related to the experimental parameters. The Hamiltonian describing the system of bosons interacting through the contact pseudo-potential (2.1) in the optical lattice (2.5), superimposed onto a generic external potential  $V_e$ , reads:

$$\hat{H} = \int dr \hat{\psi}^\dagger \left( -\frac{\hbar^2 \nabla^2}{2m} + V_e(r) + V_l(r) \right) \hat{\psi} + \frac{g}{2} \int dr \hat{\psi}^\dagger \hat{\psi}^\dagger \hat{\psi} \hat{\psi}. \quad (3.1)$$

If the periodic potential is deep enough, i.e.  $V_0$  is the largest energy scale in the problem (*tight-binding approximation*), it is more convenient to project the Bose field operator on the basis of the Wannier orbitals  $w(x)$  belonging to the lowest Bloch band,

$$\hat{\psi}(r) \simeq \sum_i w_i(r) \hat{b}_i. \quad (3.2)$$

Here  $w_i(r)$  is the Wannier function localized at the  $i$ -th lattice site and  $\hat{b}_i$  is the operator annihilating one boson at site  $i$ . In the tight-binding regime (for  $s > 5$ )

one can consider only the superposition of the nearest neighbor Wannier orbitals. The above approximation neglects the  $\hat{\psi}$  projection on higher bands (*single band approximation*); for small lattice depth, it may become necessary to take into account the higher bands Wannier orbitals. By replacing the field operator in the Hamiltonian (3.1) with (3.2), one obtains the Bose-Hubbard Hamiltonian:

$$\hat{H} = -J \sum_i (\hat{b}_i^\dagger \hat{b}_{i+1} + H.c.) + \frac{U}{2} \sum_i \hat{n}_i (\hat{n}_i - 1) + \sum_i (\epsilon_i - \mu) \hat{n}_i, \quad (3.3)$$

where  $\hat{n}_i = \hat{b}_i^\dagger \hat{b}_i$  is the site occupation operator and  $\mu$  is the chemical potential. Let us now discuss the three energy scales characterizing the Hamiltonian.

The first term expresses the kinetic energy of the particles in the tight-binding approximation; the parameter  $J$  represents the energy scale for the kinetic energy, as the energy dispersion law in the lowest lattice band is  $\epsilon(q) = -2J \cos(qd)$ . Essentially, it is the tunneling rate between nearest neighboring sites:

$$J = - \int dr w_i^*(r) \left( -\frac{\hbar^2 \nabla^2}{2m} + V_l(r) \right) w_{i+1}(r). \quad (3.4)$$

$J$  can be expressed as a function of the lattice parameter  $s$ , numerically solving the above overlapping integral:

$$\frac{J}{E_r} = 1.43s^{0.98} e^{-2.07\sqrt{s}}. \quad (3.5)$$

The tunneling energy  $J$  is thus strictly related to the depth of the optical lattice which creates the periodic potential, and can be controlled tuning the laser intensity.

The second term of the Hamiltonian describes the interactions between particles on the same lattice site. The parameter  $U$  is given by the interaction matrix element between the Wannier functions

$$U = g \int dr |w(r)|^4. \quad (3.6)$$

$U$  is the second important energy scale; it quantifies the energy-cost to put two atoms in the same lattice site compensating the collisional interaction. Here  $g$  is the coupling term expressed in Eq. (2.1). In one-dimension  $g$  should be replaced with  $\tilde{g}$ , expressed by Eq. (2.9). In any case, in the experimental setup  $U$  can be tuned and controlled, tuning the scattering length  $a$  on a Feshbach resonance.

The last term in the Hamiltonian takes into account the effect of the external potential  $V_e$ , which, in a local density approximation, produces an energy offset  $\epsilon_i$  at the site  $i$ . In experiments with optical lattices an unavoidable harmonic trapping potential is always present:

$$\epsilon_i = \frac{\alpha}{2} \sum_i (i - i_0)^2. \quad (3.7)$$

Here  $\alpha$  represents the strength of the harmonic potential and  $i_0$  is the center of the harmonic trap; in the specific case of our experiment the typical trapping frequency is 150 Hz.

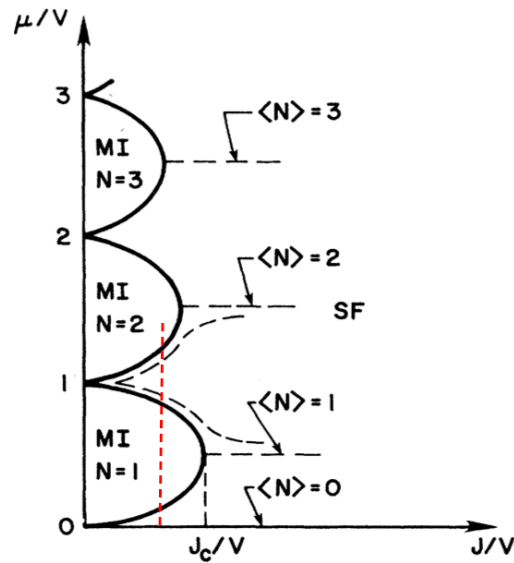


**Figure 3.1:** Zero-temperature phase diagram of the superfluid (SF) to Mott insulator (MI) transition for the homogeneous Bose-Hubbard model. The MI lobes are characterized by integer site filling  $n$ . At larger average occupancy  $\langle N \rangle$ , a larger critical interaction energy is required to enter the MI phase. In the inhomogeneous case, the system alternates different phases averaged over an extended range of local chemical potential (dashed vertical red line). The picture is rearranged from Fisher et al.<sup>37</sup>.

**Superfluid to insulator transition.** As introduced in Sec. 1.3, the Bose-Hubbard model (3.3) presents a quantum phase transition from a superfluid state at weak interactions to an insulating state at strong interactions. This transition has been widely studied in theory<sup>37</sup> with many different methods, and has been probed during the last years by different cold atoms experiments<sup>45,88</sup>. It is the consequence of the competition between the delocalizing effects of the kinetic term  $J$ , which reduces the phase fluctuations, and the localizing effects of the interaction term  $U$ , which reduces the on-site particle fluctuations. The interacting-induced insulating state is known as Mott insulator (MI) and is characterized by an energy gap (the energy required to add or remove a particle), which leads to a vanishing compressibility. The transition occurs only at integer filling whose value depends on the chemical potential  $\mu$ . The phase diagram of this model is qualitatively similar in all spatial dimensions. An example is shown in Fig. 3.1. In the inhomogeneous system, the effect of the trapping potential can be understood in terms of a local density approximation (LDA). In this framework, one approximates local quantities in the inhomogeneous system by the corresponding quantities in a homogeneous system with a local chemical potential  $\mu_i \equiv \mu_0 - \epsilon_i$ , as done in the Hamiltonian (3.3). For a harmonic trap  $\epsilon_i$  is given by Eq. (3.7). The density profiles in the trap can thus be constructed from vertical cuts across the homogeneous phase diagram 3.1, starting from  $\mu_0$  and moving towards the point  $\mu$  where the density vanishes. This leads to a wedding cake structure in which superfluid and Mott insulating domains coexist space separated. Such peculiar distribution as been experimentally observed<sup>84</sup>, as shown in Fig. 3.2.

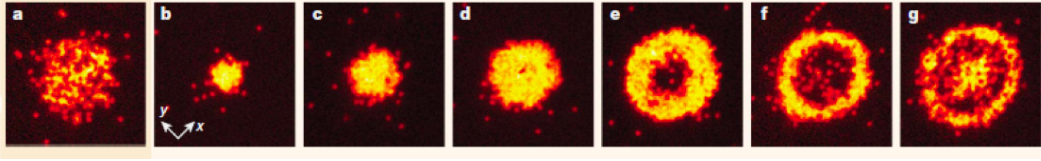


**Figure 3.2:** Fluorescence images of atoms in a two-dimensional lattice in the Mott insulator regime<sup>84</sup>. The typical wedding-cake structure is observed. Moving from the center towards the edges, alternating MI shells with even (full) and odd (empty) site occupation are shown. The images are taken for increasing number of atom.

## 3.2 The Aubry-André model

In Sec. 2.5 we introduced the bichromatic potential  $V_b$  (2.11), as the experimental realization of a disordered external potential. The Hamiltonian obtained inserting this expression in Eq. (3.1) can be solved within the framework of the Bose-Hubbard model, giving rise to a disordered Hubbard Hamiltonian. In particular, it can be demonstrated that the presence of the secondary lattice does not substantially alter the position of the minima or the shape of the Wannier functions, while it shifts the on-site energies. Thus, the quasiperiodic lattice does not modify the expressions for the tunneling energy  $J$  and the on-site interaction  $U$ , resulting only as a perturbation on the on-site energies of the lattice. In general, the distribution of  $\epsilon_i$  depends on the specific realization of the disorder. Other types of disorder, as random interactions  $U_i$  or random hopping  $J_i$  can in principle be realized, but will not be discussed here.

The properties of the non-interacting bosons in the quasiperiodic potential can be obtained by diagonalizing the Hamiltonian  $H = -(\hbar\nabla_x)^2/2m + V_b(x)$ . In the tight-binding limit, the system can be mapped onto the Harper or Aubry-André model<sup>61</sup>

$$\hat{H} = -J \sum_i (\hat{b}_i^\dagger \hat{b}_{i+1} + H.c.) + \Delta \sum_i \cos(2\pi\beta i + \phi) \hat{n}_i, \quad (3.8)$$

where  $J$  is the Bose-Hubbard tunneling rate (3.5), while  $\Delta$  measures the disorder strength and can be obtained from numerical calculations,

$$\frac{\Delta}{E_r} = \frac{s_2}{2} \beta^2 \exp\left(-\frac{2.18}{s_1^{0.6}}\right). \quad (3.9)$$

Therefore  $\Delta$  directly depends on both the lattice depths  $s_2$  and  $s_1$ , and can be easily controlled tuning the lasers intensity.

**Disorder induced localization.** The Aubry-André model<sup>9</sup> predicts a transition from extended to localized states for a finite value of the disorder,  $\Delta = 2J$ . This can be explained as follows. In a perfect periodic potential all the eigenstate are extended Bloch waves, therefore the system is conducting. The single-particle energy dispersion shows a band structure, in particular  $E(q) = E_0 - 2J \cos(qd)$  in the first band, where  $E_0$  is the ground-state energy in the single hole,  $q$  is the quasi momentum of the particles and  $d$  is the lattice spacing. In a pure random potential (random distribution of  $\epsilon_i$ ,  $\delta$ -function correlation) any trace of translational symmetry is lost and all the eigenstates are exponentially localized for any disorder, leading

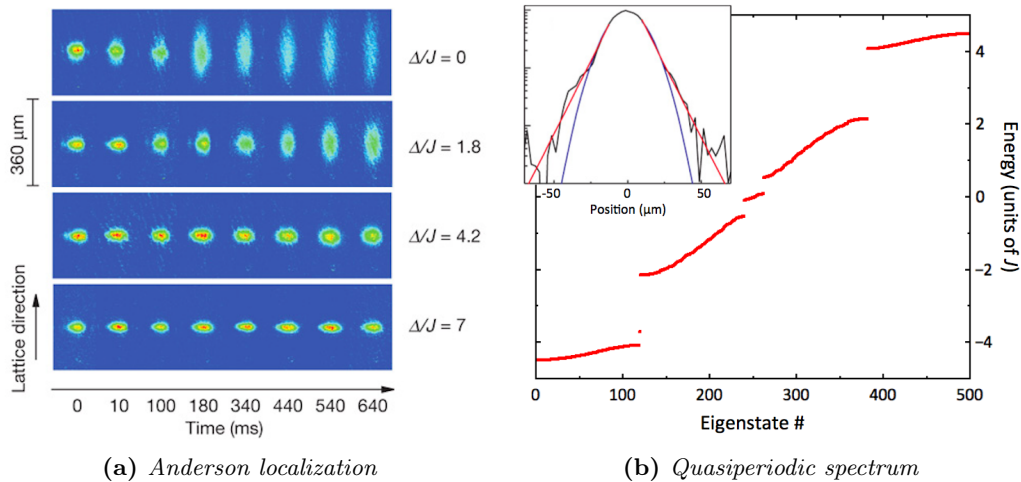


**Figure 3.3:** (a) Experimental observation of Anderson localization in a quasiperiodic lattice<sup>79</sup>. From top to bottom is shown the time evolution of the atomic cloud for increasing value of the disorder strength  $\Delta$ . For large enough disorder the cloud does not expand in the lattice revealing localized. (b) Single-particle spectrum of the quasiperiodic potential at  $\Delta = 4J$ . The minibands structure clearly appear in the spectrum. In the inset is shown the Anderson-like localized experimental profile at  $\Delta = 15J$  fitted with an exponential decaying function (in red).

to the Anderson localization, as introduced in Sec. 1.1. Instead, the quasiperiodic lattice shows non-vanishing spatial correlations. In a quasiperiodic lattice the on-site energies are shifted of about  $\Delta$ ; if  $\Delta < 2J$  the on-site energies still belong to the conducting band. For  $\Delta > 2J$  some on-site energies are out of the band, inducing localization in the whole sample. As a consequence a metal-insulator transition occurs at  $\Delta = 2J$ . From another point of view, the metal-insulator transition at  $\Delta = 2J$  can be understood by considering the duality of the Aubry-André model, which predicts localization both in the real and the momentum space<sup>29</sup>. In this context, the point where the system localizes in the real space, has to be the same point where it delocalizes in the momentum space. It is possible to see that the only self-dual point is  $\Delta = 2J$ . The disorder-induced Aubry-André transition has been experimentally proved<sup>79</sup> with cold atoms experiments, as shown for example in Fig. 3.3a.

In the quasiperiodic lattice the Anderson-like localized eigenstates display a localization length which varies with disorder as  $\xi \approx d / \ln(\Delta/2J)$ , where  $d = \lambda_1/2$  is the lattice site spacing. No mobility edges exist in the lowest band of the quasiperiodic lattice, i.e. all the states are either localized or extended, depending on the disorder strength. The spectrum of such a potential can be easily calculated, by diagonalizing the Hamiltonian. A striking feature of the spectrum is the appearance of minigaps splitting the first lattice band above the critical disorder; the bandwidth (which is  $4J$  in the regular lattice) spreads to approximately  $4J + 2\Delta$ , as shown in Fig. 3.3b. The lowest-energy eigenstates, i.e. the ones populating the lowest ‘miniband’, result separated by approximately  $D$ , since the quasiperiodic correlation function has a sinusoidal shape, with maxima of its autocorrelation separated by a quasi-period  $D$ .

### 3.3 Disorder and interactions in 1D

In Chapter 1 we introduced the dirty-bosons problem, giving the physical pictures of its phases. Besides the standard (Mott) interacting-induced and (Anderson) disordered-induced localized phases, a new compressible insulator is expected to appear, the Bose glass. Here we focus on the one-dimensional problem at strong interactions, describing a particular model (the original Bose glass model developed in Giamarchi and Schulz<sup>42</sup>) which treats the effect of disorder on interacting bosons.

In fact, while the effect of disorder on non-interacting systems is well understood, taking into account the combined effects of disorder and interactions is a tough problem. For fermions, the non-interacting system is a good starting point; the effects of interactions can be introduced in a perturbative way. Such approach is impossible with bosons, since the non-interacting bosonic case is pathological. In this case, the ground state is a highly inhomogeneous Bose-Einstein condensate, with all the particles in the lowest (localized) eigenstate of the Hamiltonian. In the absence of repulsion, a macroscopic number of particles is then in a finite region of space. Such a state is unstable to the introduction of even the weakest interaction. The interactions should thus be included into the problem from the beginning<sup>15</sup>.

In one-dimension, one way to tackle the problem is to start from the Luttinger liquid (LL) description of a uniform interacting Bose gas, then add disorder as a small perturbation. In fact, the LL theory incorporates all the interactions in a relatively simple quadratic Hamiltonian, providing a convenient starting point to study the problem. In the following, after introducing the notion of Luttinger liquids, we briefly discuss the effect of disorder within the LL framework. This description provides the evidence the Bose glass phase. A detailed description of the LL theory can be found in Cazalilla et al.<sup>15</sup>, and in the references therein contained.

#### 3.3.1 The Tomonaga-Luttinger liquid

Interacting one-dimensional fluids, no matter if the particles are fermions or bosons, belong to a universality class of systems which Haldane<sup>47</sup> named ‘Luttinger liquids’. The general property characterizing a Luttinger liquid is that its low energy excitations are collective modes with linear dispersion. The collective nature of the low energy excitations in 1D fluids can be understood as follows: in 1D, interacting particles must push their neighbors away in order to propagate; any individual motion is thus converted into a collective one. One-dimensional fluids are therefore described in terms of collective fields; this choice is behind the most successful theory treating 1D systems, the so-called bosonization technique<sup>41,15</sup>.

In the case of bosons the collective fields describing the 1D fluid, are the density  $\hat{\rho}(x)$  and the phase  $\hat{\theta}(x)$  of boson field operator,  $\hat{\psi}^\dagger(x) = \sqrt{\hat{\rho}(x)}e^{-i\hat{\theta}(x)}$ . In general, the density operator can be written as follow

$$\hat{\rho}(x) = \left( n_{1D} - \frac{1}{\pi} \partial_x \hat{\phi}(x) \right) \sum_{m \in \mathbb{Z}} \alpha_m e^{2im(\pi n_{1D} x - \hat{\phi}(x))} \quad (3.10)$$

Here  $\hat{\phi}(x)$  is a slowly varying quantum field,  $n_{1D} = \langle \hat{\rho}(x) \rangle = N/L$  is the ground state density (constant in translationally invariant systems) and  $\alpha_m$  is a non-universal coefficient depending on the microscopic details of the model. The first term in

the right hand side of this expression describes the small density deviations from  $n_{1D}$  at small excitation energies. The second oscillating term reflects instead the discreteness of the particles constituting the system, which locally (but not globally) tend to develop a crystal-like ordering with lattice spacing  $\sim n_{1D}^{-1}$ .

A representation of the Hamiltonian for the 1D interacting bosons, can be obtained introducing 3.10 in 3.1 (imposing  $V_l = V_e = 0$ ):

$$\hat{H}_{LL} = \frac{\hbar}{2\pi} \int dx \left[ vK \left( \partial_x \hat{\theta}(x) \right)^2 + \frac{v}{K} \left( \partial_x \hat{\phi}(x) \right)^2 \right]. \quad (3.11)$$

As already said, the Hamiltonian has a simple quadratic form. All the interaction effects are encoded in the two model-dependent parameters  $v$  and  $K$ . In particular, it can be shown that  $K$  controls the behavior of the correlation at long distances, while  $v$  is the velocity of propagation of density disturbances. In systems with purely local interactions,  $1 < K < \infty$ , where  $K \rightarrow \infty$  is the non-interacting limit, while  $K = 1$  represents the Tonks-Girardeau gas. In the absence of external potentials the system is always superfluid; in the case of bosons  $K$  and  $v$  are related to the Lieb-Liniger parameter  $\gamma$  (2.11) through known analytical expressions. Also the Bose-Hubbard model describes a Luttinger liquid for non integer filling or for sufficiently weak interactions at integer filling. Anyway, no analytical expressions relates the Luttinger parameters  $K$  and  $v$  to the BH energy scales.

### 3.3.2 Perturbation on 1D superfluids

**Periodic lattice.** Luttinger liquids are extremely fragile to external perturbations. If the perturbation is a weak periodic potential  $V_e(x) = V_0 \cos(Gx)$ , the system realizes the so-called sine-Gordon model<sup>20</sup>. The sine-Gordon Hamiltonian can be obtained using the expression (3.10) for the density, and reads:

$$\hat{H}_{sG} = \hat{H}_{LL} + \frac{g_u}{\pi} \int dx \cos \left( 2p\hat{\phi}(x) + \delta x \right). \quad (3.12)$$

For a weak potential  $g_u$  is the bare coupling and depends on the lattice depth  $V_0$ . The doping  $\delta \equiv nG - 2p\pi n_{1D}$  ( $n, p$  are integer numbers) measures the degree of incommensurability of the potential:  $\delta = 0$  corresponds to a commensurate number of bosons per site. For  $p = 1$  there is an integer number of bosons per site ( $n_{1D} = nG/2\pi$ ), while higher values of  $p$ , such as  $p = 2$ , correspond to integer numbers of bosons every two sites, etc. At integer filling, this Hamiltonian shows the same phase transition found in the Bose-Hubbard limit from a superfluid to a Mott insulating phase (see Sec. 3.1), allowing to study also the vanishing lattice case ( $V_0 = 0$ ). The Hamiltonian can be quantitatively studied through a renormalization group (RG) approach. The phase transition is found at a universal value of the Luttinger parameter  $K_c = 2/p^2$ , which reduces to  $K_c = 2$  for systems with purely local interactions. The system is a superfluid for  $K > K_c$ , where any shallow lattice is an irrelevant perturbation, while a Mott-gap opens for  $K < K_c$ , signaling the presence of an incompressible localized Mott phase.

**Disorder.** When the external perturbation is an on-site random disorder  $V(x)$ , such that  $\overline{V(x)V^*(x')} = \Delta\delta(x - x')$ , where  $\Delta$  is the disorder strength, the perturbed

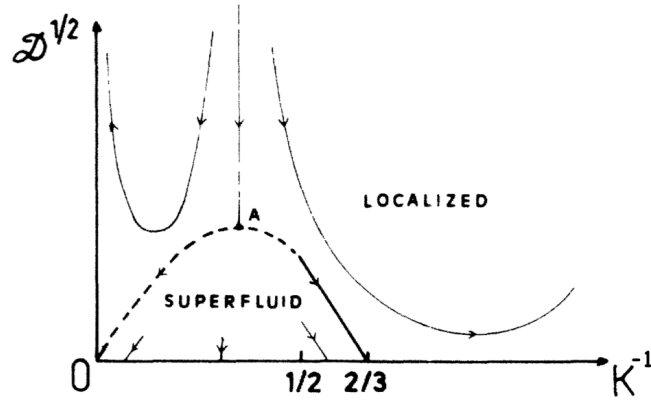


**Figure 3.4:** Phase diagrams for a disordered one-dimensional Bose gas. The dashed lines are for parts of the diagram that cannot be obtained by the bosonization technique. In the region where bosonization works (i.e. for disorder smaller than the chemical potential) the superfluid-Bose glass transition, denoted by the solid line, is described by universal exponents, and takes place at  $K^{-1}=2/3$ . The picture is taken from Giamarchi and Schulz<sup>42</sup>.

Luttinger Hamiltonian reads:

$$\hat{H}_d = \hat{H}_{LL} + \int dx V(x) \left[ -\frac{1}{\pi} \partial_x \hat{\phi}(x) + n_{1D} \left( e^{2im(\pi n_{1D} x - \hat{\phi}(x))} + H.c. \right) \right]. \quad (3.13)$$

The term  $\partial_x \hat{\phi}$  corresponds to a slowly varying chemical potential, thus describes the ‘forward’ scattering by the random potential which does not affect the system conductivity. The main disorder effects come from the ‘backscattering’ term, i.e. the term for which the momentum exchanged with the impurities is of the order of  $2\pi n_{1D}$ . This term can be treated by a RG procedure. Using this RG approach Giamarchi and Schulz<sup>42</sup> predicted a new phase transition at the universal value of the Luttinger parameter  $K^* = 3/2$ . The system is superfluid at weak interactions  $K > K^*$ , while it localizes for  $K < K^*$ , in analogy with the Tonks limit  $K = 1$  (contained in the phase  $K < 3/2$ ), for which the bosons behave as free fermions, thus (Anderson) localize in the presence of disorder. Contrarily to what happens for the periodic case the system remains *compressible* in the localized phase, as one can see again from the fermionic limit, thus no excitation gap opens. This localized gapless phase is the Bose glass (BG). Disordered bosons in 1D, whose qualitative phase diagram is shown in Fig. 3.4, provided the first derivation of the BG phase.

Until now, we have considered the case of bosons in the continuum. If the disorder perturbs a lattice, at strong enough interactions there will be a competition between Mott (commensurate) and Anderson (incommensurate) localization. This competition can be described adding to the Hamiltonian (3.13) a term as in Eq. (3.12) with  $\delta = 0$ . In this case, two effects must be considered. First, the ‘forward’ scattering term, which acts as a slowly varying chemical potential, is now in competition with the commensurate term  $\cos(2\phi)$ , thus reducing the Mott gap, and eventually, for strong enough disorders, destroying the commensurability. Therefore, the presence of disorder will reduce the stability of the Mott region, leading to a *delocalization* by the reduction of the Mott effects. On the other hand, the effect of the ‘backward’ term is to induce Anderson localization on the superfluid flow and leads to the Bose

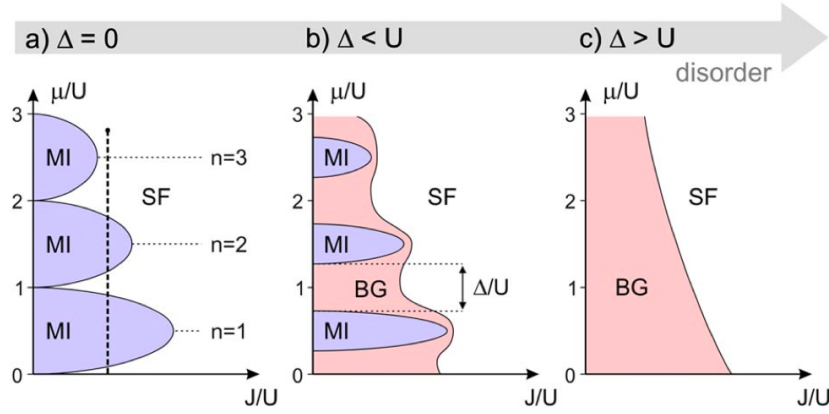


**Figure 3.5:** Phase diagram for disordered interacting bosons in a lattice. Depending on the ratio between tunneling energy  $J$ , interaction energy  $U$ , and disorder  $\Delta$ , the system forms a superfluid (SF), a Mott insulator (MI), or a Bose glass (BG). The picture is taken from Fallani et al. <sup>32</sup>.

glass phase, as discussed previously. As a result, when the disorder is increased one can naively expect a transition between a Mott insulator, which is *incompressible* and localized to a Bose glass, which is *compressible* and also localized. The qualitative diagram describing this transition is shown in Fig. 3.5. As shown in Chapter 1, in the presence of a lattice the SF-BG transition occurs in any dimension <sup>37</sup>.

**Quasiperiodic lattice.** A quasiperiodic lattice is somehow an intermediate case between a single lattice and a random potential. In fact, a random disorder can be described as a potential containing all the Fourier harmonics. In the case of the bichromatic potential only two incommensurate frequencies are present. A phase diagram of the bichromatic BH model has been numerically studied by Roux et al. <sup>81</sup>, and will be discussed in Sec. 4.4 in comparison with experimental measurements. Anyway, the phases of this system can be argued using similar arguments as before. For fillings commensurate with either the primary or the secondary lattice, the simple quadratic Luttinger Hamiltonian changes into a sine-Gordon Hamiltonian. A Mott insulator is obtained for filling commensurate with the primary lattice, and a pinned incommensurate density wave (ICDW) for filling commensurate with the secondary lattice. For fillings incommensurate with both lattices the transition towards the Bose glass phase is instead expected at a critical disorder  $\Delta \geq 2J$ , in agreement with the limiting case of free and hard-core bosons described by the Aubry-André model. For vanishing quasiperiodic potential the system should remain SF, and no Bose glass phase should exist; anyway, the fate of the localized phase in this particular regime is still under debate.

### 3.4 Open questions

In summary, the phase diagram of one-dimensional interacting bosons in disordered media appears very rich. The bosonization technique indicates the presence of a new glassy phase at strong interactions, and predicts the critical properties

of the phase transition. In the strongly correlated regime this Bose glass phase is rather analogous to the Fermi glass phase of interacting fermions in strongly disordered potentials, with the repulsive interactions playing the role of Pauli exclusion. Anyway, a direct link with the local properties of the microscopic (BH) model describing experimental systems is not straightforward. Furthermore, this perturbative approach is justified *a priori* only in the *weak disorder* limit, i.e. if the chemical potential set by the interactions is much larger than the disorder strength. The fate of such a transition in the opposite limit, i.e. at weak interactions, is still debated, even though, recently, promising beyond mean-field approaches<sup>4,91</sup> have been developed. As introduced in Sec. 1.1 at weak interactions the system seems to exhibit a different glassy phase, composed by many coherent puddles weakly coupled through the disorder potential. How the two glassy phases connects is still unknown.

# Chapter 4

## Coherence

The first experimental observable we address to study the dirty-bosons problem is the condensate correlation length, which gives indications on its coherence properties. Generally, coherence is one of the peculiar features of a Bose-Einstein condensate. In fact, for non-interacting particles, the criterion for Bose-Einstein condensation is that the occupation number for one of the single-particle energy levels should be macroscopic. When this happens all the condensed particles can be described by a single order parameter and spontaneous coherence develops between them. These coherence properties translate into a characteristic behavior for the correlation function. In particular it was demonstrated<sup>69</sup> that Bose-Einstein condensation in a three-dimensional system occurs when the single particle density matrix  $\rho(r, r') = \langle \hat{\psi}^\dagger(r') \hat{\psi}(r) \rangle$  exhibits off-diagonal long range order,

$$\lim_{|r-r'| \rightarrow \infty} \rho(r, r') = N_0 > 0. \quad (4.1)$$

In one dimension things change. Arguments similar to the three-dimensional case provide a degeneracy temperature  $T_{1D} = \hbar^2 n_{1D}^2 / mk_B$ , at which the effects of quantum statistics set in, i.e. the de Broglie wavelength become comparable to the inter-particles separation. By the way, in one dimension phase fluctuations associated with phonons, the long-wavelength excitations of the condensate, can destroy Bose-Einstein condensation and affect its correlation properties. At finite temperature,  $T < T_{1D}$ , the mean square fluctuations of the phase for the uniform one-dimensional system are expected<sup>70</sup> to diverge linearly at large separation  $x = x' - x''$ ,

$$\langle \Delta\phi(x)^2 \rangle = \langle [\phi(x') - \phi(x'')]^2 \rangle = \frac{mk_B T}{n_{1D} \hbar^2} |x|, \quad (4.2)$$

where  $n_{1D} = N/L$  is the number of particles per unit length. As a consequence the one-dimensional correlation function is expected to decay exponentially,

$$\rho(x) \simeq n_{1D} e^{-|x|/2L_\phi}. \quad (4.3)$$

In the uniform system and in the absence of external potentials (as a periodic lattice) the correlation length is  $L_\phi = n_{1D} \hbar^2 / mk_B T$ . The fact that the density matrix tends to zero as  $x \rightarrow \infty$  shows that there is no Bose-Einstein condensation. Despite the absence of long range order, coherence is not yet destroyed. The physical picture

is that of finite regions where the phase is well correlated, but with relatively weak phase coherence between different regions. The length  $L_\phi$  gives the typical distance over which there is good phase correlation, and is of the order of the square of the thermal de Broglie wavelength divided by the mean separation between particles. In general one speaks of a ‘quasicondensate’ to indicate the behavior of the density matrix in intermediate between that of a BEC, for which  $\rho(x)$  tends to a constant value at large  $x$ , and that of a normal system, in which  $\rho(x)$  drops towards zero over a typical microscopic distance.

The presence of disorder can strongly affect the correlation properties of a bosonic system, even for quasicondensates in one dimension. In the absence of interactions, the disorder induces exponential localization of the one-particle wave-functions thus destroying coherence between neighboring particles. Depending on the kind and on the strength of disorder the characteristic localization length can be even much smaller than the quasicondensate correlation length  $L_\phi$ . The resulting correlation function will decay exponentially on shorter correlation lengths. On the other hand also the presence of strong interactions can affect the correlation properties of the quasicondensate, forcing particles to stay apart from each other. An experimental mapping of the evolution of the correlation length of an interacting disordered one-dimensional Bose gas can give important indications on the different phases of the system.

## 4.1 Momentum distribution and correlation function

The experimental observable enabling the study of the correlation properties is the momentum distribution. Cold atoms experiments give the possibility to image the atomic distribution after a time of flight, i.e. after releasing atoms from the trapping confinement and letting them free to expand. If the time of flight is sufficiently large and the interactions between atoms can be neglected, the image of the atoms is acquired in the ‘far-field’ limit and it approximatively reproduces the in-trap momentum distribution,  $n_{TOF}(r) \approx \rho(p) = \langle \hat{\psi}^\dagger(p) \hat{\psi}(p) \rangle$ , where the position  $r$  and the momentum  $p$  are related by the ballistic expansion condition  $p = mr/\hbar t$ ,  $m$  is the atomic mass and  $t$  is the time of flight. Using the Wiener-Khinchin theorem, since  $\hat{\psi}(p) \propto \mathcal{F}[\hat{\psi}(r)]$ , is possible to directly relate the *spatially averaged* correlation function to the inverse Fourier transform of the experimentally measurable momentum distribution

$$g(r) = \int \rho(r', r+r') dr' = \mathcal{F}^{-1}[\rho(p)]. \quad (4.4)$$

As already said in one dimension the correlation function of a trapped gas at finite temperature decays exponentially in space, whatever the phase of the system. For a quasicondensate the correlation length is  $L_\phi$ . More generally the correlations decay on a typical length  $\xi$ . The atomic momentum distribution is therefore a Lorentzian distribution whose width is inversely proportional to the correlation length of the system

$$\rho(p) = \frac{1}{p^2 + (1/\xi)^2}. \quad (4.5)$$

Measuring the momentum width of a trapped gas is then possible to extract information on the coherence length of the system.

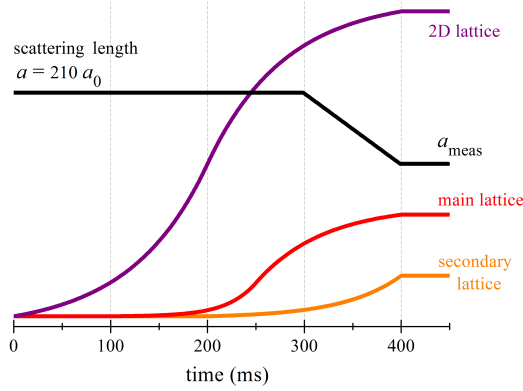


**Figure 4.1:** Experimental sequence. The loading ramp for the 2D lattice (purple) is *s*-shaped and last 400 ms. Half of the total depth is reached with a 200 ms exponential ramp, with time constant  $\tau=80$  ms; the final depth is then reached with an inverted exponential with the same  $\tau$ . The main lattice raises 100 ms after the 2D lattice. Its ramp (red) is *s*-shaped and last 300 ms. One third of the total depth is reached in 150 ms with an exponential ramp with  $\tau=30$  ms; the final depth is reached with an inverted exponential ramp with  $\tau=-70$  ms. The secondary lattice (orange) raises during the last 200 ms, with an exponential ramp with  $\tau=60$  ms. The scattering length (black) is linearly changed to the desired value after 300 ms, when the radial confinement is sufficiently strong to freeze the number of occupied tubes.

## 4.2 Experimental procedure

In this section we describe the experimental techniques used to prepare the disordered one-dimensional system at different interaction energies, and to detect its coherence properties. The main result of this experimental procedure is the diagram shown in Fig. 4.3: thanks to the ability to simultaneously control disorder and interactions, we could trace the complex evolution of the momentum width across the  $U$ - $\Delta$  plane, thus measuring the system's correlation properties.

**Loading an array of 1D traps.** As introduced in Chapter 2, the experiment starts with a condensate prepared in the ground state of a three-dimensional optical trap with mean frequency  $\omega = 2\pi \times 80$  Hz, at a scattering length  $a = 210a_0$ . The total number of atoms  $N_{tot}$  ranges from 2 to  $4 \times 10^4$ , depending on the specific dataset, and no thermal component is discernible, thus  $T$  is well below the critical temperature for Bose-Einstein condensation in three dimensions.

The experimental sequence used to load the one-dimensional traps at different disorder and interactions is sketched in Fig. 4.1. The BEC is adiabatically transferred from the dipole trap into an array of 1D tubes by ramping up the strong two-dimensional optical lattice with 400 ms *s*-shaped ramps. We remind that at typical lattice depths of 30 recoil energies, the radial trapping frequency of each tube  $\omega_{\perp} = 2\pi \times 50$  kHz, is larger than any other energy scale (including the axial trapping frequency, typically  $\omega_x = 2\pi \times 150$  Hz), and tunneling between neighboring traps is suppressed on the experimental timescale ( $\hbar/J_{\perp} \sim 0.5$  s). Each tube behaves as an effective one-dimensional system. The atom number per tube can be determined using Eq. 2.8, as discussed in Sec. 2.4

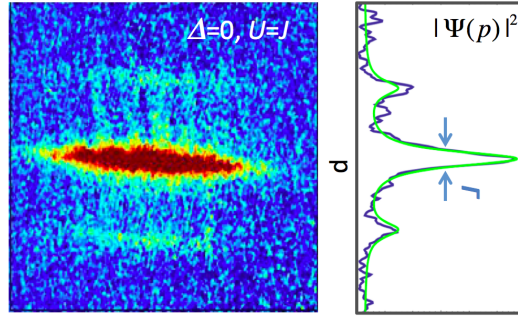


**Figure 4.2:** Typical experimental picture at  $U=J$ ,  $\Delta=0$ . The momentum distribution is integrated along the radial direction and fitted with three Lorentian peaks. The root mean square (rms) width  $\Gamma$  of the central peak gives information on the system correlation properties.

**Inside the tubes.** When the tunneling between tubes is small enough, the quasiperiodic lattice is adiabatically raised up, and the 3D scattering length is slowly changed to a final tunable value  $a$  with a magnetic Feshbach resonance, as shown in Fig 4.1. The depth of the main lattice (with spacing  $d = \lambda_1/2$ ,  $\lambda_1 = 1064$  nm) is kept fixed at around 9 recoil energies, and sets the typical tunneling energy  $J/h \sim 110$  Hz. The depth of the secondary lattice (with  $\lambda_2 = \lambda_1/\beta = 856$  nm) can be varied and sets the quasi-disorder strength  $\Delta$ . Since the depth of the primary lattice  $s_1$  is quite large, the system is well described in the Bose-Hubbard limit, as discussed in Sec. 3.1; the Hubbard Hamiltonian describing the experimental realization in the single tube reads:

$$\begin{aligned} \hat{H} = & -J \sum_i (\hat{b}_i^\dagger \hat{b}_{i+1} + H.c.) + \frac{U}{2} \sum_i \hat{n}_i (\hat{n}_i - 1) \\ & + \Delta \sum_i \cos(2\pi\beta i + \phi) \hat{n}_i + \frac{\alpha}{2} \sum_i (i - i_0)^2 \hat{n}_i, \end{aligned} \quad (4.6)$$

with  $J$ ,  $U$  and  $\Delta$  given by the expressions 3.5, 3.6 and 3.9 respectively. The strength of the interaction energy  $U$  depends on the final scattering length  $a$ .  $\alpha$  represents the harmonic confinement in the axial direction ( $\omega_x = 2\pi \times 150$ ).

**Momentum distribution detection.** The coherence properties of the system are captured by performing time of flight imaging. All the trapping potentials are suddenly switched off and the atoms are let free to expand for 16.5 ms.

A typical experimental picture is shown in Fig. 4.2. Even in the absence of disorder, the atoms are confined in a lattice, whose periodic properties are reflected in the momentum distribution. In the superfluid phase the (Wannier) wave-functions centered in each lattice site are phase-locked on length scales of the order of the correlation length; when all the trapping potentials are switched off, the wave packets overlap and interfere giving rise to sharp peaks in the momentum distribution. The distance between the peaks is  $2\hbar k_1$ , and depends on the reciprocal lattice vector  $2k_1 = 2\pi/d$ , where  $d$  is the main lattice spacing. While the envelope of the whole distribution is proportional to the square of the Fourier transform of the single site Wannier function, the peak shape reflects the coherence properties of the system.

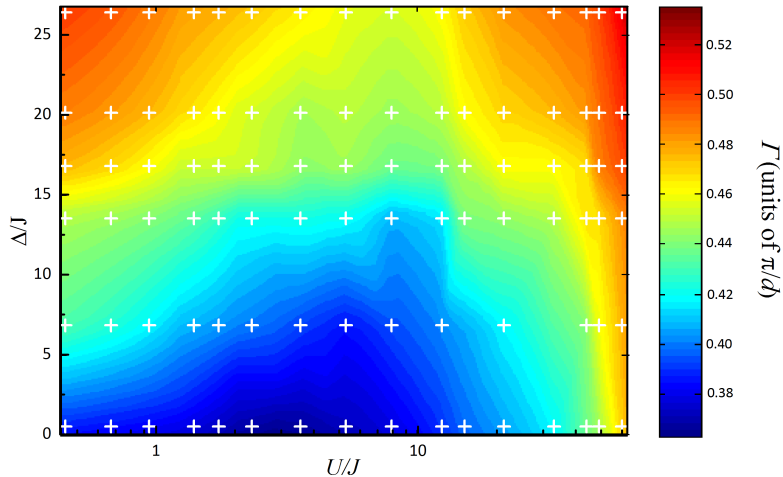


**Figure 4.3:** Coherence diagram. Evolution of the root mean square momentum width  $\Gamma$  experimentally measured in the  $U$ - $\Delta$  plane. The diagram is constructed by interpolating 94 data points, indicated with white crosses. Each point is the mean value of four measurements, with a standard deviation between 2% and 5%.

As already said, in 1D systems the correlation function decays exponentially, and each peak is a Lorentzian distribution, whose width is inversely proportional to the correlation length  $\xi$ . In less coherent samples, the correlations decay on smaller length scales (even smaller than the lattice spacing), resulting in a broadening of the Lorentzian distribution.

The simpler experimental observable one can extract from the measured distribution is the root mean square (rms) width  $\Gamma$  of the central peak. We estimate it in the first Brillouin zone. This quantity is linked to the Lorentzian width  $1/\xi$ , it is fit-independent and can be directly measured from the bare experimental profiles. By fitting the measured distribution with a Lorentzian function is also possible to directly derive the correlation length  $\xi$ .

### 4.3 Experimental $U$ - $\Delta$ diagram

The evolution of the root mean square momentum width  $\Gamma$  is shown in Fig. 4.3. The diagram is constructed by interpolating 94 data points taken at different disorder and interactions and homogeneously distributed. Each point is the average of four different experimental measurements, with a standard deviation between 2% and 5%.

The momentum width  $\Gamma$  features a clear variation across the  $U$ - $\Delta$  plane, suggesting the presence of different disorder/interaction-induced quantum regimes. Coherent and incoherent regimes are well detectable even though the unavoidable harmonic trapping ( $\omega_z = 2\pi \times 150$  Hz) limits the size of the system and transforms sharp quantum phase transitions into crossovers. Along the  $\Delta = 0$  line,  $\Gamma$  increases with  $U$  due to the progressive formation of an incoherent Mott insulator, which in our inhomogeneous system coexists with a remaining superfluid fraction. At large  $U$ , in fact, the Poissonian fluctuations in atom number are energetically costly and tunneling from site to site is suppressed, as discussed in Sec. 3.1. The coherence is lost on length scales of the order of the lattice spacing. For increasing disorder along

the non-interacting line, an Anderson insulator forms above the critical  $\Delta = 2J$  of the Aubry-André model, see Sec. 3.2. The general behavior for finite  $U$  and  $\Delta$  indicates the presence of a reentrant incoherent regime characterized by small correlation lengths, extending from small  $U$  and  $\Delta > 2J$  to large  $U$ , surrounding a more coherent one for moderate disorder and interaction. This observation strongly reminds the insulating regimes discussed in Chapter 1. At small  $U$  the interactions weaken the disorder-induced localization; a crossover from the incoherent (Anderson localized) regime towards more coherent regimes is observed when the interaction energy  $nU$  becomes of the order of  $\Delta$ , in agreement with theoretical predictions. At stronger  $U$  a second crossover towards less coherent regimes occurs. An interaction-induced Mott insulator is expected to survive in the disordered potentials only for moderate disorder  $\Delta < U/2$ . In this region, the interaction energy cooperates with disorder in destroying the system coherence, suggesting the presence of a new insulating regime besides the disordered Mott insulator, which will prove to be the Bose glass.

**Temperature.** The experiment is realized at finite temperature. As discussed in Sec. 1.3, the effect of temperature can be twofold in the  $U$ - $\Delta$  diagram; at weak interactions a finite temperature could compete with the interaction energy, reducing the spatial density of the system, thus not preventing its localization in the disordered landscape. In this context theoretical studies<sup>2</sup> predicted a temperature-independent metal-insulator transition, up to a crossover temperature  $T_0 \approx \sqrt{nUT_{1D}}/k_B$ . On the other hand at strong interactions the thermal energy should compete with the disorder, weakening the localization effects. For instance a melting temperature  $T_0 \approx 0.2U$  is expected<sup>40</sup> for the Mott insulating phase. To clearly distinguish and characterize the different quantum regimes, a good estimate and control of thermal effects is thus required.

A good measurement of the temperature in a lattice is not trivial. In the uniform system and in the absence of a lattice an experimental indication might be extracted from the momentum width at zero disorder and weak interactions, where the bosons form a quasicondensate, relating  $\Gamma$  to the correlation length  $L_\phi$ . Actually, the presence of the lattice and the inhomogeneity of the experimental system strongly affect this relation, changing the evolution of the correlation length with temperature. Detailed studies on  $\xi(T)$  will be presented in Sec. 4.5, in order to characterize the role of a finite temperature in the different regimes observed in the experiment. From finite-temperature simulations we can estimate  $T \sim 3J$  for the quasicondensate, not larger than the other energy scales characterizing the system (actually smaller in many regions of the phase-diagram), well below the degeneracy temperature  $T_{1D} \sim 8J$ . However, in this system the temperature can be estimated only in the weakly-interacting regime at  $\Delta = 0$ ; in other regions of the phase diagram a direct measure of the temperature is not easily available.

**Entropy.** An experimental observable related to the thermal energy present in the system is its entropy  $S$ . While the temperature is not directly addressable in the whole  $U$ - $\Delta$  plane, the entropy can be measured everywhere, giving informations on the heating in the system. The entropy is measured as follows: in a 3D trap, the entropy depends explicitly on the temperature of the system<sup>14</sup>, which can be

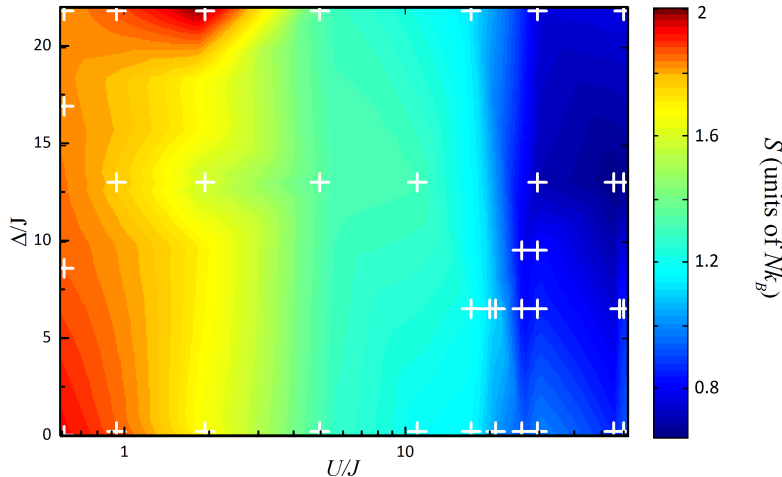


**Figure 4.4:** Measured entropy per particle,  $S/Nk_B$ . The 2D graph is constructed by interpolating the data points whose position is shown by the white crosses.

measured by time of flight images. For a condensate  $S = 4N_{tot}k_B\zeta(4)/\zeta(3)(T/T_c)^3$ , where  $T_c$  is the critical temperature for condensation and  $\zeta$  is the Riemann Zeta function. For a thermal cloud,  $S = N_{tot}k_B[4 - \log(N_{tot}(\hbar\omega/k_B T)^3)]$ . In our setup it is not possible to directly assess the entropy of the one-dimensional system, but we can measure the entropy after transferring the atoms into the 1D tubes and back into the 3D trap, and compare it with the initial entropy in the 3D trap. We assume the mean value of the initial and the final entropies as an indication of the entropy in the 1D tubes.

The evolution of the entropy along the  $U$ - $\Delta$  diagram is shown in Fig. 4.4. Though this observation is not an absolute measurement of the temperature, it gives indications on the relative heating in the different regions of the phase-diagram. Generally we measure entropies  $S \sim Nk_B$ . The overall increase of  $S$  towards small  $U$  suggests a slight heating of the sample at weak interactions. This is probably due to a less adiabatic preparation of the one-dimensional systems at vanishing interactions, and could lead to an overestimation of the temperature in regions with larger  $U$ . For increasing  $\Delta$  the entropy is constant: the presence of the disordered potential does not affect the temperature of the sample. The strong local increase of  $S$  for large  $\Delta$  and vanishing  $U$  is instead presumably caused by the presence of strongly localized single particle states keeping the system far from its ground state during the loading procedure.

## 4.4 Comparison with theory

Many theoretical works<sup>42,37,81,80</sup> studied the quantum phases of an interacting Bose gas in the quasiperiodic potential. Anyway, most of the theories were developed at zero-temperature and in the absence of harmonic confinement, i.e in homogeneous systems. In Roux et al.<sup>81</sup>, density-matrix renormalization group (DMRG) algorithms were used to treat the soft-core Bose-Hubbard model in a quasiperiodic potential. Different observables were computed: the correlation length  $\xi$  and the superfluidity

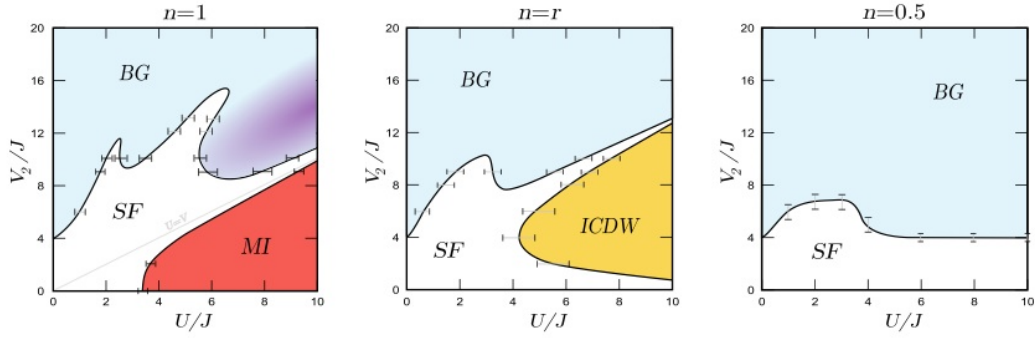


**Figure 4.5:** Phase diagrams of the quasiperiodic Bose-Hubbard model for densities  $n=1$ ,  $n=r$  (the ratio of the potential wave-lengths,  $\lambda_1/\lambda_2$ ), and  $n=0.5$ . The diagrams are shown as a function of the interaction strength  $U$  and the quasiperiodic potential strength  $V_2$ , proportional to  $\Delta$ , both normalized by the hopping  $J$ . Lines are guides to the eyes. The picture is taken from Roux et al. <sup>81</sup>.

density  $\rho_s$  gave informations on the coherence and the mobility of the system, suggesting the presence of localized or delocalized phases. On the other hand, the one-particle gap  $\Delta_c$  (a quantity directly related to the computable chemical potential  $\mu$ ), gave indications on its compressibility. All the observables were evaluated at different densities  $n$ , and their evolution in the  $U$ - $\Delta$  plain allowed the detection of different quantum phases. A summary of the main theoretical results is depicted in Fig 4.5, which gather the phase diagrams for commensurate ( $n=1$ ) and incommensurate ( $n=0.5$ ,  $n=r$ ) densities. Here  $V_2$  is the depth of the secondary lattice, proportional to  $\Delta$ , and  $r = \lambda_1/\lambda_2$  the ratio between the bichromatic potential wave-lengths. The observed quantum regimes strongly depend on the density  $n$ . Anyway, generally three main different phases are found, in agreement with the general discussion developed in Sec 3.3.2: a superfluid-compressible phase (SF), present at weak interaction and weak disorder, transforms in an insulating and incompressible Mott phase (MI) at strong interactions, or in a incommensurate density wave (ICDW), depending on the system commensurability. For  $\Delta > 2J$  the Bose glass (BG) phase emerges. As introduced in Chapter 1, this peculiar phase, extending from weak to strong interactions, is globally insulating, but characterized by local coherence, thus resulting in a finite compressibility and in a gapless excitation spectrum.

The reentrant shape of the experimental diagram shown in Fig. 4.3 reminds the behavior of this Bose glass phase found in theoretical studies at  $T = 0$  for the homogeneous systems. The experimental situation is, however, much more complex. The experiment is in fact composed by several one-dimensional inhomogeneous systems with different atomic densities, at finite-temperature. In order to identify the observed incoherent regimes with predicted theoretical phases, a close comparison between the experimental data and theory is thus needed. We achieve the closest experiment-theory comparison by performing a DMRG study of the inhomogeneous systems described by Hamiltonian (4.6), and then extending the zero-temperature results to finite  $T$ . The calculations have been performed in cooperation with Guillaume Roux and Thierry Giamarchi, using the experimental parameters given in Sec. 4.2.

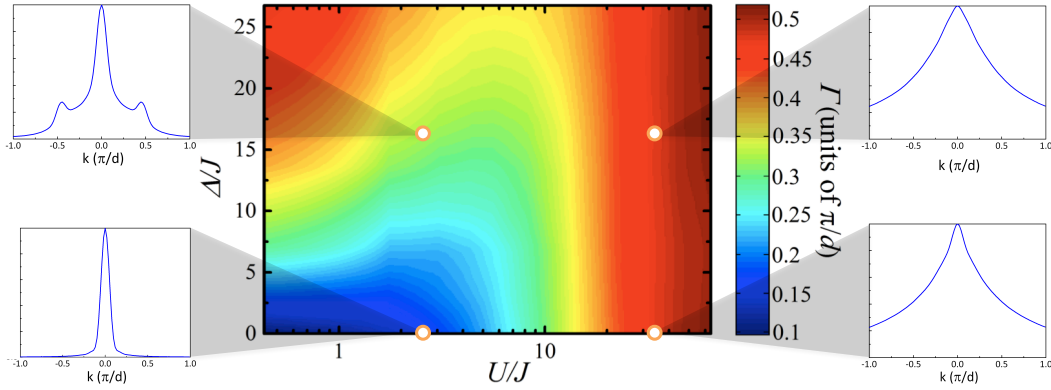
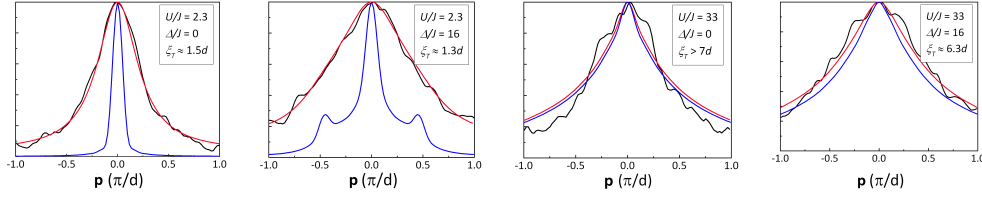


**Figure 4.6:** Theoretical coherence at  $T=0$  in the inhomogeneous system. Momentum width  $\Gamma$  at  $T=0$ , calculated for individual tubes, and then averaged over the distribution of tubes. The diagram is built with 94 data points at the same positions of the experimental data in Fig. 4.3. The insets show four typical momentum distributions calculated at  $U=2.3J$  and  $\Delta=0$ ,  $U=2.3J$  and  $\Delta=16J$ ,  $U=33J$  and  $\Delta=0$ ,  $U=33J$  and  $\Delta=16J$ .

#### 4.4.1 Zero- $T$ phase diagram in inhomogeneous systems

Zero-temperature DMRG calculations<sup>81</sup> give access to all the single-particle correlations  $g_{mn} = \langle \hat{b}_m^\dagger \hat{b}_n \rangle$  in the ground-state, which are then averaged over the whole distribution of tubes in order to account the experiment's inhomogeneity. The  $T = 0$  momentum distribution is obtained using Eq. (4.4),  $\rho(p) = |W(p)|^2 \sum_{m,n} e^{ip(m-n)} g_{mn}$ , where  $W(p)$  is the Fourier transform of the numerically computed Wannier function. Few representative results, in different  $U$ - $\Delta$  zones, are displayed in the inset of Fig. 4.6. The overall evolution of the rms momentum width along the  $U$ - $\Delta$  plane is shown in Fig. 4.6. The presence of a strong harmonic potential affects the shape of the  $U$ - $\Delta$  diagram. In fact, different phases are now coexisting at a given disorder and interaction strength, due to the different atomic densities present in each one-dimensional system. The resulting phase-diagram is thus a ‘combination’ of several theoretical homogeneous phase diagrams with different occupancies of the lattice sites. As a consequence, the theoretical sharp transitions of the homogeneous system broaden into crossovers between different regimes. Moreover, the inhomogeneity washes out the peculiar finger-like structure of the SF phase found for the homogeneous system; the overall shape is actually very similar to the experimental one.

Of course, the great difference between theory and experiment is in the values of  $\Gamma$ : in the experiment we measure much bigger widths than the ones estimated by the zero-temperature theory, at least at weak interactions ( $U < 10J$ ). This suggest the presence of relevant thermal broadening in the weakly-interacting region. At strong interactions and low disorder instead, experimental and theoretical-zero-temperature widths are not so different, suggesting negligible thermal effects in this regime. Finite-temperature simulations we will present in section 4.5, will clarify the different behavior of the correlation length versus temperature.

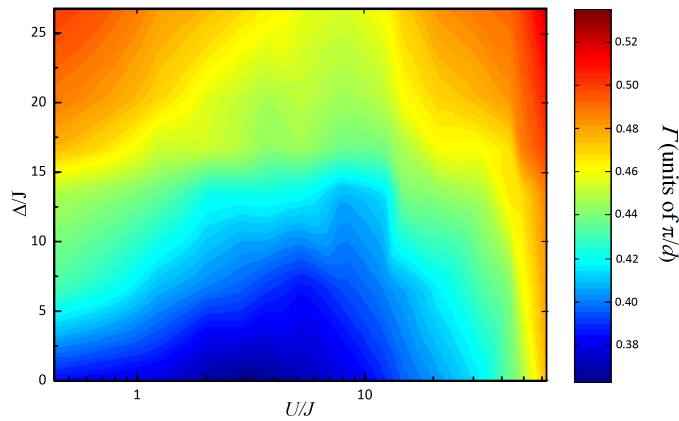
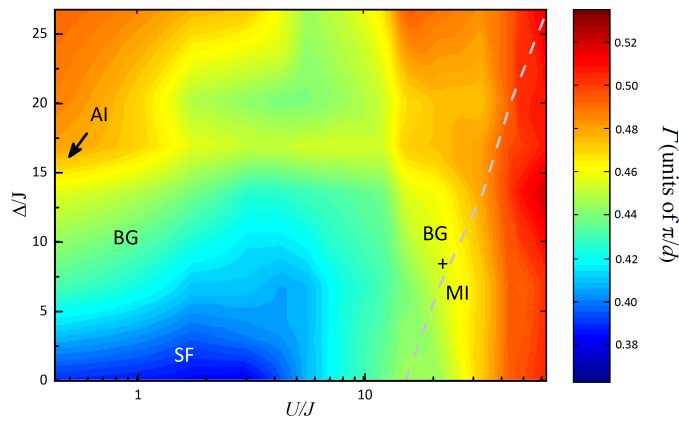
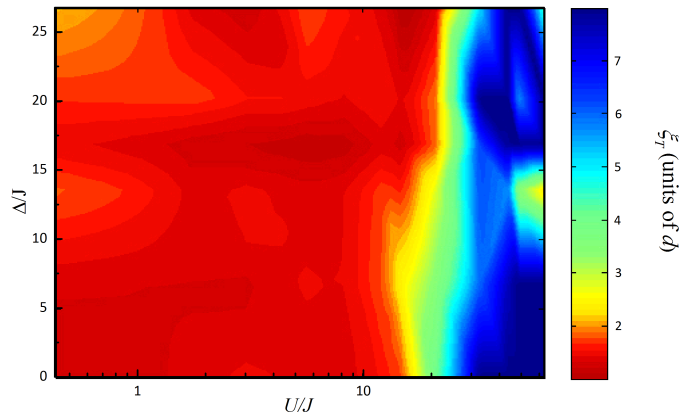


**Figure 4.7:** Measured and calculated momentum distributions. The experimental momentum distributions (black) are compared with  $T=0$  DMRG calculations (blue lines) supplemented by the introduction of a thermal correlation length  $\xi_T$  (red lines), in four typical regions of the phase diagram

#### 4.4.2 Finite-temperature: a phenomenological approach

A phenomenological account of temperature effects is introduced by multiplying the correlation function by  $e^{-|m-n|/\xi_T}$ , where  $\xi_T$  is a phenomenological thermal correlation length. In the superfluid regime, for homogeneous systems, the Luttinger liquid theory justifies this assumption and predicts  $\xi_T \propto 1/T$  in the continuum (i.e. in the absence of a lattice). For the sake of simplicity, we take the same  $\xi_T$  for all distances and all tubes. This qualitatively amounts to convolve the  $T = 0$  momentum distribution with a Lorentzian of width  $1/\xi_T$ ; the resulting ‘thermal’  $\rho(p)$  is reproduced by red curves in Fig. 4.7 and compared with the  $T=0$  DMRG distributions (blue lines) and the experimental profiles (black lines). The evolution of the ‘thermal’ rms momentum width in the  $U$ - $\Delta$  plane, is shown in Fig. 4.8b, and compared with the experimental one (Fig. 4.8a).  $\xi_T$  is left as a free fitting parameter, which we adjust on the experimental profiles, the black curves in Fig 4.7. As shown in Fig. 4.7a-4.7b-4.7d, this approach well reproduces the experimental momentum distribution in all regimes, realizing quite good agreement between theory and experiment in the whole  $U$ - $\Delta$  plane (see Fig. 4.8a-4.8b), with the exception of the large- $U$ , low- $\Delta$  region. The evolution of  $\xi_T$  is shown in Fig. 4.8c and suggests the presence of two distinct regions in the  $U$ - $\Delta$  diagram, one at weak interactions, say  $U < 10J$ , strongly affected by the thermal excitations, the other at strong  $U$ , weakly dependent on temperature.

In the weakly interacting region  $\xi_T$  is indeed rather short ( $\sim d$ ), revealing a relevant thermal broadening of the momentum width, but it is essentially constant. The presence of a finite temperature results in a reduction of the typical correlation length, but does not affect the crossover lines between more and less coherent phases. This suggests a strong link between the experimentally observed regimes and the theoretically computed quantum phases. As already noticed, the shape of the experimental diagram is not different from the computed  $T = 0$ , in agreement with the expectation<sup>2</sup> of a temperature-independent metal-insulator crossover for our temperature  $T \sim 3J$  of the order of  $T_0 \approx \sqrt{nUT_{1D}/k_B}$ . In particular, in the weakly-interacting region at  $\Delta > 2$ , interactions tend to restore coherence between single-particle localized states, thus weakening the Anderson localization and leading to a delocalization transition from a weakly-interacting Bose glass to a superfluid phase. Both the experiment and the theoretical study locate this crossover at  $nU \sim \Delta$ , where the interactions are large enough to screen disorder effects, as already observed in three-dimensional systems<sup>26</sup>.

(a) *Experimental  $U$ - $\Delta$  diagram.*(b) *DMRG  $U$ - $\Delta$  diagram.*(c)  *$\xi_T$  across the  $U$ - $\Delta$  plane.*

**Figure 4.8:** Coherent and incoherent regimes across the  $U$ - $\Delta$  plane. Momentum width  $\Gamma$  measured (a) and calculated (b) as described in the text. The dominant phases in the typical system from the  $T=0$  theory are labeled in the calculated diagram. The grey dots indicate the interaction values above which one finds Mott insulating domains; for large  $U$  this interaction is about  $2\Delta$ . Both diagrams are built with 94 individual data points. (c) Fitted  $\xi_T$  across the  $U$ - $\Delta$  plane.

At strong interactions,  $\xi_T$  increases substantially ( $\xi_T \sim 7d$ ), thus indicating that the strongly-correlated phases are only weakly affected by the finite temperature. In the large- $U$  small- $\Delta$  region the thermal broadening approach fails; the theoretical ‘thermal’ phase diagram is not well reproducing the experimental one. Here, in fact, the situation is more complex; at zero temperature at least two phases coexist in our inhomogeneous system. The fraction of the atoms which is commensurate with the lattice periodicity forms a Mott insulator well localized at the lattice sites by interactions; on the other hand the remaining incommensurate fraction behaves as a weakly-interacting Fermi gas, i.e., in absence of disorder, as a fluid of fermions (see Fig. 4.5). The coherence properties and the typical correlation lengths of these phases are not expected to be equal. In particular we will show that the evolution of  $\xi(T)$  with temperature behaves quite differently for the commensurate and the incommensurate phase. Actually, looking at the profiles in Fig 4.7c, the use of one single correlation length does not perfectly fit the experimental data, probably leading to an overestimation of the computed theoretical  $\Gamma$ .

For increasing disorder the incommensurate-fluid fraction (Anderson) localizes, and its correlation properties resembles more and more the commensurate-insulating one even for  $T > 0$ , leading to a better agreement between theory and experimental data. As already pointed out, the coherence diagram exhibits a new crossover, clearly different from what would be expected for a simple MI surviving in the presence of disorder (i.e.  $U > 2\Delta$ , the dashed line in Fig. 4.8b), suggesting the presence of an additional disorder-induced phase besides the MI, the strongly-correlated Bose glass. As discussed in Chapter 1, this new phase, predicted by zero-temperature theory, arises from the localization of the strongly-interacting incommensurate fluid fraction, thus displaying finite compressibility and gapless response in the excitation spectrum. Finite temperature simulations, and further experimental observations, such as the excitation spectrum measurement, will prove this preliminary observation in the next sections.

## 4.5 Finite temperature effects

The phenomenological approach described above, suggests a strong link between the coherent and incoherent regimes observed in the experiment and the quantum phases predicted by theory at  $T = 0$ . To get a rigorous connection between the measured  $\rho(p)$  and theoretical results at  $T = 0$  we realized exact diagonalization studies of the Hamiltonian (4.6) at finite- $T$ . An extensive numerical study of the inhomogeneous problem is something very difficult, at present out of reach. We therefore performed exact diagonalization on small homogeneous clusters with size up to  $L = 12d$  and variable mean site occupations up to  $n = 1$ , and then extracted the characteristic correlation length  $\xi$  by exponentially fitting the tails of the computed correlation function. In this section we discuss the evolution of the correlation length with temperature in the different zones of the  $U$ - $\Delta$  diagram.

### 4.5.1 Weakly-interacting side: an experimental thermometer

The conceptually simpler case is the non-disordered SF phase obtained at  $\Delta=0$  and weak interactions ( $U \sim J$ ); the evolution of  $\xi^{-1}(T)$  at  $U = 2J$  is shown in Fig.

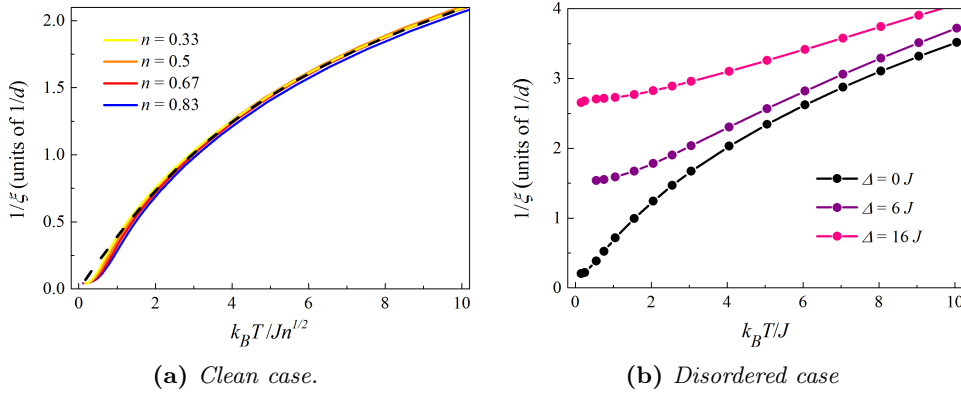


**Figure 4.9:** (a) Temperature evolution of the inverse correlation length, calculated by exact diagonalization of small homogeneous systems for  $\Delta=0$ ,  $U = 2J$  and various site occupancies. The horizontal scale has been rescaled by  $n^{1/2}$  to show that all the curves are well reproduced by  $d/\xi = \text{arcsinh}(k_B T / 2.5 J n^{1/2})$  (dashed black line). (b) Temperature evolution of  $1/\xi$  for  $U = 2J$ ,  $n=0.46$  and 3 different disorder strengths.

4.9a, for different densities. Additional numerics suggest little or no dependence on  $U$ , at least in the weakly-interacting regime. Here, the  $T = 0$  correlation length is negligible, and  $\xi$  can be identified with  $\xi_T$ . The presence of a finite temperature affects the coherence properties of the system, reducing its correlation length, as noted previously. As a consequence  $\xi$  can be employed as a thermometer for the system. In particular, for temperatures  $2J < k_B T < 100J$  and densities  $n \leq 1$ , the correlation length scales as

$$\xi = \frac{d}{\text{arcsinh}\left(\frac{k_B T}{\alpha J \sqrt{n}}\right)}, \quad (4.7)$$

where  $\alpha$  is a numerical constant. This behavior has never been found in previous studies on bosonic systems; anyway, a similar result,  $\xi \sim d / \text{arcsinh}(k_B T / J)$ , is known for spinless fermions in a lattice<sup>85</sup>, representing the  $U = \infty$  bosonic limit. The weak logarithmic temperature dependence of  $\xi$  for  $k_B T > J$  is due to the presence of the lattice, resulting in a finite bandwidth. For vanishing  $T$ , eq. (4.7) tends instead to  $\xi \sim Jd / k_B T$ , showing the usual linear scaling in  $T$  of the Luttinger liquid theory. Presumably, we enter this regime only for  $k_B T \ll J$  (see Fig. 4.9a), in contrast to standard assumptions in previous studies; anyway finite size effects prevent us from more detailed studies of the low- $T$  phase.

Eq. (4.7) can be used to estimate the experimental temperature from the correlation length measured in the superfluid phase. We account the experimental inhomogeneity, employing a local-density approximation and averaging the finite temperature momentum distribution,  $\rho(p) \sim 1/[2\pi\xi(p^2 + 1/\xi^2)]$ , over the zero temperature density distribution in the trap. In the experiment, at  $U = 2.3J$ , we measure  $\xi_T = 1.38(13)d$ ; exploiting this procedure we obtain  $k_B T = 3.1(4)(3)J$ , where the first uncertainty is the statistical error on  $\xi_T$  and  $n$ , and the second one is the systematic error on the calibration of  $N_{tot}$  ( $\sim 50\%$ ). At lower interaction energies we observe an increase of the temperature up to  $k_B T = 5.4(8)(4)J$  for  $U = 0.4J$ ,

suggesting a not fully adiabatic preparation of the system, as already shown by entropy measurements discussed above.

At finite disorder and weak interactions, we still observe a comparable thermal broadening, as shown in Fig. 4.9b (in this case  $U = 2J$ ), confirming a rather strong impact of thermal fluctuations also on the correlation properties of the weakly-interacting Bose glass.

### 4.5.2 Strongly-correlated phases

Fig. 4.10a shows the evolution of  $\xi^{-1}(T)$  at large interaction ( $U = 44J$ ) and finite disorder ( $\Delta = 10J$ ) for commensurate and incommensurate densities ( $n = 1$  and  $n = 0.46$ ). In the strongly-interacting regime the correlation length  $\xi$  is essentially  $T$ -independent at low temperatures, and thermal effects become relevant only above a crossover temperature  $T_0$ , both in the commensurate-MI and in the incommensurate-BG regimes. In fact, the Mott insulator is an incompressible phase, characterized by an energy gap of the order of the on-site interaction energy, and it is therefore expected to melt for thermal energies comparable with some fraction of the energy gap. Surprisingly also the gapless Bose glass shows a similar behavior.

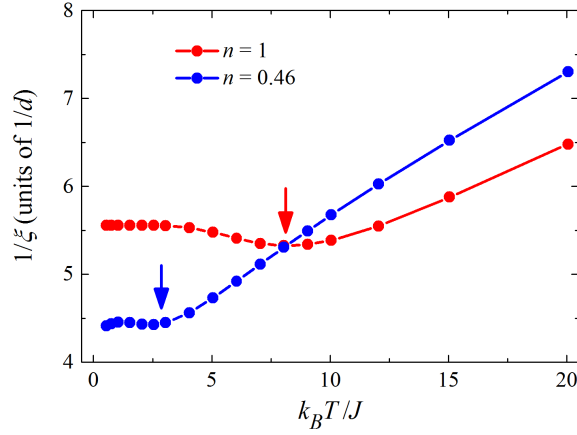
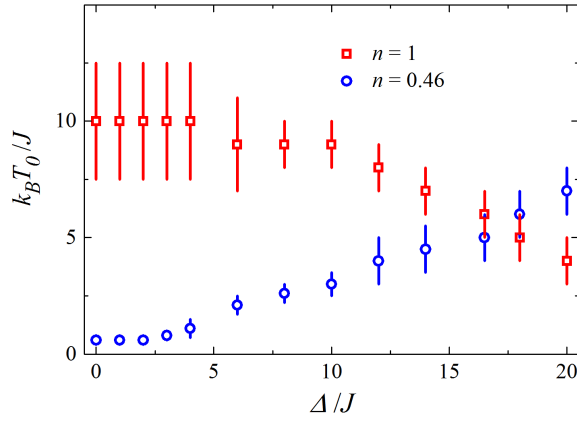
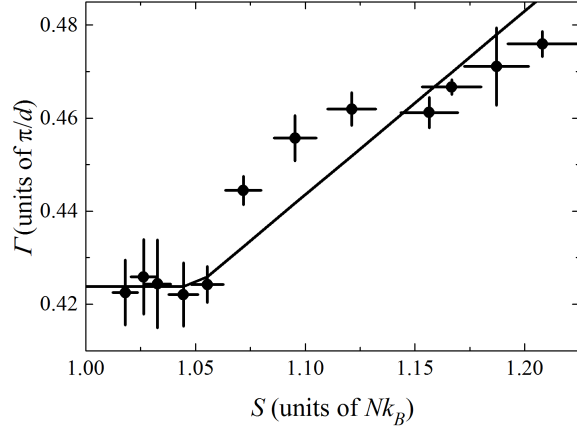
In Fig. 4.10b we plot the evolution of  $T_0$  with  $\Delta$  for one representative interaction ( $U = 44J$ ) in the commensurate and incommensurate cases. At  $\Delta = 0$ , the crossover temperature is  $k_B T_0 = 0.23(6)U$  for the MI, in agreement with the predicted ‘melting’ temperature  $k_B T \sim 0.2U$ <sup>40</sup>, while it decreases with increasing  $\Delta$ , consistently with the predicted reduction of the energy gap in presence of a finite disorder. In the BG phase the crossover temperature shows instead a linear increase with  $\Delta$ . This apparently surprising result was already observed in numerical simulations<sup>64</sup>, and could be intuitively justified by considering the  $\Delta$ -scaling of the effective Fermi energy in the Bose glass phase.

We experimentally verified the existence of a large  $T_0$  for the coexisting BG and disordered-MI phases. Amplitude and phase fluctuations of the optical lattices induce on the experimental system a background heating approximately linear with time, with rate  $8.5(1.4)Js^{-1}$  at  $U = J$ . Exploiting this heating mechanism, we measured the evolution of the width of  $\rho(p)$  as a function of the system entropy (our temperature-related observable) in the strongly-interacting regime ( $U = 23.4J$  and  $\Delta = 6.6J$ ). As shown in Fig. 4.10c, at low entropy  $\Gamma$  is constant for increasing entropies, before reaching the regime of thermal broadening. In this strongly-correlated phase we cannot reliably associate a temperature to the measured entropy; we can only state the corresponding range of temperatures in the SF regime,  $k_B T = 3.1(1) - 4.7(2)J$ . This observation, in cooperation with theory, indicates that, for large enough disorder, the  $T = 0$  quantum phases should persist in the experimental range of temperatures.

### 4.5.3 Thermal effects in the $U$ - $\Delta$ plane

An overview of the thermal effects across the whole  $U$ - $\Delta$  plane, is shown in Fig. 4.11. Here we plot the evolution of the computed momentum width (the analogous of our experimental observable) for commensurate and incommensurate fillings at two different temperatures,  $T = 0$  and  $k_B T = 4J$ .

In the weakly-interacting side of the phase diagram thermal effects are quite important, as revealed by the widening of the momentum width at  $k_B T = 4J$ .

(a)  $\xi^{-1}(T)$ , theoretical evolution.(b)  $T_0$  vs.  $\Delta$ (c)  $\xi^{-1}(S)$ , experimental observation.

**Figure 4.10:** (a) Temperature evolution of the calculated  $1/\xi$  for  $U = 44J$  and  $\Delta = 10J$  for 2 different densities.  $1/\xi$  is essentially constant up to a crossover temperature  $T_0$ , which is identified with the location of the zero of the first derivative of  $1/\xi$  (arrows). (b) Evolution of  $T_0$  with the disorder strength for  $U = 44J$  and 2 different densities. The error bar is set by the discretization of the data in (a). (c) Experimentally measured width for  $U = 23.4J$  and  $\Delta = 6.6J$  vs the entropy per particle. The corresponding temperature in the SF regime varies from  $3.1(1)J$  to  $4.7(2)J$ . The line is a guide to the eye. The error bars are the s.d. of about 10 measurements.

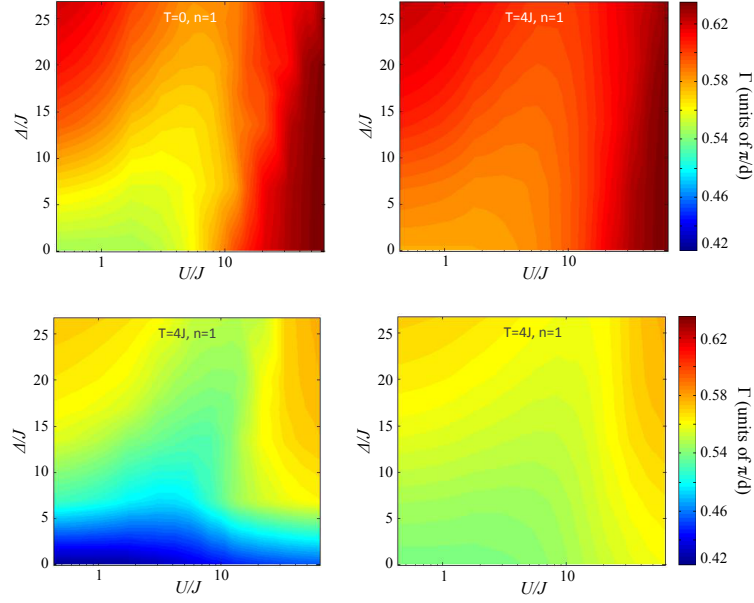


**Figure 4.11:** Coherence from exact diagonalization. Width  $\Gamma$  of the momentum distribution calculated with exact diagonalization for a small system with length  $L$ , for two different densities  $n=1$  ( $L=8d$ ) and  $n=0.46$  ( $L=13d$ ), for  $T=0$  and finite- $T$ . The width still captures the main regions of the phase diagram.

Anyway, the large thermal broadening of  $\rho(p)$  does not necessarily prevent a connection between the finite temperature experimental results and the  $T=0$  properties. As already said, theory predicts a  $T$ -independent fluid-insulator transition for 1D systems in a relatively large range of temperatures<sup>2</sup>, up to a crossover temperature of the order of  $\sqrt{nUT_{1D}/k_B}$ , comparable with the temperature in the experiment. In the following chapter we will show transport measurements consistent with these predictions. In the weakly-interacting regime, the shape of the experimental diagram is substantially equal to the theoretical one calculated at zero-temperature, and the phenomenological thermal correlation length is constant at weak interactions; all these observations strongly indicates that the observed crossover towards less coherent phases in the  $U$ - $\Delta$  diagram is not induced by temperature, but by the interplay between disorder and interactions.

On the other hand, in the large- $U$  regime, finite- $T$  and zero- $T$  widths are generally very similar, confirming that temperatures of the order of  $4J$  does not affect the correlation properties of the MI and strongly-correlated BG phases. The only exception is the weakly-disordered incommensurate case, where even at large interactions the SF regime is dominated by the thermal correlation. In fact, at large interactions and small disorder two different crossover temperatures are estimated for the SF/BG (incommensurate) phase and the MI (commensurate) phase, therefore the single- $\xi_T$  phenomenological approach used in Fig. 4.8b does not reproduce the observed  $\rho(p)$ .

## Chapter 5

# Transport

The existence of a Bose-Einstein condensate – or, in one dimension, of a quasi-condensate – i.e. a macroscopically occupied quantum state, is intimately connected with the macroscopic quantum phenomena of superfluidity and superconductivity. While a microscopic definition of BEC is straightforward, at least in principle, the notion of superfluidity is more subtle. Generally, superfluidity is a state of matter which behaves as a fluid with zero viscosity. On a phenomenological level, the basic properties of superfluids may be explained by introducing a complex order parameter<sup>73</sup>  $\psi(x) = \sqrt{n_s}e^{i\phi(x)}$ , whose magnitude squared gives the superfluid density  $n_s$ , while the phase  $\phi(x)$  determines the superfluid velocity via  $v_s = (\hbar/m)\nabla\phi(x)$ . This relation immediately implies that the superfluid flow is irrotational and its circulation is quantized in an integer number of circulation quanta  $h/m$ . According to a perturbative mechanism proposed by Landau, superfluidity is broken when the velocity of the flow exceeds a critical value at which it is energetically favorable to emit elementary excitations. This mechanism has been explicitly verified in  $^4\text{He}$ <sup>3</sup>,  $^3\text{He-B}$ <sup>13</sup>, and Bose-Einstein condensates<sup>3,16</sup>.

Anyway, the presence of defects or even a periodic lattice can affect the transport properties of physical systems, due to the occurrence of phase slips. In low-dimensional systems especially, phase fluctuations play a crucial role, strongly affecting the superfluid and superconducting phases. Quantum and thermal fluctuations allow the amplitude of the superfluid order parameter to vanish and its phase to unwind, destroying the coherent motion of particles already at small velocities and eventually inducing localization.

On the other hand, the quantum transport properties of a system are intimately related to the underlying symmetries of the Hamiltonian. In disordered potentials, where every trace of translational symmetry is lost, the one-particle wave-functions at zero temperature are expected to exponentially localize. More precisely, this means that, on the average, depending on the strength of disorder, their amplitudes are exponentially decaying in space, thus inhibiting transport and destroying conductivity.

Measuring the dynamical properties of the one-dimensional bosonic system in the presence of disorder and interactions, can give deeper indications on the nature of the coherent and incoherent regimes already observed from equilibrium measurements in Chapter 4. Are these incoherent regimes insulators? How does the conducting phase depend on the condensate velocity? How does disorder affect the superfluid? In this Chapter, after describing the experimental procedure (Sec. 5.1), we first

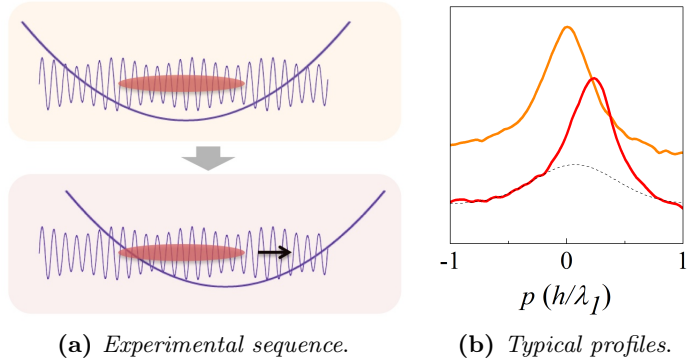


**Figure 5.1:** (a) The dynamics is induced shifting the harmonic potential confining the atoms by controlling a gravity-compensating a magnetic-field gradient. (b) Momentum distribution at  $t=0$  (orange) and  $t=0.8\mu\text{s}$  (red), for a non-disordered lattice at  $U/J=1.26$ .

discuss the transport in the non-disordered case (Sec. 5.2). A close comparison of the experimental results with theoretical studies suggests a phase-slip mechanism destroying superfluidity at an interaction-dependent critical momentum already in the absence of disorder. In Sec. 5.3, we use a similar approach to study the dynamics in the disordered system, in order to locate the metal-insulator transition driven by disorder at weak interactions. Some of the results here reported have been published in Tanzi et al.<sup>90</sup>. Finally, in Sec. 5.4, we report mobility measurements performed from weak to strong interactions.

## 5.1 Experimental procedure

The transport properties of the disordered system are studied exciting a collective oscillation of the one-dimensional quasicondensates of  $^{39}\text{K}$  atoms trapped in the quasiperiodic lattice. The loading procedure of the 1D traps has been already described in Sec. 4.2 (see Fig. 4.1). A 3D Bose-Einstein condensate is split into a few hundreds 1D quasicondensates with a deep two-dimensional lattice in the horizontal plane. Each subsystem contains on average fifty atoms and its longitudinal (transverse) trapping frequency is  $\omega_x = 2\pi \times 150$  Hz ( $\omega_\perp = 2\pi \times 50$  kHz). The quasiperiodic lattice is loaded along the longitudinal direction. The typical tunneling energy, set by the primary lattice, is  $J/h \sim 150$  Hz. The mean atom number per site  $n$ , which scales approximately as  $U^{-1/3}$ , varies in the range of 2 (at strong interactions) to 4 (at weak interactions). From the width of the momentum distribution of the weakly interacting quasicondensate, we estimate an equilibrium temperature of the order of  $k_B T \sim 3J$ . The oscillation is induced using a controllable magnetic-field gradient able to shift the trap center respect to the atomic position in the vertical direction.

In order to study the dynamics of the system, we apply an impulse on the trapped quasicondensate: as shown in Fig. 5.1a, we suddenly displace the trap center along the vertical direction by the small amount  $x_0 = 3.9 \mu\text{m}$ , switching off the magnetic-field gradient. We then let the system free to evolve for a variable time  $t$  in the shifted potential, before detecting the momentum acquired by the atoms. Once again our

experimental observable is the momentum distribution  $\rho(p)$ , which we record after  $t_{exp}=16.5$  ms of free expansion. An example of momentum distribution at two different evolution times  $t=0$  and  $t=0.8 \mu\text{s}$  is reported in Fig. 5.1b. We typically observe an evolving asymmetry of  $\rho(p)$ , presumably due to the presence of an inhomogeneous damping rate braking a part of the sample, as we will discuss later. This asymmetry leads to a systematic shift between the mean position and the peak position of the distribution. We decided to study the evolution of the peak position, which we identify with the averaged momentum  $p_0$  acquired by the atoms. To reduce the effect of the experimental noise, we measure  $p_0$  by fitting the data with a Lorentzian distribution plus a slope. As already observed in Sec. 4.1, time-of-flight images approximately reproduces the in-trap momentum distribution,  $n_{TOF}(x) \approx \rho(p)$ . More precisely, the position in time-of-flight is related to the in-trap momentum by  $x_{TOF}(t) = x(t) + t_{exp}p(t)/m + t_{exp}^2g/2$ , where  $x(t)$  and  $p(t)$  are the *in-situ* position and momentum of the atoms at time  $t$ . Therefore, the peak position in TOF at time  $t$ , moved from the initial position of  $x_{TOF}(t) - x_{TOF}(0) = x(t) + t_{exp}p(t)/m$ , since our initial conditions are  $x(0) = 0$ ,  $p(0) = 0$ . Actually, the contribution of the *in-situ* position  $x(t)$  is negligible at short evolution times (of the order of a fraction of a micrometer), and we can safely identify the measured  $n_{TOF}(x)$  with  $\rho(p)$ , and  $[x_{TOF}(t) - x_{TOF}(0)] \propto p_0$ .

## 5.2 Dynamics in a clean lattice

### 5.2.1 Physical picture and theoretical expectations

The first, fundamental case we investigate is the non-disordered one. In a single lattice, the system at the equilibrium is superfluid even in one dimension; anyway, a dynamical phase transition is expected to occur for increasing velocities<sup>86</sup>, when the wave vector associated with the condensate momentum exceeds a critical value  $p_c$  — one-quarter of the reciprocal lattice constant, i.e.  $p_c = \pi/2$ , at zero interactions. For  $p > p_c$  the coherent motion of the condensate becomes unstable, causing the loss of superfluidity. This transition, experimentally measured in 3D systems<sup>31</sup>, is of classical origin, resulting as an instability in the Gross-Pitaveskii equations of motion in the presence of a single lattice.

For increasing interactions, quantum fluctuations enhance, inducing a ground-state transition from superfluid to insulator, and drive the system towards the Mott-insulating state. As  $p$  increases, the single-particle effective mass grows resulting in a reduction of the effective hopping amplitude  $J_{eff}$  along the current direction. As a consequence, quantum fluctuations, which are determined by the ratio  $U/nJ_{eff}$ , become stronger with  $p$ , implying a concomitant increase of quantum depletion and of the superfluid density  $n_s$ . In the presence of interactions, the dynamical phase transition is thus expected to occur at smaller critical momenta  $p_c < \pi/2$ , already at the mean-field level. In particular, near the superfluid-insulator transition,  $n_s$  is both very small and very sensitive to variation of  $J_{eff}$ , and  $p_c$  is expected to be close to zero. A theoretical mean-field phase diagram, separating regions of stable and unstable motion for the condensate, has been estimated in Altman et al.<sup>5</sup> and is shown in Fig. 5.2a, as a function of the interaction energy and at different dimensionality.

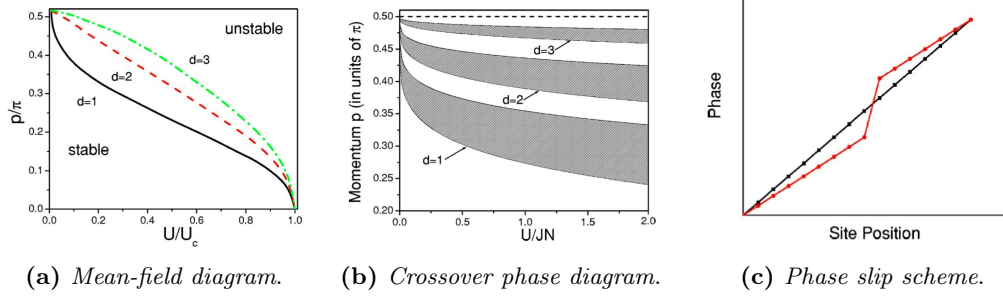


**Figure 5.2:** (a) Mean-field phase diagram separating stable and unstable motion for a condensate. The vertical axis is the condensate momentum in the inverse lattice units and the horizontal axis is the normalized interaction. The results have been obtained for integer filling  $n=1$  at different spatial dimensions. (b) Zero-temperature phase diagram for the non-equilibrium superfluid-insulator transition. The dashed line represents the mean-field transition at  $p = \pi/2$ . The shaded regions correspond to the tunneling action satisfying  $1 \leq S \leq 3$ , obtained within the discrete phase model in different spatial dimensions. Below the shaded regions the tunneling action is large and the current decay is slow, so the superfluid state is stable for long time scales. Above the shaded regions the current decays very fast and the superfluid state is unstable. (c) Schematic representation of a phase slip. Dots represent phases on different sites for uniform and perturbed systems, the lines are guides to the eye. All the figures are adapted from Polkovnikov et al.<sup>74</sup>.

**Beyond mean-field approach.** In one dimension the mean-field approach fails. Quantum and thermal fluctuations are strongly enhanced, thus generating phase slips which induce a decay of the superfluid (or superconducting) flow at even smaller critical momenta. An illustrative phase configuration for a particular phase slip is shown in Fig. 5.2c. Basically a phase slip corresponds to the generation of a large phase difference on a particular link (or close to this link) and a simultaneous reduction of the phase gradient (proportional to the superfluid velocity  $v_s = p/m$ ) in the rest of the chain. As a consequence, by generating phase slips the system reduces its superfluid current, causing a broadening of the mean-field transition.

The nucleation rate of quantum and thermal phase slips in one-dimensional systems has been calculated in Polkovnikov et al.<sup>74</sup>. Here the authors mapped the Bose-Hubbard Hamiltonian (3.3) into the  $O(2)$  quantum rotor model

$$H = \sum_{\langle jk \rangle} -2Jn \cos(\phi_k - \phi_j) + \sum_j \frac{U}{2} n_j^2, \quad (5.1)$$

with  $\phi_j$  and  $n_j$  the conjugate phase and particles number on the site  $j$ , and used the celebrated instanton formula<sup>19,12</sup>  $\Gamma \propto e^{-S}$  to analytically predict the phase slips nucleation rate. Here  $S$  is the action for the bounce solution (instanton) of the classical equations of motion. When the temperature is low enough, thermal fluctuations are suppressed and the nucleation of phase slips is due to quantum tunneling. At temperature higher than a characteristic value  $T_0$ , phase slips are instead thermal activated. The above-mentioned theories<sup>74</sup> estimates this crossover temperature of the order of the Josephson energy,  $k_B T_0 = c\sqrt{nJU}$ , with  $c$  a momentum-dependent factor smaller than unity. The quantum phase slips nucleation rate is found to scale

in interaction energy, density and momentum as,

$$\Gamma_q = e^{-7.1\sqrt{\frac{nJ}{U}}\left(\frac{\pi}{2}-p\frac{\lambda_1}{2\hbar}\right)^{\frac{5}{2}}}, \quad (5.2)$$

in the limit  $p \rightarrow \pi/2$ . On the other hand, the thermal nucleation rate scales as,

$$\Gamma_t \propto e^{-\frac{4nJ}{3k_B T}\left(\frac{\pi}{2}-p\frac{\lambda_1}{2\hbar}\right)^3}. \quad (5.3)$$

The complete description and mathematical derivation of Eqs. (5.2-5.3) is in Danshita and Polkovnikov<sup>25</sup>. As already noticed, for small enough  $nJ/U$ , quantum fluctuations start to dominate and the phase slip nucleation rate exponentially grows, thus destroying superfluidity, whatever the momentum  $p$ . In fact, a strong inhibition of transport already at small momenta has been observed in experiments with low-density ( $n \simeq 1$ ) 1D bosons in a lattice<sup>35,63</sup>. The zero-temperature crossover phase diagram in Fig. 5.2b, shows that the classical transition from stable phases (where the nucleation rate is small, and the tunneling action is large, say  $S > 3$ ) to unstable ones (where there is no exponential suppression of the phase slip rate, say  $S < 1$ ) broadens, at least in 1D, turning into a wide crossover (the shaded region).

### 5.2.2 Experimental observation

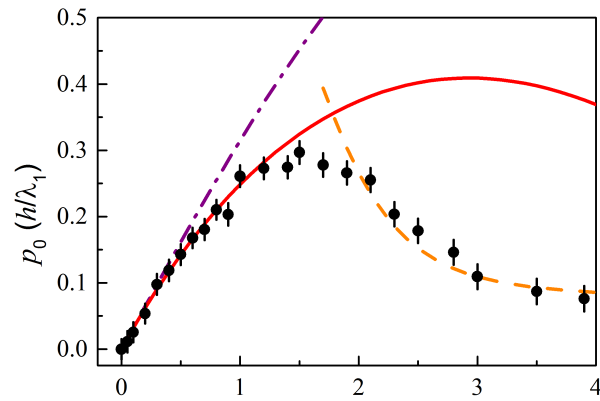
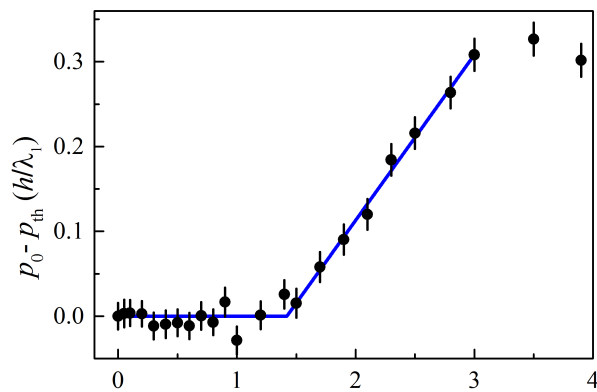
A typical observation of the evolution of  $p_0$  in the single lattice is shown in Fig. 5.3a, at the specific interaction energy  $U = 1.26J$  and density  $n = 3.6$ . Surprisingly, we clearly observe a rather sharp transition from a weakly dissipative regime at low momenta to a strongly unstable one at large  $p$ . In order to quantitatively comprehend the experimental observation, we perform a close comparison with the theoretical solution of the semiclassical equations of motion.

The motion of the atoms in the harmonic oscillator in the presence of a lattice can be modeled by solving the system of equations:

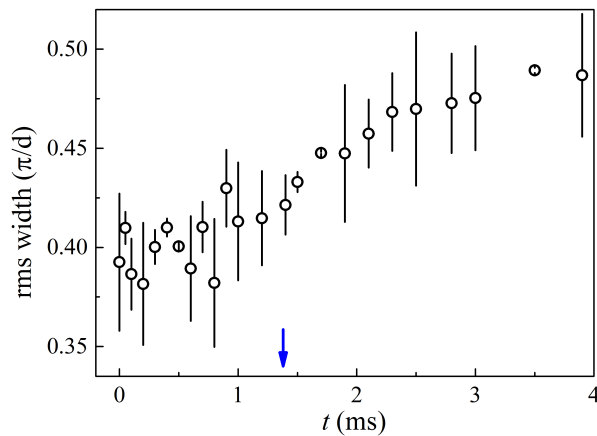
$$\begin{cases} \dot{p} = -m\omega_x^2 x - 2m\gamma\dot{x} \\ \dot{p} = m^*(p)\ddot{x} \end{cases} \quad (5.4)$$

where  $m^*(p) = \hbar^2 \cos(pd/\hbar)/2Jd^2$  is the atomic effective mass in the lattice. In the absence of any dissipation, the atoms would oscillate with a frequency  $\omega^* = \omega_x \sqrt{m/m^*} \simeq 2\pi \times 90$  Hz, where  $m^* = m^*(0) \simeq 2.8m$ . For non vanishing dissipation  $\gamma$ , the displacement of the peak momentum  $p_0$  could instead be approximated with a damped oscillation  $p_0(t) = m^*\omega^{*2}x_0/\omega' \sin(\omega't)e^{-\gamma^*t}$ , where  $\omega' = \sqrt{\omega^{*2} - \gamma^{*2}}$  and  $\gamma^* = \gamma m/m^*$ .

We fit the evolution of the peak momentum  $p_0$  with the function  $x(t) + p(t)t_{exp}/m$  (as explained in Sec. 5.1), where  $x(t)$  and  $p(t)$  are the solution of Eqs. (5.4), leaving  $\gamma$  as a free fitting parameter. We identify two different regimes in the dynamical evolution of the system. At short times we find almost constant damping rates  $\gamma = 2\pi \times (20-300)$  Hz, depending on the interaction energy. At longer times, as  $p_0$  increases towards the center of the Brillouin zone ( $p = h/2\lambda_1$ ), we observe a sudden increase of  $\gamma$  which stops the growth of  $p_0$ . The following decay of  $p_0$  towards zero momentum can be again fit with a constant damping rate of the order of 1 kHz.

(a) Time-evolution of  $p$ .

(b) Difference between fit and experimental data.



(c) Time-evolution of the rms width.

**Figure 5.3:** Transport in nondisordered lattices. (a) Time evolution of the peak momentum for  $U=1.26J$  and  $n=3.6$ . The experimental data (dots) are fitted at short times with a damped oscillation with  $\gamma/2\pi = 135(10)$  Hz (continuous line) and at long times with  $\gamma/2\pi = 600(50)$  Hz (dashed line). The dash-dotted line is the expected oscillation in the absence of damping. (b) The difference between the fit to the initial damped motion and the experimental data (dots) is fitted (continuous line) to estimate the critical momentum. (c) Time evolution of the momentum rms width.

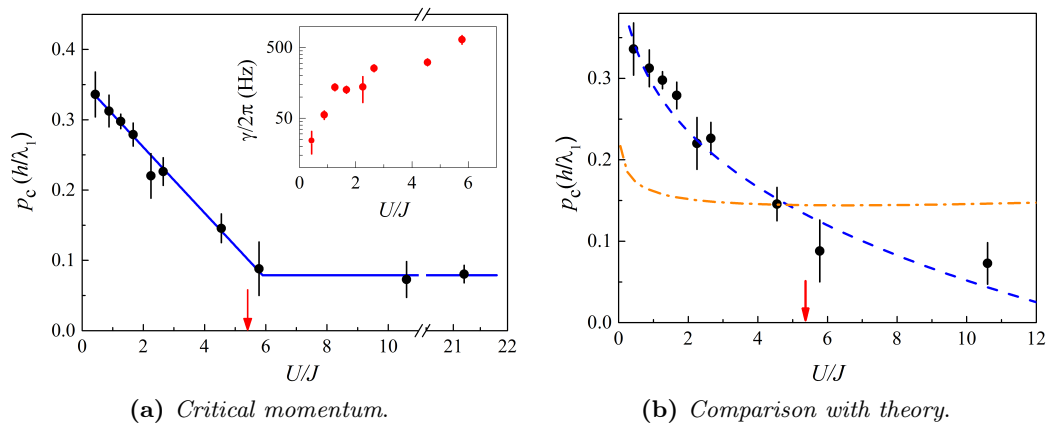


**Figure 5.4:** (a) Critical momentum for non disordered lattices (dots) versus the interaction energy. The continuous line is a linear fit, the arrow marks the critical  $U/J$  required for the superfluid-Mott insulator transition at  $n=2$ . In the inset is plotted the evolution of the initial damping rate  $\gamma$  versus the interaction energy. (b) The critical momentum (dots) is compared with the predictions for the phase-slip nucleation rate in the quantum (blue dashed line) and thermal (orange dash-dotted line) regimes.

This change of behavior is accompanied by a sudden increase of the width of  $\rho(p)$ , as shown in Fig. 5.3c, followed by a steady broadening for increasing time.

This observation is in contrast with what has been previously observed in low-density experiments<sup>63</sup>. This is probably a consequence of the high density  $n$  present in our inhomogeneous system; while the low-density fraction of the system stops already at small momenta, the observed sudden instability is induced by the higher- $n$  component, for which the theoretical expressions (5.2-5.3) predict a fast exponential increase of  $\Gamma$  with  $p$ . In fact, Eqs. (5.2-5.3) strongly depend on  $n$ , which appears in the exponent of the function. The hypothesis of an inhomogeneous nucleation rate is actually supported by the observation of asymmetric momentum profiles  $\rho(p)$  at large  $p$ , as shown for example in Fig. 5.1b.

**Critical momentum.** We estimate the critical momentum  $p_c$  separating the initial regime of weaker dissipation from the strongly unstable one, by linearly fitting the difference between the experimental data and the fit of the initial oscillation, as shown in Fig. 5.3b. We performed similar dynamical measurements for different interaction energies  $U$ . The measured  $p_c$  features a clear decrease for increasing  $U$  at constant  $J$ , as shown in Fig. 5.4a. Eventually,  $p_c$  approaches zero as  $U$  approaches the predicted critical value for the Mott insulator ( $U_c/J=2 \times 2.674$  for the calculated<sup>24</sup> mean occupation  $n=2$ ). Actually, even deep into the insulating regime we observe a small but finite  $p_c$  of the order of the inverse size of the system, as previously observed<sup>63</sup>. A piecewise fit of the data, gives us a critical interaction comparable with theoretical expectation:  $U_c/J=5.9(2)(4)$ , where the uncertainties are statistical and systematic, respectively, allowing us to precisely determinate the onset of the Mott insulating regime by measuring a vanishing transport even in 1D, as already observed in 3D systems<sup>63</sup>.

**Damping rate.** From the evolution of the peak momentum  $p_0$  at momenta smaller than  $p_c$ , i.e. before the system breaks, we can extract the oscillation damping rate  $\gamma$ , a quantity strictly related to the phase slip nucleation rate  $\Gamma$ , via  $\gamma \propto \Gamma/p$ , at least for vanishing momenta<sup>23</sup>. No theoretical models estimate the phase slip nucleation rate for our specific regime of time-dependent large momenta  $p$ , and inhomogeneous density. We then try to compare the experimental observations with the existing theoretical models discussed in Sec. 5.2.1. For our experimental parameters the Josephson energy is in the range  $(1 - 4)J$ , depending on the interaction energy, of the same order of the system temperature  $\sim 3J$ . We therefore expect that both the thermal and the quantum mechanisms are significant in the activation of the phase-slip processes.

The evolution of the fitted damping with the interaction energy is plotted in the inset of Fig. 5.4a; as already noticed  $\gamma$  increases for increasing  $U$ , since quantum and thermal fluctuations become important. Anyway, a direct comparison between our measured damping  $\gamma$  and the calculated nucleation rates (5.2-5.3), cannot be easily performed: in the experiment in fact,  $p$  is rapidly changing from zero to large values, strongly affecting the nucleation rate, thus preventing a precise measure of  $\Gamma$ . We thus employed the two models (5.2-5.3) to estimate the critical momentum required to enter the strongly dissipative regime at different interactions, i.e.  $p_c(U)$  such that  $\gamma(p_c)/2\pi \simeq 1\text{kHz}$ , as in the experiment. In the calculation we use the experimental parameters, we impose  $T=3J$ , and we adjust an arbitrary constant to reproduce the observed  $p_c$  at  $U/J=4.5$ . The experimental data and the theoretical predictions for  $p_c$  are shown in Fig. 5.4b. While the quantum nucleation rate capture the observed evolution of  $p_c(U)$ , the thermal rate at constant temperature shows only a weak dependence on  $U$ , thus suggesting a more relevant role of the quantum mechanism. Anyway, these are preliminary results; a more precise investigation on the quantum/thermal origin of phase slips could be obtained studying the evolution of  $\gamma$  with  $p$  at variable temperatures.

### 5.3 Dynamics in a disordered lattice

In the previous section we analyzed the motion of one-dimensional quasicondensates in a periodic potential; here repulsive interactions and lattice effects can generate quantum fluctuations able to drive the system into an insulating phase. We now investigate the impact of disorder on this superfluid-insulator transition, studying the dynamics of one-dimensional bosons moving in a quasiperiodic lattice. Disorder, in fact, is considered the main source of dissipation in many physical systems, ranging from superconductors to superfluid Helium. Experiments employing strongly disordered nanowires close to the superconductor-insulator transition, observed phenomena related to the quantum phase-slip nucleation mechanism<sup>8</sup>, and few models of dissipation due to disorder have been developed<sup>52,1</sup>. We exploit our ability to control simultaneously disorder and interactions to address the dynamics of a superfluid state in disordered potential. In particular, here we focus on the weakly interacting regime  $U/J < 3$ , where  $p_c$  for the non-disordered lattice can be very precisely measured. In the next section we will study the bosonic transport from weak to strong interactions.

The experimental scheme is described in Sec. 5.1; a finite disorder  $\Delta$  is now loaded

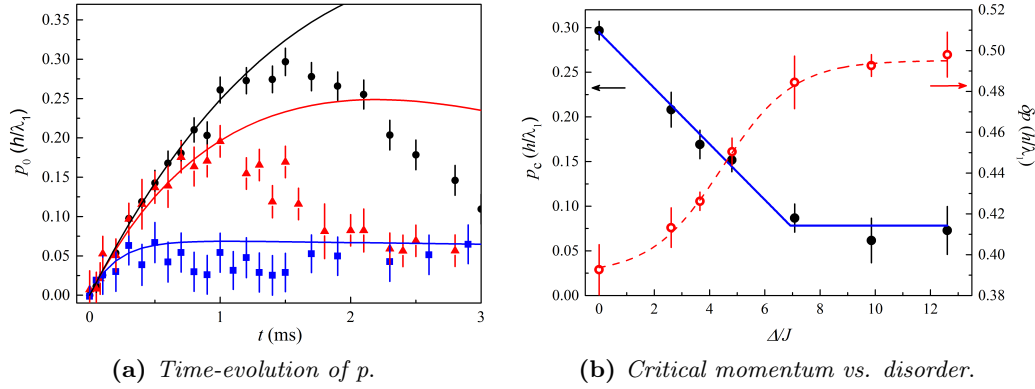


**Figure 5.5:** Transport in disordered lattices. (a) Time-evolution of the peak momentum at  $U=1.26J$  for  $\Delta/J=0$  (dots),  $\Delta/J=3.6$  (triangles) and  $\Delta/J=10$  (squares). The lines are fits to the initial oscillation with the semiclassical equations of motion. The fitted damping rates are  $\gamma/2\pi=130(10)\text{Hz}$ ,  $\gamma/2\pi=250(30)\text{Hz}$  and  $\gamma/2\pi=1.1(6)\text{kHz}$ , respectively. (b) Critical momentum  $p_c$  (full circles) and initial rms momentum width  $\delta p$  (open circles) for a fixed interaction energy ( $U/J=1.26$ ) and increasing disorder strength. A linear fit (continuous line) is used to estimate  $\Delta_c$ , while the dashed line is a sigmoidal fit of  $\delta p$ .

together with the main lattice, and the system evolve in a quasiperiodic potential. Fig. 5.5a shows the impact of increasing disorders on the evolution of  $p_0$  at fixed  $U$ ; the experimental data are analyzed as in Sec. 5.2.2: again we clearly distinguish two dynamical regimes, and we extrapolate the average damping rate  $\gamma$  of the stable regime and the critical momentum  $p_c$ . A small disorder  $\Delta$  results in a moderate increase of  $\gamma$ , and in an anticipated instability; at large disorder,  $\gamma$  drastically increase and the system immediately breaks. A summary of the evolution of the critical momentum  $p_c$  at different  $\Delta$  and fixed  $U$  is shown in Fig. 5.5b;  $p_c$  features a clear decreasing trend for increasing disorder. Above a critical disorder strength  $\Delta_c$  of the order of the total interaction energy per atom  $nU$ ,  $p_c$  stops decreasing and stabilize around a small value close to zero, as observed for the Mott-insulator regime. This is actually the regime where a weakly interacting Bose glass is predicted to appear, i.e. where the disorder induces a new localized regime, overcoming the delocalization effect of the interaction.

Both the increase of  $\gamma$  and the reduction of  $p_c$  with increasing  $\Delta$ , can be justified by the following heuristic picture: in the presence of disorder, the hopping amplitude  $J$  reduces, resulting in an effective tunneling  $J_{\text{eff}}(\Delta) < J$ , thus inducing an increase of the phase-slips nucleation rates (5.2-5.3) which exponentially depend on  $J$ . In fact, a related phase-slip model<sup>52</sup> developed for disordered superconductors suggests nucleation rates scaling exponentially with  $\Delta$ . Anyway, to our knowledge, the existing theoretical models only concern weakly interacting systems in absence of a lattice and at small momenta, thus preventing a direct comparison to our experimental case. The development of rigorous theoretical models calculating the phase-slips nucleation rate in the disordered case is clearly necessary.

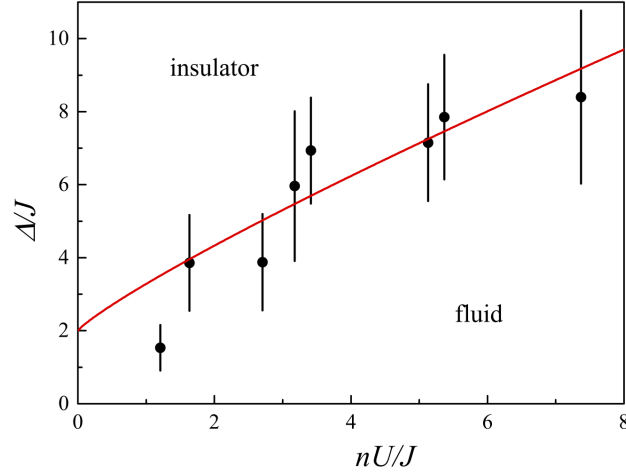


**Figure 5.6:** Critical disorder to enter the insulating phase vs interaction energy. The experimental data from the critical momentum (dots) are fitted with the model described in the text (line). The uncertainty is dominated by a 20% error on the calibration of  $\Delta$ .

### 5.3.1 Transport diagram

Motivated by the possibility to discriminate the fluid regime from the insulating one, thus locating a transition line in the  $U$ - $\Delta$  diagram, we studied how  $\Delta_c$  evolves with  $U$ . For each  $U$ , we estimate  $\Delta_c$  by fitting the evolution of  $p_c(\Delta)$  with a piecewise function, as already shown for  $U = 1.26J$  in Fig. 5.5b. The summary of these measurements is reported in Fig. 5.6, and compared with the coherence diagram in Fig. 4.3.  $\Delta_c$  clearly increases with the interaction energy, confirming that, as the interactions grow, the critical momentum (which measure the conductivity of the system) is less affected by disorder. The large uncertainty on the experimental data is due to the unavoidable 20% error on the calibration of  $\Delta$ ; anyway, the experimental transition is clearly visible, and can be compared to known theoretical models.

**Comparison with theory.** The transition from fluid to (BG) insulating phases in a weakly-interacting system of disordered bosons has been studied in many theoretical works, using different approaches. All the theoretical studies considered random or gaussian correlated disorder, no one ever focused on the bichromatic case. In Fontanesi et al.<sup>38</sup> the quantum phase transition was studied in the framework of the Bogoliubov theory, i.e. linearly expanding the solution of the mean-field Gross-Pitaevskii equation. As shown in Fig. 5.7a, the mean field phase transition at zero temperature exhibits two different trends, depending on the ratio between the interaction energy and the characteristic energy associated to the correlation length of the disordered potential  $\eta$ ,  $E_c = \hbar^2/(2m\eta^2)$ . In the limit  $E_{\text{int}} \ll E_c$ , the healing length is much longer than the disorder correlation length; as a consequence the disorder is effectively an uncorrelated white noise (WN) potential. The opposite case  $E_{\text{int}} \gg E_c$  marks the Thomas-Fermi (TF) regime, where the healing length is smaller than  $\eta$ . The numerical results give two power-law dependencies of the

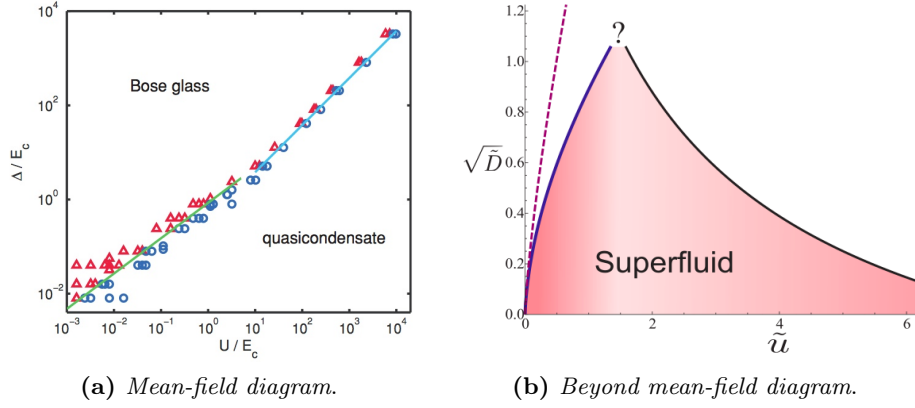


**Figure 5.7:** Theoretical phase diagrams. (a) Sketch of the mean-field phase diagram of the 1D Bose gas as a function of interaction and disorder. Triangles represent the Bose glass, circles the quasicondensate. Picture taken from Fontanesi et al.<sup>38</sup>. (b) Beyond mean-field disorder-interaction diagram. The continuous blue boundary at weak interactions corresponds to the set of points mapped to the separatrix of the RG flow. The dashed red line marks the points where the classical theory predicts a transition. The phase boundary at strong interactions is obtained from the weak disorder theory of Giamarchi and Schulz<sup>42</sup>. Picture taken from Vosk and Altman<sup>91</sup>.

fluid-to-insulator transition in the two limiting cases:

$$\frac{\Delta}{E_c} = A \left( \frac{E_{\text{int}}}{E_c} \right)^\alpha, \quad (5.5)$$

with  $\alpha$  equal to 3/4 and 1, respectively, and  $A \sim 1$ .

Quantum corrections to the mean-field approach, were obtained by Vosk and Altman<sup>91</sup>. Here the authors studied the superfluid to insulator transition in the one-dimensional disordered system using a real-space renormalization-group (RG) approach<sup>4</sup>. The RG flow was computed by deriving an effective quantum Josephson array model (conventionally described by the O(2) quantum rotor Hamiltonian (5.2)) for the weakly-interacting condensate fragmented into many puddles weakly coupled by the disorder potential

$$H = \sum_i -J_i \cos(\phi_{i+1} - \phi_i) + \sum_i \frac{U_i}{2} n_i^2, \quad (5.6)$$

and estimating the distribution of  $U_i$  and  $J_i$ , both in the WN and TF regimes. Here  $U_i$  is the charging energy of the puddle  $i$  and  $J_i$  is the Josephson coupling between puddle  $i$  and puddle  $i + 1$ . Actually, the physical model is the same one used in Sec. 5.2.1 to evaluate the evolution of the phase-slip nucleation rate via the instanton method, and assumed to be responsible of the observed damped dynamics in the absence of disorder. The beyond-mean field phase diagram is shown in Fig. 5.7b. Here the continuous line represents the RG transition, while the dashed line shows the mean-field transition; the diagram is given in terms of dimensionless disorder  $\tilde{D}$  and interaction  $\tilde{u}$ . The predicted exponent is  $\alpha = \alpha(U) < 1$ .

A close comparison between the experimental transition observed in Fig. 5.6 and these theoretical models is not straightforward. Theoretical studies deal with

zero-temperature homogeneous systems in gaussian correlated random potentials. In the experiment, besides the finite-temperature problem, we investigate a particular kind of spatially correlated disorder, the quasiperiodic lattice, which shows specific properties (see Sec. 2.5). As shown in Sec. 3.2, the single-particle fluid to insulator transition in the quasiperiodic potential, is at a nonzero critical disorder  $\Delta = 2J$ , affecting the shape of the expected phase diagram, at least for vanishing interactions. In the absence of any analytical model for the SF-BG transition in the quasiperiodic lattice, we fit the experimental data with the function  $(\Delta_c - 2)/J = A(nU/J)^\alpha$ , in order to account the critical  $\Delta/J \simeq 2$  required to localize the non-interacting system. This choice is supported by the results of the DMRG study in Roux et al.<sup>81</sup>, already discussed in Sec. 4.4.1. The fit gives an exponent  $\alpha = 0.86(22)$  and a coefficient  $A = 1.3(4)$ . We exclude from the fit the data point at  $\Delta/J < 2$ , which should be described by a different mechanism of competition between the mini-band structure of the quasiperiodic lattice and the interaction energy.

The correlation function of a quasiperiodic potential is non-decaying, which implies a vanishing correlation energy  $E_c$  on a system with infinite length. Anyway, the actual length of the experimental system is relatively small; we can thus estimate an upper bound for  $E_c$  from the half-width of the first oscillation of the correlation function,  $E_c \simeq 8\hbar^2(\beta - 1)^2/m\lambda_1^2 \simeq J$ , where  $\beta = \lambda_1/\lambda_2$ . For our parameters,  $E_c/J \simeq 0.7$ , almost one order of magnitude smaller than the explored range of  $E_{\text{int}} = nU$ , therefore the experimental problem is the TF (or smooth disordered) limit. The experimental exponent is compatible with both the mean-field prediction  $\alpha=1$  for correlated Gaussian disorder in the Thomas-Fermi regime, and the beyond mean-field expectation  $\alpha = \alpha(U) < 1$ . Unfortunately the large uncertainty on the experimental data does not allow us to discriminate between the two approaches. Anyway, a careful assessment of finite-size and finite- $T$  effects and a theoretical study considering the quasiperiodic disordered landscape is required to establish a direct relation between the observed critical line and the theoretical fluid-insulator transition.

**Transport and coherence.** The existence of a critical disorder  $\Delta_c$  above which the system is insulating, whatever the impulse, is a signature of the presence of a weakly interacting Bose glass phase. In fact, the decrease of  $p_c$  is accompanied by the increase of the equilibrium (i.e.,  $t = 0$ ) rms momentum width  $\delta p$  – essentially the inverse correlation length  $\xi^{-1}$  (see Sec. 4.1). As shown in Fig. 5.5b, at fixed interaction,  $\delta p$  starts to increase already at disorder smaller than  $\Delta_c$ , signaling the progressive crossover of the system into a regime with reduced correlation length. For disorder larger than  $\Delta_c$ , when  $p_c$  is almost zero and the system is insulating, the coherence is lost and the correlation length is of the order of the lattice spacing,  $\xi \simeq d$ .

In Fig. 5.8 we compare the complementary information obtained by measuring the dynamical properties of the system – signaling a fluid to insulator transition, with the evolution of its momentum width (measured in Fig. 4.3) – revealing its coherence properties. In the weakly-interacting side of the phase diagram, the two quantity evolve similarly, following the same crossover line. While transport measurements allow the direct detection of fluid and insulating regimes, the evolution of the correlation length suggests a broad crossover between coherent and incoherent

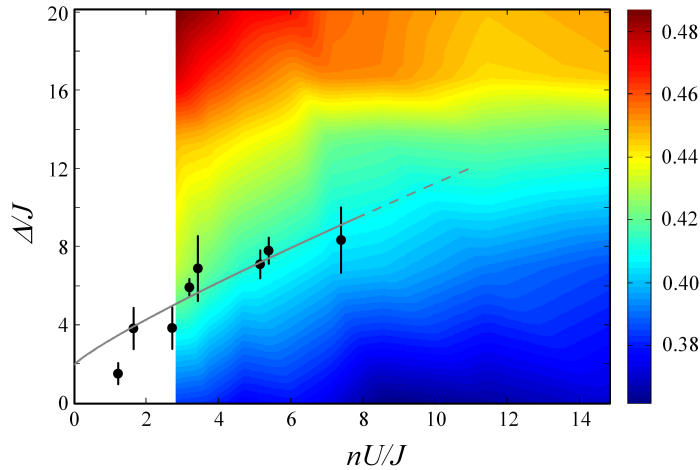


**Figure 5.8:** The experimental dynamical diagram shown in Fig. 5.6 signaling the onset of the fluid-insulator transition is compared with the coherence diagram, revealing the crossover from correlated to uncorrelated regimes. The points in the coherence diagram are adapted from Fig. 4.3, rescaling  $U/J$  with  $nU/J$ , where  $n$  is the mean site occupation at the interaction  $U$ .

regimes, as already discussed in Sec. 4.3. Anyway, the conducting/insulating nature of the system results intimately related to its coherence properties. Once again the physical picture is that of a weakly-interacting condensate fragmented into many puddles weakly coupled through the disorder potential. Every puddle has a well defined phase, and phase coherence between puddles, which define the coherence properties of the system, depends on the local interaction energy, i.e. on the local density. Disorder tends to uncouple different puddles. When coherence is locally broken, the superfluid phase unwinds, and the superfluid flow vanishes, as shown for example from RG calculations, affecting the transport properties of the system. In the experiment we deal with a strongly inhomogeneous system. In a generic point of the  $U$ - $\Delta$  diagram, depending on the local density, coherence is broken in some tubes, while it survives in others (where most of the puddles is still coherently coupled). The fraction of coherent tubes contributes to transport, thus resulting in a finite conductivity when some external force is applied to the system. When instead coherence is broken in most of the tubes (for example at strong disorder, or at vanishing interactions), transport is completely suppressed, and the system acts as an insulator. In other words, transport techniques measure a property of the conducting part of the system; in fact, we observe a sharp transition separating fluid and insulating phases, even in the inhomogeneous setup. On the other hand the momentum width measures an averaged correlation length of the system, which depends on the fraction of coherent and incoherent tubes; as a consequence in the coherence diagram sharp transitions broadens into smooth crossovers.

## 5.4 Mobility from weak to strong interactions

In Sec. 4.3 we plotted a diagram of the momentum width in the  $U$ - $\Delta$  plane, showing crossovers from coherent to incoherent regimes, at both weak and strong

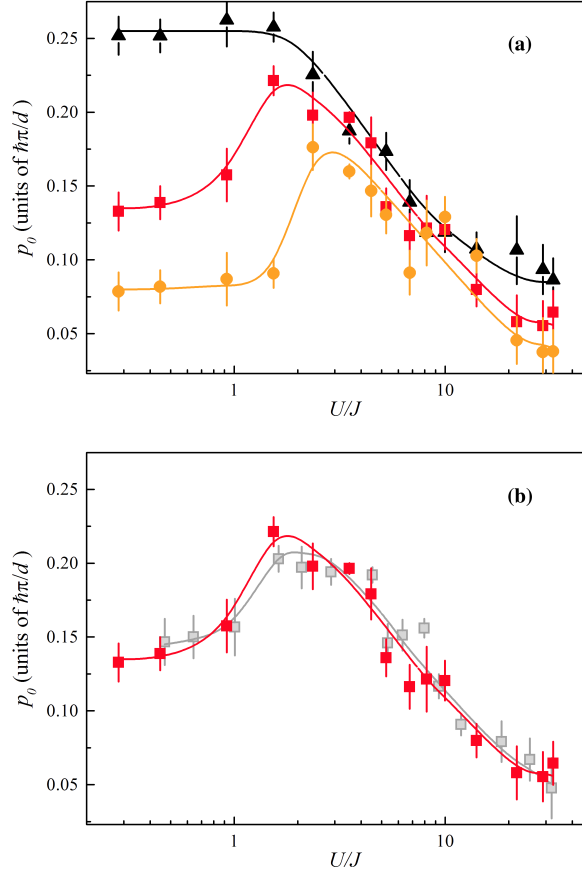


**Figure 5.9:** Effective mobility vs disorder and interaction. (a) Mean momentum  $p_0$  acquired by the system after a fixed evolving time  $t = 0.9\text{ms}$  in the tilted potential for three different disorder strengths,  $\Delta=0$  (black triangles),  $\Delta=6.2J$  (red squares) and  $\Delta=8.8J$  (orange circles). The lines are a guide to the eye. The error bars are the standard deviation of typically 5 measurements. (b) The  $\Delta=6.2J$  measurements is acquired for two temperatures of the SF component,  $k_B T=3.1(4)J$  (red) and  $k_B T=4.5(7)J$  (grey).

interactions, see Fig. 4.3. In order to confirm the insulating nature of the observed incoherent regime in the whole  $U$ - $\Delta$  diagram, we performed transport measurements from weak to strong interactions, in the same experimental conditions of Sec. 4.2. The experimental technique used to transfer an impulse to the trapped atoms is as described in Sec. 5.1. We apply a sudden shift to the harmonic confinement by  $x_0 = 3.9 \mu\text{m}$ , which corresponds to a force  $F \sim mg/3$  (with  $g$  the gravity acceleration). At large  $U$  the system is strongly incoherent and its momentum width broadens, thus making the transport measurement dirtier. To simplify the experimental procedure, we decided to acquire the accumulated mean momentum  $p_0$  after a fixed evolving time  $t = 0.9\text{ms}$ , just before the breaking of the clean system at vanishing interactions. Once again,  $p_0$  essentially measures the drift velocity in presence of the force  $F$ , and it can thus be related to an effective mobility of the system.

Fig. 5.9a shows the evolution of  $p_0$  with  $U$  for three different values of  $\Delta$ . In the clean case ( $\Delta = 0$ )  $p_0$  reduces smoothly across the superfluid-Mott insulator transition, due to the progressive enhancement of (quantum and thermal) phase

slips for increasing interactions. At finite  $\Delta$  and vanishing interaction energy, the system is an Anderson insulator, featuring a reduced mobility (which is however not zero, because of the finite  $F$ ). The presence of a weak interaction restores coherence, as described in the previous section, inducing an increased mobility. At strong interactions the physical picture drastically change. As discussed in Sec 1.2, the strongly-correlated Bose gas can be localized in the presence of a finite disorder. This is confirmed by the experimental observations: at large  $U$  disorder and interactions cooperate in destroying mobility; the resulting disordered insulating state is even less mobile than the standard Mott insulator. The measurements here reported are not exhaustive, and clearly cannot be compared to theoretical predictions. A more detailed experimental study, using for example the experimental techniques introduced in the previous sections, thus measuring the time-evolution of  $p_0$  even in the strongly correlated regime, is required. Anyway, these observations give a first indication of the mobility across the whole  $U$ - $\Delta$  plane, confirming that both the incoherent regimes at small and large  $U$  are actually insulating regimes, not simply incoherent excited phases.

By exploiting an experimental heating mechanism (see Sec. 4.5.2), we measured the transport properties of the system also at a higher temperature. The measurement is shown in Fig. 5.9b, and indicates that the mobility for intermediate disorder strength is essentially  $T$ -independent in the explored range  $k_B T = (3.1 - 4.5)J$ , as expected by theory<sup>2</sup>. This measure, combined with the observation of a constant thermal correlation length at weak interactions, confirms the idea that the thermal regimes observed in the experiment are effectively related to zero- $T$  phases.



## Chapter 6

# Excitation spectrum

A crucial ingredient to characterize the quantum phases composing a many-body system is the low-energy excitation spectrum, i.e. the system response to a weak perturbation. As shown in Sec. 3.3, at low temperatures disorder and interactions deeply affects the phases of condensed bosons. In the absence of disorder, the quasicondensate is in a superfluid phase, characterized by the typical phonon dispersion relation at low energies. In a lattice, strong interactions localize the system, opening a Mott gap; the elementary excitations are then particles and holes and the absorption occurs only at frequencies of the order of the interaction energy ( $h\nu \sim U$ , with  $U$  is given by Eq. 3.6 in the Hubbard regime). On the other hand, in the presence of disorder, even the incommensurate part of the system (Anderson) localizes, but now the excitation spectrum is expected to be gapless. The resulting general picture of the excitation spectrum predicted in the lattice-disordered system is depicted in Fig. 6.1. The low frequency absorption  $0 < h\nu < W$ , with  $W$  the effective lattice bandwidth, is a consequence of the formation of a Bose glass at incommensurate fillings. The second distribution centered at frequency  $h\nu \approx U$ , comes from particle-holes excitations generating doubly occupied sites.

In Chapters 4-5 we investigated the coherence and transport properties of the system of disordered interacting bosons, revealing the presence of a reentrant incoherent-localized regime at strong interactions. In this Chapter we will focus on its excitations properties from weak to strong interactions, in order to eventually probe the nature of the observed insulating phases.

### 6.1 Inelastic scattering and Bragg spectroscopy

In general, the information concerning the excitation spectrum of a many-body system are extracted from inelastic scattering experiments. In condensed-matter systems, scattering neutrons off crystalline samples provided fundamental insights into the microscopic and the energetic structure of matter; for example, neutrons scattering was used in the early sixties to measure the energy-momentum phonon-like dispersion relation for the superfluid  $^4\text{He}$ . A schematic of such experiments is shown in Fig. 6.2a: a monochromatic neutron beam (i.e. a beam of neutrons with a single wavelength or energy) is sent onto the sample. When the neutrons penetrate the sample they scatter the atoms; if the neutrons excite the atoms they lose the

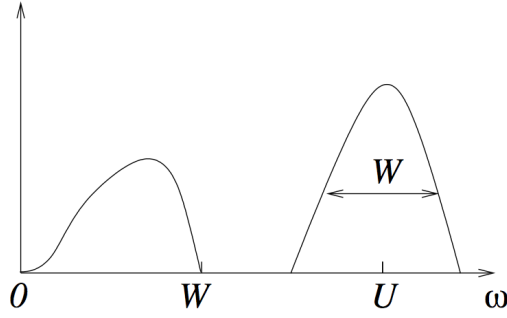


**Figure 6.1:** Sketch of the full absorption spectrum of disordered lattice bosons. The peak at  $\omega \sim U$  stems for the particle-hole excitations, whereas the low-frequency absorption appears as a consequence of the presence of a Bose glass at incommensurate filling.  $W$  is the effective lattice bandwidth. The image is taken from Orso et al.<sup>66</sup>

energy  $\hbar\omega$  absorbed by the excitation, and acquire a momentum  $\hbar q$ , diverting their output direction. A detector placed at some angle beyond the sample, allows to count the number of remaining neutrons and to analyze possible changes in their energy, thus measuring the partial differential cross section for the overall process, i.e. the number of neutrons scattered per second into a certain small solid angle and within a certain small energy range. This number, the scattering cross section, is proportional to the dynamical structure factor  $S(q, \omega)$ , which is essentially the Fourier transform of the density-density correlation function, a central quantity in the theoretical description of many-body systems. Therefore, inelastic scattering experiments allow to directly measure the dynamical structure factor. Generally  $S(q, \omega)$ , at fixed transferred momentum  $\hbar q$  and for varying transferred energies  $\hbar\omega$ , measures the energy of the elementary excitations in the system, thus allowing us to extract its excitation spectrum.

In the context of cold atoms, inelastic scattering experiments are realized in a different way: instead of diffracting particles on a grating of atoms, atoms are diffracted on a grating of coherent light. This process induces Bragg scattering, a stimulated two-photon transition connecting two different momentum states of the same internal ground state. The schematics of the Bragg transitions is shown in Fig. 6.2b: the atomic gas is shone with two simultaneous off-resonant light pulses (Bragg beams), with a tunable frequency-difference  $\delta\nu$ . The wavelength of the Bragg beams and the angle  $\theta$  between them set the momentum  $q$  imprinted on the sample. During the Bragg pulse, the atoms absorb photons from one beam and are stimulated to emit photons in the second beam, crossing a virtual state. The initial and final momentum states form an effective two-level system coupled by a two-photon Raman process. The transition is resonant provided that energy and momentum are conserved: atoms with initial momentum  $p_i$  end up in the same internal state with a final momentum  $p_f = p_i + \hbar q$ , while the energy difference between the initial and final states is given by the frequency-difference between the two Bragg beams ( $\hbar\omega = h\delta\nu$ ). Therefore, changing the relative detuning of the two Bragg beams at fixed transferred momentum  $q$ , one can tune the energy of the excitation created into the system. As neutron scattering in condensed-matter experiments, this process directly measures the dynamical structure factor  $S(q, \omega)$ ; it

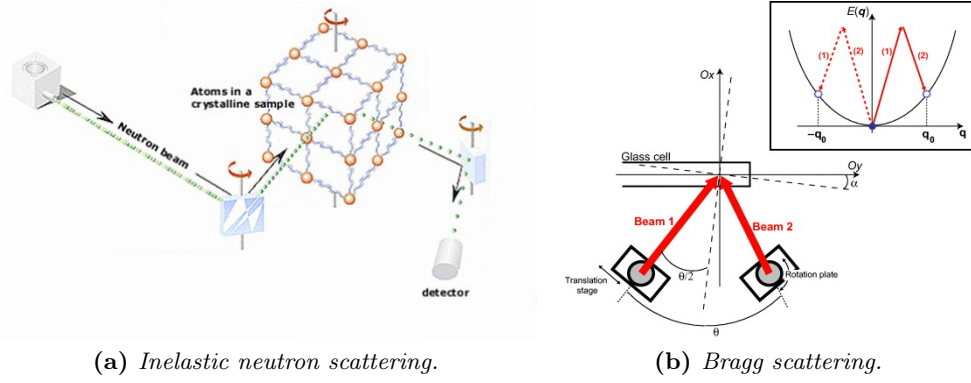


**Figure 6.2:** (a) Schematic of an inelastic neutrons scattering experiment. A monochromatic neutron beam hit the sample exciting the atoms. A detector counts the number of neutrons scattered per second into a certain small solid angle and within a certain small energy range thus measuring the scattering cross section for the overall process. (b) Schematic of the Bragg scattering. Two off-resonant light pulses (Bragg beams), with frequency-difference  $\delta\nu$  and angle-displacement  $\theta$  are shone onto the atomic gas, inducing a Bragg transition (inset), as explained in the text. Picture readapted from Clément et al. <sup>18</sup>

can therefore be used (and actually has been used) to probe the density fluctuations of the system <sup>87</sup> and its excitation spectrum <sup>88,32,17</sup>.

## 6.2 Experimental procedure

A simple way to realize a two-photon Bragg scattering experiment is to modulate in amplitude the external lattice potential (2.5), thus performing, in some sense, a lattice modulation spectroscopy experiment. This is the kind of spectroscopy we use to investigate the system excitations. The experimental sequence is the following: after the standard loading procedure of the interacting one-dimensional system in the quasiperiodic lattice (see Sec. 4.2), the primary lattice is modulated in amplitude for a fixed time  $t_{mod}$ . The resulting lattice potential have the form:

$$V(x, t) = (V_0 + A_{mod} \sin(2\pi\nu_{mod}t)) \cos^2(kx), \quad (6.1)$$

where  $k = 2\pi/\lambda$  is the wave-vector of the optical lattice, while  $A_{mod}$  and  $\nu_{mod}$  are the amplitude and the tunable frequency of the modulation, respectively. The modulation introduces two sidebands with frequencies  $\pm\nu_{mod}$  relative to the lattice laser frequency  $c/\lambda$ , defining the energy  $h\nu_{mod}$  of the excitation. Because of the Bragg condition, atoms scattering two photons receive a momentum transfer of  $0\hbar k$  or  $2\hbar k$ . Tuning the frequency of the modulation it is then possible to experimentally measure the excitations of the system at fixed transferred momentum  $q = 2\hbar k$ .

After the excitation, the lattice potentials are ramped down in 300 ms with exponential ramps, allowing the system to re-thermalize via atom-atom collisions. The absorbed energy is extracted from the temperature increase, which is measured through standard time-of-flight images. In the BEC regime, the temperature is estimated from the measured condensed fraction  $\eta(\omega)$ , with  $\omega = 2\pi\nu$ . Since typically  $\eta < 0.3$ , we use the first order approximation  $\Delta T(\omega) = -T_c(\eta(\omega) - \eta_0)/3$ , where  $\eta_0$  is

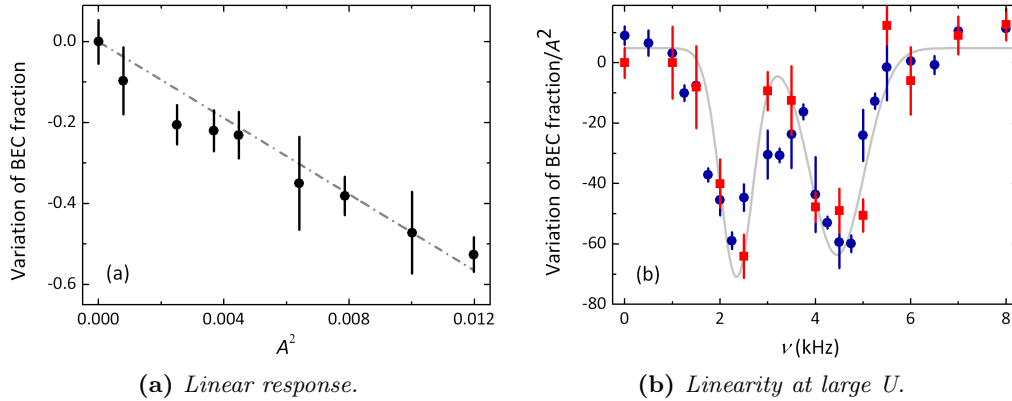


**Figure 6.3:** Linear response. (a) Relative variation of the condensed fraction for  $\Delta=0$  and  $U=5.4J$ , versus the square of the modulation amplitude. (b) Excitation spectrum for  $\Delta=0$  and  $U=26J$ , for two different modulation amplitudes,  $A=0.05$  (red) and  $A=0.1$  (blue), normalized to the square of the modulation amplitude.

the unperturbed condensed fraction. On the other hand, in the thermal regime  $T/T_c > 1$ ,  $T$  is extracted from the thermal width  $\sigma(\omega)$ :  $\Delta T(\omega) = m(\sigma^2(\omega) - \sigma_0^2)/k_B t_{exp}^2$ , where  $t_{exp}=16$  ms is the expansion time and  $\sigma_0$  is the unperturbed width.

The modulation time  $t_{mod}=200$  ms is chosen as long as possible, as allowed by the system background heating, in order to have the maximum sensitivity at low frequencies. Usually, the energy absorption rate can be calculated within the linear response theory. The modulation amplitude  $A_{mod} \sim 0.1$ , is in fact chosen small enough to stay in the linear response regime, as shown in Fig. 6.3a, where we plot the relative variation of the condensed fraction at  $\Delta=0$  and  $U=5.4J$  versus the square of the modulation amplitude is plotted. We also checked that the excitation spectrum in the strongly correlated regime ( $\Delta=0$ ,  $U=26J$ ) is not changing for two different modulation amplitudes ( $A=0.05$ ,  $A=0.1$ ), as shown in Fig. 6.3b.

### 6.3 Excitations in the strongly-correlated regime

First of all, we investigate the excitations properties of the disordered bosons in the strongly-correlated regime. As discussed in Sec. 4.5.2, at large interactions, even in the presence of disorder, the typical correlation length characterizing the system is small (few lattice sites) and therefore temperature-independent, at least in the experimental temperature range,  $k_B T \approx 3J$ . As a consequence, in this regime the experimental observations directly reflect the properties of the  $T=0$  quantum phases.

The typical response in the clean case ( $\Delta=0$ ) at large  $U$  is shown in Fig. 6.4. The excitation spectrum shows the standard Mott insulator response<sup>54,17</sup>: at low frequencies,  $h\nu < U$ , essentially no absorption is visible. A first excitation peak appears at the Mott-gap,  $h\nu=U$ . This absorption peak is due to particle-hole excitations in the MI plateaus, that form in the inhomogeneous trapped system. For our typical densities we estimate MI domains with single site occupation  $n=1-3$ , depending on the trap zone. A second peak is instead centered at  $h\nu=2U$ , and stems from particles hopping from single- into doubly-occupied lattice site. This peak

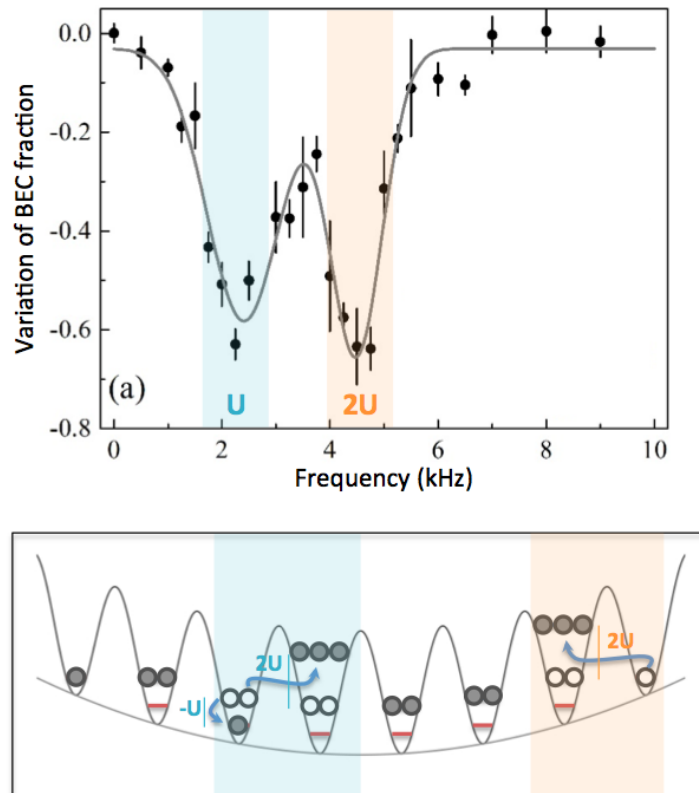


**Figure 6.4:** (a) Excitation spectrum at  $U=26J$  and  $\Delta=0$ . At low frequencies the system is not responding; a first excitation peak appears at the Mott-gap,  $h\nu=U$ , and a second one at about  $2U$ , due to the system inhomogeneity. (b) Schematics of the activation mechanism of an elementary excitation in the inhomogeneous Mott insulator. When a particle hops between sites with the same occupancy the energy cost is  $U$ . When instead a particle hops into a lattice site already occupied by two other particles, the energy cost is  $2U$

confirms the presence of MI domains with different occupation in individual tubes, due to the system inhomogeneity (see Fig. 6.4). The MI domains are connected by additional SF components with density incommensurate with the lattice periodicity (i.e.  $n$  different from an integer), which do not respond to the excitation in the regime of  $U \gg J$ .

When a finite disorder  $\Delta$  is included, the system response to the external perturbation modifies. The typical response for varying  $\Delta$  is shown in Fig. 6.5. The MI peaks broaden of approximately  $\Delta$ , as already observed in previous experiments<sup>32</sup>, since the energy required to create particle-hole excitations is now site-dependent, and  $\Delta$  quantifies the spreading of the on-site energies. More surprisingly, a further peak appears in the gap, at  $h\nu \sim \Delta$ . This observation strongly reminds the general picture discussed in Orso et al.<sup>66</sup> and summarized in Fig. 6.1, predicting a similar response for the strongly-correlated Bose glass phase at finite disorder. In fact, at large interactions, the incommensurate fraction composing our experimental inhomogeneous system is expected<sup>42</sup> to behave as a weakly-interacting Fermi gas, which essentially undergoes Anderson localization, showing such a peculiar response around the characteristic disorder energy. Even though the experimental unavoidable finite resolution at low frequencies does not allow us to clearly distinguish a gapless response, the presence of the extra peak strongly indicates this Bose glass phase. In the next paragraph we close compare our experimental results with theoretical expectations, giving evidence of this glassy phase.

**Comparison with theory.** In Fig. 6.6, the experimental data are compared to the theoretical prediction for the excitation spectrum, evaluated with a fermionized-boson model, on the line of Orso et al.<sup>66</sup>. The calculations are performed in the hard-core limit  $U \gg \Delta, J$ , where bosons can be mapped onto non-interacting spinless fermions. The energy absorption rate (EAR) is derived using the linear response theory<sup>50</sup>. For the incommensurate component, which provides the Bose-glass response, the EAR reads:

$$\dot{E}(\omega) = \frac{\delta J^2 \pi \omega}{2} \sum_{a,b} \overline{K_{ab} [f_{FD}(\epsilon_a) - f_{FD}(\epsilon_b)] \delta(\hbar\omega + \epsilon_a - \epsilon_b)}, \quad (6.2)$$

where  $\delta J$  is the perturbation on the tunneling energy  $J$  induced by the primary lattice modulation (6.1). Here  $K_{ab} = |\sum_i \psi_a^*(i+1)\psi_b(i) + \psi_a^*(i)\psi_b(i+1)|^2$  is calculated over pairs  $(a, b)$  of single-particle eigenstates of the quasiperiodic lattice at two different disorder  $\Delta = 6.5J$  and  $\Delta = 9.5J$ , while  $f_{FD}(\epsilon)$  is the Fermi-Dirac distribution at finite temperature. The bar represents averages over different realizations of the potential. Each spectrum is calculated evaluating Eq. (6.2) at different frequencies  $\omega$  on a 200-sites lattice confined in a harmonic potential with frequency  $\nu_x=150$  Hz, as in the experiment. The calculations are performed at finite temperature  $k_B T=3J$ . In the experiment the interaction energy  $U$  is not infinite, as assumed in the theoretical model; as a consequence the single site occupation  $n$  is often bigger than unity (in some zones of the harmonic potential we have  $n=2-3$ ). In the calculations, this is taken into account employing an extended-fermionization approach<sup>75</sup>, i.e. neglecting the coupling between layers with different occupations ( $n \leq 1$ ,  $1 < n \leq 2$ ,  $2 < n \leq 3$ ), and calculating their response independently. The larger kinetic energy of the fermionic excited bands is properly taken into account in the numerics. In fact, this approach

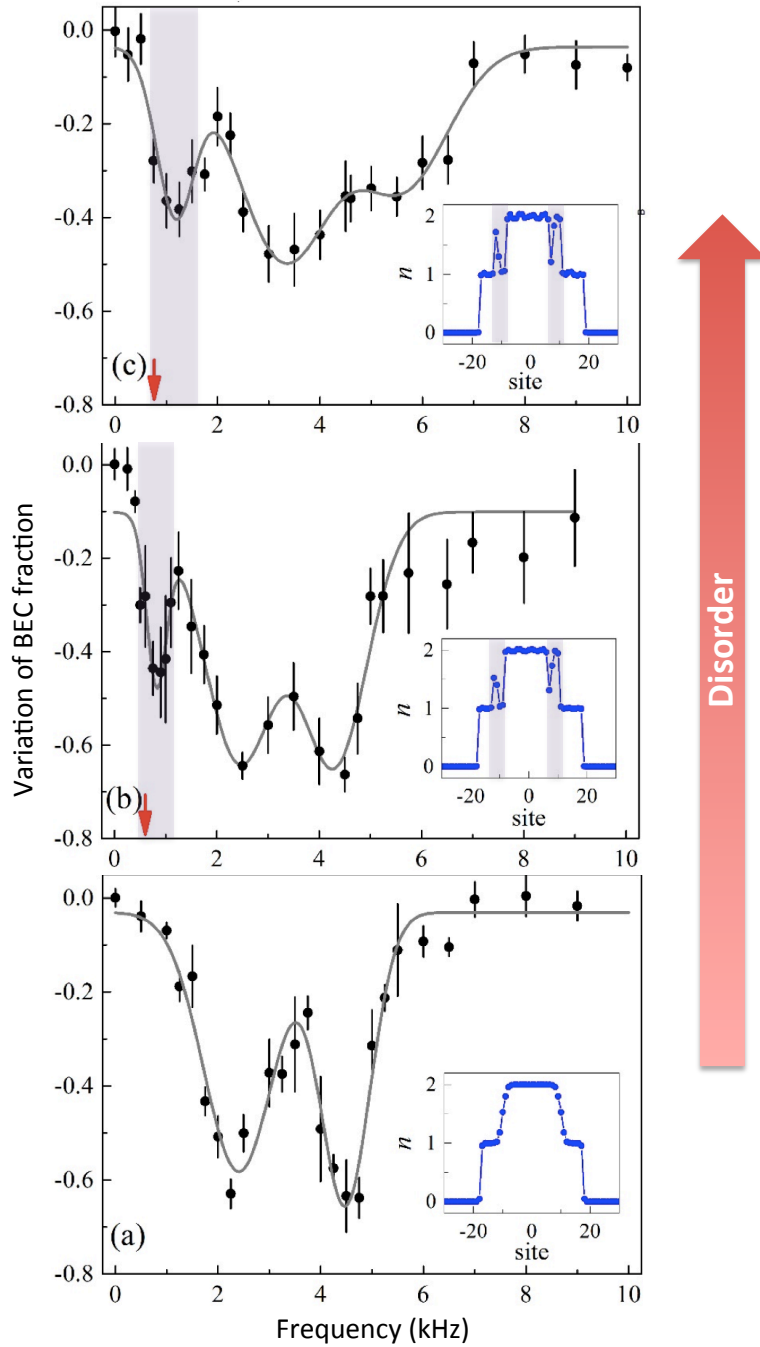


**Figure 6.5:** Emergence of a strongly correlated Bose glass. Excitation spectrum at  $U=26J$  and SF temperature  $k_B T \approx 3J$ , for increasing disorder strengths. (a)  $\Delta=0$ : the system does not respond at low frequency, while a first excitation appears at around  $U$ , which is the expected Mott gap energy, and a second one due to the system inhomogeneity at around  $2U$ ; (b)  $\Delta=6.5J$ : the two Mott peaks are broadened, and a new peak centered around  $1.5 \Delta$  appears; (c)  $\Delta=9.5J$ : the low-frequency peak shifts and broadens with  $\Delta$ , and the Mott peaks are further broadened. The arrows are at  $h\nu = \Delta$  and the lines are a fit with multiple Gaussians. The insets are the density profiles calculated for  $N=55$ .

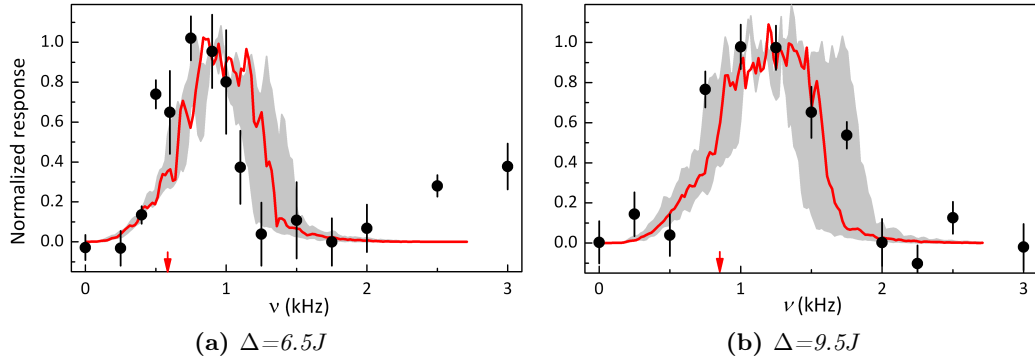


**Figure 6.6:** Experiment-theory comparison of the low-frequency response in Fig. 6.5 spectra, for two disorder strengths: (a)  $\Delta=6.5J$  (b)  $\Delta=9.5J$ . The red curve is calculated spectrum at the nominal  $\Delta$ , and the grey region shows the effect of the 20% uncertainty on  $\Delta$ . The red arrows mark the disorder strength in frequency units,  $\Delta/h$ .

is known to work rather well already at relatively small interactions  $U$ , provided that the Mott-gap is open. Each of the excitation spectra shown in Fig. 6.6, is the average of the spectra calculated for individual tubes over the whole distribution of tubes in the experiment. Both the theoretical and the experimental peak responses have been normalized to unity; moreover, we subtracted from the experimental data a Gaussian background, due to the first Mott peak. Grey shaded areas show how the experimental uncertainty on  $\Delta$  affects the calculated spectra.

As shown in Fig. 6.6, the calculated absorption peak well reproduces the experimental observation, confirming the qualitative picture depicted in Fig. 6.1. The systematic shift of the experimental data towards lower frequencies might be a consequence of the  $U = \infty$  approximation employed in the theoretical model. Anyway, the appearance of such extra peak experimentally probes the presence of a strongly-correlated BG coexisting with the disordered MI. Moreover, the theoretical analysis of the density distribution in the insets of Fig. 6.5 shows the expected spatial arrangement of the commensurate and incommensurate components in the typical tube, confirming that the smooth SF density is turned by the disorder into a strongly varying one, as expected for a Bose glass.

## 6.4 Excitations from weak to strong interactions

In this section we explore the condensate excitations properties in a disordered potential from weak to strong interactions. As shown in Sec. 4.3, at weak interactions the entropy enhances; as a consequence in this regime it is easier to measure the energy absorption from the increase of the thermal width, once the sample has been transferred back into the 3D trap. Furthermore, at small  $U$  the typical correlation length of the zero-temperature system is large and the presence of a finite temperature broadens its momentum width, as shown in Sec. 4.4.2 and deeply discussed in Sec. 4.5. Therefore at low interactions we are dealing with a finite-temperature system, which however gives strong indications and might be quantitatively connected to the zero-temperature expected phases. Coherence and transport measurements revealed

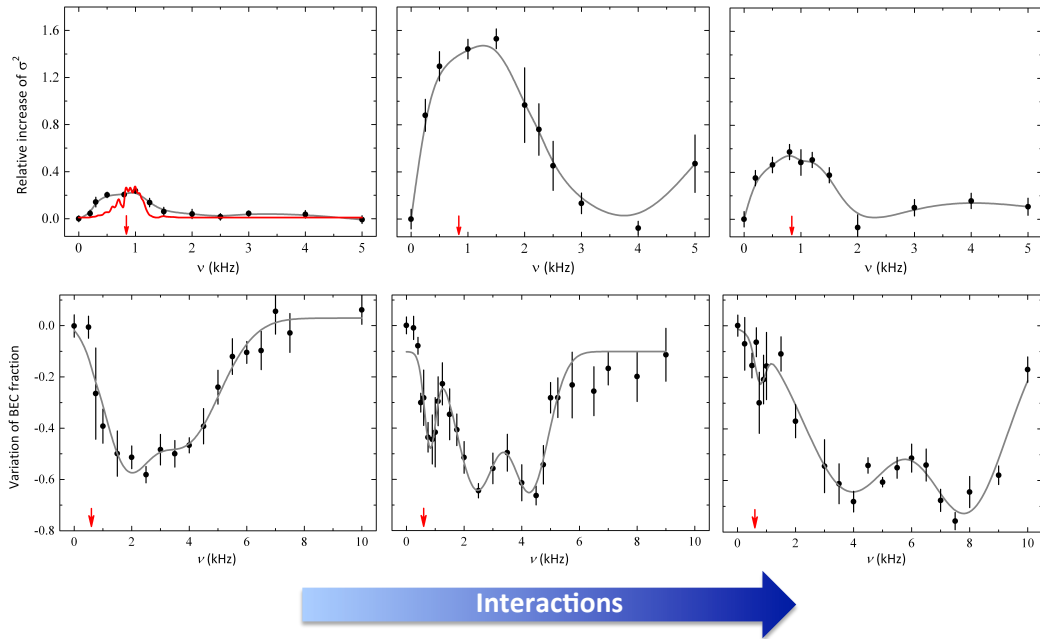


**Figure 6.7:** Excitation spectrum from weak to strong interactions. Top figures: measured excitation spectrum for fixed disorder,  $\Delta = 7J$ , and increasing interaction:  $U < 0.05J$  (top-left),  $U \sim 0.2J$  (top-center),  $U \sim 0.3J$  (top-right). Bottom figures: measured excitation spectrum for fixed disorder,  $\Delta = 6.5J$ , and increasing interaction:  $U = 20J$  (bottom-left),  $U = 26J$  (bottom-center),  $U = 58J$  (bottom-right). The arrows mark  $\Delta/h$ . The red line is the theory for non-interacting bosons and the grey lines are a guide to the eye. Error bars represent the standard deviation of 5 measurements.

the presence of a finite-temperature insulator even in this side of the  $U$ - $\Delta$  diagram. We now explore its excitations spectrum, comparing it to the characteristic response at large interactions.

The typical excitation spectra for varying  $U$  are shown in Fig. 6.7. The nature of the excitations at weak interactions contrasts with the fermion-like response observed in the strongly-correlated regime. At small  $U$  in fact, bosons do not behave as fermions, and the excitations show the typical bosonic response. For vanishing  $U$  a weak excitation peak centered at  $\Delta$  appears, as expected for an Anderson insulator; the system is incoherent and difficult to excite. A non-interacting bosonic model, built replacing  $f_{FD}(\epsilon_a) - f_{FD}(\epsilon_b)$  with the Bose-Einstein distribution  $f_{BE}(\epsilon_a)$  in the fermionic model used previously, captures relatively well the atomic response at  $\Delta=7J$ . This response greatly enhances and broadens when a small  $U \leq \Delta$  is added, signaling the crossover into a weakly-interacting disordered-induced insulating regime, consistent with a finite-temperature Bose glass. Eventually, at larger  $U$ , this regime is undistinguishable from a clean superfluid. This behavior, combined with the evolution of the momentum width (shown in Fig. 4.3) and the transport properties (see Fig. 5.8), confirms the nature of such weakly-interacting phase: in the bosonic case, a small repulsive interaction favors the coupling of single-particle states, gradually restoring the superfluidity. In fact, the low-frequency response of the system at weak interactions enhances if compared to its strongly-correlated counterpart, indicating the possibility of longer-distance excitations at small  $U$ , while at large  $U$  the excitations occur only on small length scales. As discussed in Chapter 1, the role of the interactions in bosonic samples is different in the weakly- and in the strongly-correlated limit. While weak interactions compete with disorder and screen the disorder-induced localization, restoring coherence between particles, strong interactions act as the Pauli exclusion, ‘fermionizing’ the bosonic sample and favoring (Anderson) localization in disordered media.

At large  $U$ , a peak centered at  $\Delta$  appears in the excitation spectrum, signaling the presence of a strongly-correlated BG. This  $\Delta$ -peak can be observed only in a limited region of  $U$ - $\Delta$  values, as shown for example in Fig. 6.7. Indeed, when  $\Delta$  is comparable with  $U$ , the larger MI peak overlaps with the smaller BG one. When instead  $U$  is much larger than  $\Delta$ , the incommensurate density component that can form a BG is strongly reduced.

# Conclusions

In this thesis we used a one-dimensional Bose-Einstein condensate in a quasiperiodic lattice to investigate the very general problem of dirty bosons, i.e. the effect of disorder in an interacting bosonic sample. Thanks to the ability to tune and control both the disorder and the interaction strength, we probed the physical properties of this system in the whole interaction-disorder plane, identifying a Bose glass at strong interactions, coexisting with a disordered Mott insulator. Three experimental observables, the system correlation length, its transport properties and the spectrum of its excitations, give the evidence of the several quantum regimes.

The combination of coherence and transport measurements reveals a reentrant insulating phase, surrounding a coherent superfluid phase from weak to strong interactions, besides the well known disorder-induced Anderson insulator (in the absence of interactions) and interaction-induced Mott insulator (in the non-disordered lattice).

At strong interactions we spectrally separate a new disordered insulator from the disordered Mott insulator; the spectral feature is well reproduced by the low- $T$  theory for the Bose glass, consistently with a gapless insulator. We test the different spectral response of the insulator on the two sides of the diagram, highlighting the fermionic nature of the Bose glass phase at strong interactions, and the bosonic nature of the insulating phase at weak interactions. The combination of these measurements with the coherence diagram shows the opposite role of a weak or a strong interaction energy: while a weak interaction couples localized states on large length scales, a strong interaction ‘fermonize’ the bosonic gas, inducing its localization in disorder.

At weak interactions we study in detail the system dynamics, observing a sharp crossover from a weakly dissipative regime to a strongly unstable one at a disorder-dependent critical momentum. In the clean lattice limit these observations suggest the contribution of quantum phase slips to the dissipation. This method allows us to locate the fluid-insulator transition driven by disorder at weak interactions, across the interaction-disorder plane. We find this transition consistent with the broad crossover observed from coherence measurements, and with the predicted zero-temperature superfluid-Bose glass transition.

An exhaustive theoretical model for the experimental system is not trivial, since the experiment is performed in an inhomogeneous setup and at finite temperature. DMRG simulations done by the group of T. Giamarchi allow to reproduce the  $T=0$  correlation function of the inhomogeneous experimental system; a close comparison with the experimental results suggests the presence of a Bose glass phase also at weak interactions. The effects of a finite-temperature are assessed in various ways. We study the evolution of the correlation length with temperature, both

experimentally and theoretically, employing a phenomenological approach on the inhomogeneous experiment-like system, and an exact diagonalization technique on small homogeneous systems. We find that the strongly-correlated regime is not affected by a finite temperature and we measure a constant correlation length in a large temperature range. This observation indicates that the  $T=0$  quantum phases persist in the experimental range of temperatures, confirming the observation of a strongly-correlated Bose glass. Instead, at weak interactions we predict and observe a large thermal broadening; anyway we find a constant broadening in the  $U$ - $\Delta$  plane, suggesting a direct connection with the  $T=0$  phases. Moreover, transport measurements shows no detectable changes in the mobility with temperature in the whole range of interactions, suggesting a temperature-independent metal-insulator transition at the experimental temperatures.

This work opens the way to various future studies. The spectroscopic technique we used to probe the one-dimensional system can be applied to other types of disorder and to higher dimensionality. A speckle potential could be used to study the Bose glass physics in the absence of a lattice, thus avoiding overlaps with the Mott-insulator physics and effectively decreasing the thermal effects. In this context, momentum-dependent transport measurements could give informations on the phase transition at strong interactions and vanishing disorder, establishing a link to the Luttinger-liquid theory for the superfluid-Bose glass transition. On the other hand, in higher dimensions, bosons are generally predicted to be much more resistant to disorder, and the evolution of the insulating phases in the interaction-disorder plane is still not clear. While in 3D the correlated regime is not easily achievable and a Bose glass phase could be observed only in the presence of a lattice, in two-dimensional systems the strongly correlated regime could be experimentally realized. At weak interactions instead we deal with a finite-temperature insulator; despite the large thermal effects we still observe an insulating phase. As discussed in the thesis, this could be the first hint of a many-body localization occurring in this regime. Future work could characterize this localized phase, studying its evolution with temperature.

# Bibliography

- [1] M. Albert, T. Paul, N. Pavloff, and P. Leboeuf. Dipole Oscillations of a Bose-Einstein Condensate in the Presence of Defects and Disorder. *Phys. Rev. Lett.*, 100:250405, Jun 2008. doi: 10.1103/PhysRevLett.100.250405. URL <http://link.aps.org/doi/10.1103/PhysRevLett.100.250405>.
- [2] I. L. Aleiner, B. L. Altshuler, and G. V. Shlyapnikov. A finite-temperature phase transition for disordered weakly interacting bosons in one dimension. *Nat Phys*, 6:900–904, Nov 2010.
- [3] D. R. Allum, P. V. E. McClintock, and A. Phillips. The Breakdown of Superfluidity in Liquid  $^4\text{He}$ : An Experimental Test of Landau’s Theory. *Philosophical Transactions of the Royal Society of London. Series A, Mathematical and Physical Sciences*, 284(1320):179–224, 1977. doi: 10.1098/rsta.1977.0008. URL <http://rsta.royalsocietypublishing.org/content/284/1320/179.abstract>.
- [4] E. Altman, Y. Kafri, A. Polkovnikov, and G. Refael. Phase Transition in a System of One-Dimensional Bosons with Strong Disorder. *Phys. Rev. Lett.*, 93:150402, Oct 2004. doi: 10.1103/PhysRevLett.93.150402. URL <http://link.aps.org/doi/10.1103/PhysRevLett.93.150402>.
- [5] E. Altman, A. Polkovnikov, E. Demler, B. I. Halperin, and M. D. Lukin. Superfluid-Insulator Transition in a Moving System of Interacting Bosons. *Phys. Rev. Lett.*, 95:020402, Jul 2005. doi: 10.1103/PhysRevLett.95.020402. URL <http://link.aps.org/doi/10.1103/PhysRevLett.95.020402>.
- [6] P. W. Anderson. Absence of Diffusion in Certain Random Lattices. *Phys. Rev.*, 109:1492, 1958.
- [7] A. Aspect and M. Inguscio. Anderson localization of ultracold atoms. *Physics Today*, 62(8):30, 2009.
- [8] O. V. Astafiev, L. B. Ioffe, S. Kafanov, Y. A. Pashkin, K. Y. Arutyunov, D. Shahar, O. Cohen, and J. S. Tsai. Coherent Quantum Phase Slip. *Nature*, 484:355–358, Apr 2012.
- [9] S. Aubry and G. André. Analyticity breaking and Anderson localization in incommensurate lattices. *Ann. Israel. Phys. Soc.*, 3:33, 1980.
- [10] J. Billy, V. Josse, Z. Zuo, A. Bernard, B. Hambrecht, P. Lugan, D. Clement, L. Sanchez-Palencia, P. Bouyer, and A. Aspect. Direct observation of Anderson

- localization of matter waves in a controlled disorder. *Nature*, 453:891–894, Jun 2008.
- [11] I. Bloch, J. Dalibard, and W. Zwerger. Many-body physics with ultracold gases. *Rev. Mod. Phys.*, 80:885–964, Jul 2008. doi: 10.1103/RevModPhys.80.885. URL <http://link.aps.org/doi/10.1103/RevModPhys.80.885>.
- [12] C. G. Callan and S. Coleman. Fate of the false vacuum. II. First quantum corrections. *Phys. Rev. D*, 16:1762–1768, Sep 1977. doi: 10.1103/PhysRevD.16.1762. URL <http://link.aps.org/doi/10.1103/PhysRevD.16.1762>.
- [13] C. A. M. Castelijns, K. F. Coates, A. M. Guénault, S. G. Mussett, and G. R. Pickett. Landau critical velocity for a macroscopic object moving in superfluid  $^3\text{B}$ : Evidence for gap suppression at a moving surface. *Phys. Rev. Lett.*, 56:69–72, Jan 1986. doi: 10.1103/PhysRevLett.56.69. URL <http://link.aps.org/doi/10.1103/PhysRevLett.56.69>.
- [14] J. Catani, G. Barontini, G. Lamporesi, F. Rabatti, G. Thalhammer, F. Minardi, S. Stringari, and M. Inguscio. Entropy exchange in a mixture of ultracold atoms. *Phys. Rev. Lett.*, 103:140401, Sep 2009. doi: 10.1103/PhysRevLett.103.140401. URL <http://link.aps.org/doi/10.1103/PhysRevLett.103.140401>.
- [15] M. A. Cazalilla, R. Citro, T. Giamarchi, E. Orignac, and M. Rigol. One dimensional bosons: From condensed matter systems to ultracold gases. *Rev. Mod. Phys.*, 83:1405–1466, Dec 2011. doi: 10.1103/RevModPhys.83.1405. URL <http://link.aps.org/doi/10.1103/RevModPhys.83.1405>.
- [16] A. P. Chikkatur, A. Görlitz, D. M. Stamper-Kurn, S. Inouye, S. Gupta, and W. Ketterle. Suppression and Enhancement of Impurity Scattering in a Bose-Einstein Condensate. *Phys. Rev. Lett.*, 85:483–486, Jul 2000. doi: 10.1103/PhysRevLett.85.483. URL <http://link.aps.org/doi/10.1103/PhysRevLett.85.483>.
- [17] D. Clément, N. Fabbri, L. Fallani, C. Fort, and M. Inguscio. Exploring Correlated 1D Bose Gases from the Superfluid to the Mott-Insulator State by Inelastic Light Scattering. *Phys. Rev. Lett.*, 102:155301, Apr 2009. doi: 10.1103/PhysRevLett.102.155301. URL <http://link.aps.org/doi/10.1103/PhysRevLett.102.155301>.
- [18] D. Clément, N. Fabbri, L. Fallani, C. Fort, and M. Inguscio. Multi-band spectroscopy of inhomogeneous Mott-insulator states of ultracold bosons. *New Journal of Physics*, 11(10):103030, 2009. URL <http://stacks.iop.org/1367-2630/11/i=10/a=103030>.
- [19] S. Coleman. Fate of the false vacuum: Semiclassical theory. *Phys. Rev. D*, 15:2929–2936, May 1977. doi: 10.1103/PhysRevD.15.2929. URL <http://link.aps.org/doi/10.1103/PhysRevD.15.2929>.
- [20] S. Coleman. *Aspects of Symmetry*. Cambridge University Press, 1988.

- [21] P. A. Crowell, F. W. Van Keuls, and J. D. Reppy. Onset of superfluidity in  $^4\text{He}$  films adsorbed on disordered substrates. *Phys. Rev. B*, 55:12620–12634, May 1997. doi: 10.1103/PhysRevB.55.12620. URL <http://link.aps.org/doi/10.1103/PhysRevB.55.12620>.
- [22] G. A. Csáthy, J. D. Reppy, and M. H. W. Chan. Substrate-Tuned Boson Localization in Superfluid  $^4\text{He}$  Films. *Phys. Rev. Lett.*, 91:235301, Dec 2003. doi: 10.1103/PhysRevLett.91.235301. URL <http://link.aps.org/doi/10.1103/PhysRevLett.91.235301>.
- [23] I. Danshita. Universal Damping Behavior of Dipole Oscillations of One-Dimensional Ultracold Gases Induced by Quantum Phase Slips. *Phys. Rev. Lett.*, 111:025303, Jul 2013. doi: 10.1103/PhysRevLett.111.025303. URL <http://link.aps.org/doi/10.1103/PhysRevLett.111.025303>.
- [24] I. Danshita and A. Polkovnikov. Superfluid-to-Mott-insulator transition in the one-dimensional Bose-Hubbard model for arbitrary integer filling factors. *Phys. Rev. A*, 84:063637, Dec 2011. doi: 10.1103/PhysRevA.84.063637. URL <http://link.aps.org/doi/10.1103/PhysRevA.84.063637>.
- [25] I. Danshita and A. Polkovnikov. Quantum phase slips in one-dimensional superfluids in a periodic potential. *Phys. Rev. A*, 85:023638, Feb 2012. doi: 10.1103/PhysRevA.85.023638. URL <http://link.aps.org/doi/10.1103/PhysRevA.85.023638>.
- [26] B. Deissler, M. Zaccanti, G. Roati, C. D’Errico, M. Fattori, M. Modugno, G. Modugno, and M. Inguscio. Delocalization of a disordered bosonic system by repulsive interactions. *Nat Phys*, 6:354–348, May 2010.
- [27] B. Deissler, E. Lucioni, M. Modugno, G. Roati, L. Tanzi, M. Zaccanti, M. Inguscio, and G. Modugno. Correlation function of weakly interacting bosons in a disordered lattice. *New Journal of Physics*, 13(2):023020, 2011. URL <http://stacks.iop.org/1367-2630/13/i=2/a=023020>.
- [28] C. D’Errico. Osservazione di risonanze di Fano-Feshbach in miscele atomiche K-Rb. Master’s thesis, University of Florence, 2005.
- [29] C. D’Errico. *Anderson localization of a weakly interacting Bose-Einstein condensate*. PhD thesis, University of Florence, 2008.
- [30] C. D’Errico, M. Zaccanti, M. Fattori, G. Roati, M. Inguscio, G. Modugno, and A. Simoni. Feshbach resonances in ultracold  $^{39}\text{K}$ . *New Journal of Physics*, 9(7):223, 2007. URL <http://stacks.iop.org/1367-2630/9/i=7/a=223>.
- [31] L. Fallani, L. De Sarlo, J. E. Lye, M. Modugno, R. Saers, C. Fort, and M. Inguscio. Observation of Dynamical Instability for a Bose-Einstein Condensate in a Moving 1D Optical Lattice. *Phys. Rev. Lett.*, 93:140406, Sep 2004. doi: 10.1103/PhysRevLett.93.140406. URL <http://link.aps.org/doi/10.1103/PhysRevLett.93.140406>.

- [32] L. Fallani, J. E. Lye, V. Guarrera, C. Fort, and M. Inguscio. Ultracold Atoms in a Disordered Crystal of Light: Towards a Bose Glass. *Phys. Rev. Lett.*, 98:130404, Mar 2007. doi: 10.1103/PhysRevLett.98.130404. URL <http://link.aps.org/doi/10.1103/PhysRevLett.98.130404>.
- [33] U. Fano. Sullo spettro di assorbimento dei gas nobili presso il limite dello spettro d'arco. *Nuovo Cimento*, 12:156, 1935.
- [34] F. Ferlaino. *Atomic Fermi gases in an optical lattice*. PhD thesis, University of Florence, 2004.
- [35] C. D. Fertig, K. M. O'Hara, J. H. Huckans, S. L. Rolston, W. D. Phillips, and J. V. Porto. Strongly Inhibited Transport of a Degenerate 1D Bose Gas in a Lattice. *Phys. Rev. Lett.*, 94:120403, Apr 2005. doi: 10.1103/PhysRevLett.94.120403. URL <http://link.aps.org/doi/10.1103/PhysRevLett.94.120403>.
- [36] H. Feshbach. A Unified Theory of Nuclear Reactions. *Ann. Phys.*, 5:357, 1958.
- [37] M. P. A. Fisher, P. B. Weichman, G. Grinstein, and D. S. Fisher. Boson localization and the superfluid-insulator transition. *Phys. Rev. B*, 40:546–570, Jul 1989. doi: 10.1103/PhysRevB.40.546. URL <http://link.aps.org/doi/10.1103/PhysRevB.40.546>.
- [38] L. Fontanesi, M. Wouters, and V. Savona. Mean-field phase diagram of the one-dimensional Bose gas in a disorder potential. *Phys. Rev. A*, 81:053603, May 2010. doi: 10.1103/PhysRevA.81.053603. URL <http://link.aps.org/doi/10.1103/PhysRevA.81.053603>.
- [39] B. Gadway, D. Pertot, J. Reeves, M. Vogt, and D. Schneble. Glassy Behavior in a Binary Atomic Mixture. *Phys. Rev. Lett.*, 107:145306, Sep 2011. doi: 10.1103/PhysRevLett.107.145306. URL <http://link.aps.org/doi/10.1103/PhysRevLett.107.145306>.
- [40] F. Gerbier. Boson Mott Insulators at Finite Temperatures. *Phys. Rev. Lett.*, 99:120405, Sep 2007. doi: 10.1103/PhysRevLett.99.120405. URL <http://link.aps.org/doi/10.1103/PhysRevLett.99.120405>.
- [41] T. Giamarchi. *Quantum Physics in One Dimension*. Oxford University Press, 2004.
- [42] T. Giamarchi and H. J. Schulz. Anderson localization and interactions in one-dimensional metals. *Phys. Rev. B*, 37:325–340, Jan 1988. doi: 10.1103/PhysRevB.37.325. URL <http://link.aps.org/doi/10.1103/PhysRevB.37.325>.
- [43] M. Girardeau. Relationship between Systems of Impenetrable Bosons and Fermions in One Dimension. *J. Math. Phys.*, 1:516, 1960.
- [44] J. W. Goodman. *Speckle Phenomena in Optics: Theory and Applications*. Roberts and Company Publishers, 2007.

- [45] M. Greiner, O. Mandel, T. Esslinger, T. W. Hansch, and I. Bloch. Quantum phase transition from a superfluid to a Mott insulator in a gas of ultracold atoms. *Nature*, 415:39–44, January 2002.
- [46] R. Grimm, M. Weidemüller, and Y. B. Ovchinnikov. Optical dipole traps for neutral atoms. *Advances in Atomic, Molecular and Optical Physics*, 42:95, 2000.
- [47] F. D. M. Haldane. 'Luttinger liquid theory' of one-dimensional quantum fluids. I. Properties of the Luttinger model and their extension to the general 1D interacting spinless Fermi gas. *Journal of Physics C: Solid State Physics*, 14(19):2585, 1981. URL <http://stacks.iop.org/0022-3719/14/i=19/a=010>.
- [48] H. Hu, A. Strybulevych, J. H. Page, S. E. Skipetrov, and B. A. van Tiggelen. Localization of ultrasound in a three-dimensional elastic network. *Nat Phys*, 4: 945–948, Dec 2008.
- [49] S. Inouye, M. R. Andrews, J. Stenger, H.-J. Miesner, D. M. Stamper-Kurn, and W. Ketterle. Observation of Feshbach resonances in a Bose-Einstein condensate. *Nature*, 392:151–154, Mar 1998.
- [50] A. Iucci, M. A. Cazalilla, A. F. Ho, and T. Giamarchi. Energy absorption of a Bose gas in a periodically modulated optical lattice. *Phys. Rev. A*, 73:041608, Apr 2006. doi: 10.1103/PhysRevA.73.041608. URL <http://link.aps.org/doi/10.1103/PhysRevA.73.041608>.
- [51] K. V. Kheruntsyan, D. M. Gangardt, P. D. Drummond, and G. V. Shlyapnikov. Finite-temperature correlations and density profiles of an inhomogeneous interacting one-dimensional bose gas. *Phys. Rev. A*, 71:053615, May 2005. doi: 10.1103/PhysRevA.71.053615. URL <http://link.aps.org/doi/10.1103/PhysRevA.71.053615>.
- [52] S. Khlebnikov and L. P. Pryadko. Quantum Phase Slips in the Presence of Finite-Range Disorder. *Phys. Rev. Lett.*, 95:107007, Sep 2005. doi: 10.1103/PhysRevLett.95.107007. URL <http://link.aps.org/doi/10.1103/PhysRevLett.95.107007>.
- [53] T. Kinoshita, T. Wenger, and D. S. Weiss. Observation of a one-dimensional tonks-girardeau gas. *Science*, 305(5687):1125–1128, 2004. doi: 10.1126/science.1100700. URL <http://www.sciencemag.org/content/305/5687/1125.abstract>.
- [54] C. Kollath, A. Iucci, T. Giamarchi, W. Hofstetter, and U. Schollwöck. Spectroscopy of Ultracold Atoms by Periodic Lattice Modulations. *Phys. Rev. Lett.*, 97:050402, Jul 2006. doi: 10.1103/PhysRevLett.97.050402. URL <http://link.aps.org/doi/10.1103/PhysRevLett.97.050402>.
- [55] B. Kramer and A. MacKinnon. Localization: theory and experiment. *Reports on Progress in Physics*, 56(12):1469, 1993. URL <http://stacks.iop.org/0034-4885/56/i=12/a=001>.

- [56] Y. Lahini, A. Avidan, F. Pozzi, M. Sorel, R. Morandotti, D. N. Christodoulides, and Y. Silberberg. Anderson Localization and Nonlinearity in One-Dimensional Disordered Photonic Lattices. *Phys. Rev. Lett.*, 100:013906, Jan 2008. doi: 10.1103/PhysRevLett.100.013906. URL <http://link.aps.org/doi/10.1103/PhysRevLett.100.013906>.
- [57] M. Landini, S. Roy, G. Roati, A. Simoni, M. Inguscio, G. Modugno, and M. Fattori. Direct evaporative cooling of  $^{39}\text{K}$  atoms to Bose-Einstein condensation. *Phys. Rev. A*, 86:033421, Sep 2012. doi: 10.1103/PhysRevA.86.033421. URL <http://link.aps.org/doi/10.1103/PhysRevA.86.033421>.
- [58] E. H. Lieb and W. Liniger. Exact Analysis of an Interacting Bose Gas. I. The General Solution and the Ground State. *Phys. Rev.*, 130:1605–1616, May 1963. doi: 10.1103/PhysRev.130.1605. URL <http://link.aps.org/doi/10.1103/PhysRev.130.1605>.
- [59] E. Lucioni, B. Deissler, L. Tanzi, G. Roati, M. Zaccanti, M. Modugno, M. Larcher, F. Dalfovo, M. Inguscio, and G. Modugno. Observation of Subdiffusion in a Disordered Interacting System. *Phys. Rev. Lett.*, 106:230403, Jun 2011. doi: 10.1103/PhysRevLett.106.230403. URL <http://link.aps.org/doi/10.1103/PhysRevLett.106.230403>.
- [60] E. Lucioni, L. Tanzi, C. D’Errico, M. Moratti, M. Inguscio, and G. Modugno. Modeling the transport of interacting matter waves in a disordered system by a nonlinear diffusion equation. *Phys. Rev. E*, 87:042922, Apr 2013. doi: 10.1103/PhysRevE.87.042922. URL <http://link.aps.org/doi/10.1103/PhysRevE.87.042922>.
- [61] M. Modugno. Exponential localization in one-dimensional quasi-periodic optical lattices. *New Journal of Physics*, 11:033023, March 2009.
- [62] O. Morsch and M. Oberthaler. Dynamics of Bose-Einstein condensates in optical lattices. *Rev. Mod. Phys.*, 78:179–215, Feb 2006. doi: 10.1103/RevModPhys.78.179. URL <http://link.aps.org/doi/10.1103/RevModPhys.78.179>.
- [63] J. Mun, P. Medley, G. K. Campbell, L. G. Marcassa, D. E. Pritchard, and W. Ketterle. Phase Diagram for a Bose-Einstein Condensate Moving in an Optical Lattice. *Phys. Rev. Lett.*, 99:150604, Oct 2007. doi: 10.1103/PhysRevLett.99.150604. URL <http://link.aps.org/doi/10.1103/PhysRevLett.99.150604>.
- [64] N. Nessi and A. Iucci. Finite-temperature properties of one-dimensional hard-core bosons in a quasiperiodic optical lattice. *Phys. Rev. A*, 84:063614, Dec 2011. doi: 10.1103/PhysRevA.84.063614. URL <http://link.aps.org/doi/10.1103/PhysRevA.84.063614>.
- [65] M. Olshanii. Atomic Scattering in the Presence of an External Confinement and a Gas of Impenetrable Bosons. *Phys. Rev. Lett.*, 81:938–941, Aug 1998. doi: 10.1103/PhysRevLett.81.938. URL <http://link.aps.org/doi/10.1103/PhysRevLett.81.938>.

- [66] G. Orso, A. Iucci, M. A. Cazalilla, and T. Giamarchi. Lattice modulation spectroscopy of strongly interacting bosons in disordered and quasiperiodic optical lattices. *Phys. Rev. A*, 80:033625, Sep 2009. doi: 10.1103/PhysRevA.80.033625. URL <http://link.aps.org/doi/10.1103/PhysRevA.80.033625>.
- [67] B. Paredes, A. Widera, V. Murg, O. Mandel, S. Folling, I. Cirac, G. V. Shlyapnikov, T. W. Hansch, and I. Bloch. Tonks-girardeau gas of ultracold atoms in an optical lattice. *Nature*, 429:277–281, May 2004.
- [68] M. Pasienski, D. McKay, M. White, and B. DeMarco. A disordered insulator in an optical lattice. *Nat Phys*, 6:677–680, Sep 2010.
- [69] O. Penrose and L. Onsager. Bose-einstein condensation and liquid helium. *Phys. Rev.*, 104:576–584, Nov 1956. doi: 10.1103/PhysRev.104.576. URL <http://link.aps.org/doi/10.1103/PhysRev.104.576>.
- [70] C. J. Pethick and H. Smith. *Bose-Einstein Condensation in Dilute Gases*. Cambridge University Press, 2008.
- [71] D. S. Petrov, G. V. Shlyapnikov, and J. T. M. Walraven. Regimes of Quantum Degeneracy in Trapped 1D Gases. *Phys. Rev. Lett.*, 85:3745–3749, Oct 2000. doi: 10.1103/PhysRevLett.85.3745. URL <http://link.aps.org/doi/10.1103/PhysRevLett.85.3745>.
- [72] D. S. Petrov, D. Gangardt, and G. V. Shlyapnikov. Low-dimensional trapped gases. *J. Phys. IV France*, 116:5–44, 2004. doi: 10.1051/jp4:2004116001. URL <http://dx.doi.org/10.1051/jp4:2004116001>.
- [73] L. Pitaevskii and S. Stringari. *Bose-Einstein Condensation*. Clarendon Press, Oxford, 2003.
- [74] A. Polkovnikov, E. Altman, E. Demler, B. Halperin, and M. D. Lukin. Decay of superfluid currents in a moving system of strongly interacting bosons. *Phys. Rev. A*, 71:063613, Jun 2005. doi: 10.1103/PhysRevA.71.063613. URL <http://link.aps.org/doi/10.1103/PhysRevA.71.063613>.
- [75] G. Pupillo, A. M. Rey, C. J. Williams, and C. W. Clark. Extended fermionization of 1d bosons in optical lattices. *New Journal of Physics*, 8(8):161, 2006. URL <http://stacks.iop.org/1367-2630/8/i=8/a=161>.
- [76] Z. Ristivojevic, A. Petković, P. Le Doussal, and T. Giamarchi. Phase transition of interacting disordered bosons in one dimension. *Phys. Rev. Lett.*, 109:026402, Jul 2012. doi: 10.1103/PhysRevLett.109.026402. URL <http://link.aps.org/doi/10.1103/PhysRevLett.109.026402>.
- [77] G. Roati. *Quantum degenerate Potassium-Rubidium mixtures*. PhD thesis, University of Trento, 2003.
- [78] G. Roati, M. Zaccanti, C. D’Errico, J. Catani, M. Modugno, A. Simoni, M. Inguscio, and G. Modugno.  $^{39}\text{K}$  Bose-Einstein Condensate with Tunable Interactions. *Phys. Rev. Lett.*, 99:010403, Jul 2007. doi: 10.1103/PhysRevLett.99.010403. URL <http://link.aps.org/doi/10.1103/PhysRevLett.99.010403>.

- [79] G. Roati, C. D'Errico, L. Fallani, M. Fattori, C. Fort, M. Zaccanti, G. Modugno, M. Modugno, and M. Inguscio. Anderson localization of a non-interacting Bose-Einstein condensate. *Nature*, 453:895–898, 2008.
- [80] T. Roscilde. Bosons in one-dimensional incommensurate superlattices. *Phys. Rev. A*, 77:069903, Jun 2008. doi: 10.1103/PhysRevA.77.069903. URL <http://link.aps.org/doi/10.1103/PhysRevA.77.069903>.
- [81] G. Roux, T. Barthel, I. P. McCulloch, C. Kollath, U. Schollwöck, and T. Giamarchi. Quasiperiodic Bose-Hubbard model and localization in one-dimensional cold atomic gases. *Phys. Rev. A*, 78:023628, Aug 2008. doi: 10.1103/PhysRevA.78.023628. URL <http://link.aps.org/doi/10.1103/PhysRevA.78.023628>.
- [82] B. Sacepe, T. Dubouchet, C. Chapelier, M. Sanquer, M. Oviaia, D. Shahar, M. Feigel'man, and L. Ioffe. Localization of preformed Cooper pairs in disordered superconductors. *Nat Phys*, 7:239–244, Mar 2011.
- [83] T. Schwartz, G. Bartal, S. Fishman, and M. Segev. Transport and anderson localization in disordered two-dimensional photonic lattices. *Nature*, 446:52–55, Mar 2007.
- [84] J. F. Sherson, C. Weitenberg, M. Endres, M. Cheneau, I. Bloch, and S. Kuhr. Single-atom-resolved fluorescence imaging of an atomic Mott insulator. *Nature*, 467:68–72, Sep 2010.
- [85] J. Sirker and A. Klümper. Thermodynamics and crossover phenomena in the correlation lengths of the one-dimensional t-J model. *Phys. Rev. B*, 66:245102, Dec 2002. doi: 10.1103/PhysRevB.66.245102. URL <http://link.aps.org/doi/10.1103/PhysRevB.66.245102>.
- [86] A. Smerzi, A. Trombettoni, P. G. Kevrekidis, and A. R. Bishop. Dynamical Superfluid-Insulator Transition in a Chain of Weakly Coupled Bose-Einstein Condensates. *Phys. Rev. Lett.*, 89:170402, Oct 2002. doi: 10.1103/PhysRevLett.89.170402. URL <http://link.aps.org/doi/10.1103/PhysRevLett.89.170402>.
- [87] J. Stenger, S. Inouye, A. P. Chikkatur, D. M. Stamper-Kurn, D. E. Pritchard, and W. Ketterle. Bragg spectroscopy of a bose-einstein condensate. *Phys. Rev. Lett.*, 82:4569–4573, Jun 1999. doi: 10.1103/PhysRevLett.82.4569. URL <http://link.aps.org/doi/10.1103/PhysRevLett.82.4569>.
- [88] T. Stöferle, H. Moritz, C. Schori, M. Köhl, and T. Esslinger. Transition from a Strongly Interacting 1D Superfluid to a Mott Insulator. *Phys. Rev. Lett.*, 92:130403, Mar 2004. doi: 10.1103/PhysRevLett.92.130403. URL <http://link.aps.org/doi/10.1103/PhysRevLett.92.130403>.
- [89] M. Störzer, P. Gross, C. M. Aegerter, and G. Maret. Observation of the critical regime near anderson localization of light. *Phys. Rev. Lett.*, 96:063904, Feb 2006. doi: 10.1103/PhysRevLett.96.063904. URL <http://link.aps.org/doi/10.1103/PhysRevLett.96.063904>.

- [90] L. Tanzi, E. Lucioni, S. Chaudhuri, L. Gori, A. Kumar, C. D'Errico, M. Inguscio, and G. Modugno. Transport of a bose gas in 1d disordered lattices at the fluid-insulator transition. *Phys. Rev. Lett.*, 111:115301, Sep 2013. doi: 10.1103/PhysRevLett.111.115301. URL <http://link.aps.org/doi/10.1103/PhysRevLett.111.115301>.
- [91] R. Vosk and E. Altman. Superfluid-insulator transition of ultracold bosons in disordered one-dimensional traps. *Phys. Rev. B*, 85:024531, Jan 2012. doi: 10.1103/PhysRevB.85.024531. URL <http://link.aps.org/doi/10.1103/PhysRevB.85.024531>.
- [92] D. S. Wiersma, P. Bartolini, A. Lagendijk, and R. Righini. Localization of light in a disordered medium. *Nature*, 390:671–673, Dec 1997.
- [93] R. Yu, L. Yin, N. S. Sullivan, J. S. Xia, C. Huan, A. Paduan-Filho, N. F. Oliveira Jr, S. Haas, A. Steppke, C. F. Miclea, F. Weickert, R. Movshovich, E.-D. Mun, B. L. Scott, V. S. Zapf, and T. Roscilde. Bose glass and Mott glass of quasiparticles in a doped quantum magnet. *Nature*, 489:379–384, 2012.
- [94] M. Zaccanti. *Tuning of the interactions in ultracold K-Rb quantum gases*. PhD thesis, University of Florence, 2007.